To Veronika

UNIVERSITÉ DE SHERBROOKE

Effects of Isoproterenol, an Adrenergic Agonist, on

Resting Skeletal Muscle

par

Gabor Gyurkovics

Département de physiologie et biophysique

Faculté de médecine

Thèse présentée à la Faculté de médecine et des sciences de la santé
en vue de l'obtention du grade de
philosophiae doctor (Ph.D.) en Physiologie - Biophysique

November 2009

Membres du jury:

Pr Éric ROUSSEAU, Ph.D., Département de physiologie et biophysique, Université de Sherbrooke, Président

Pr Jean-Marc RENAUD, Ph.D., Université d'Ottawa, Département de médecine cellulaire et moléculaire
Évaluateur externe

Pr Guillaume GRENIER, Ph.D., Département de chirurgie, Université de Sherbrooke
Évaluateur interne

Pr Paul PAPE, Ph.D., Département de physiologie et biophysique, Université de Sherbrooke
Directeur de recherche

Canada

I. Table of Contents

v

RÉSUMÉ

Cette étude démontre l'effet de l'isoprotérénol (ISO), un agoniste β-adrénergique, sur le contenu total en calcium dans le réticulum sarcoplasmique (SR), désigné $[Ca_T]_{SR}$. Un indicateur d'ions Ca^{2+} de basse affinité (K_D = 2.6 mM), le tétraméthylmuréxide (TMX), perméable aux membranes, a été utilisé afin d'évaluer le contenu en Ca^{2+} libre dans le SR, désigné $[Ca^{2+}]_{SR}$. La fraction du TMX lié à du Ca^{2+} dans le SR (fCa) est proportionnel à $[Ca^{2+}]_{SR}$ laquelle peut être utilisée pour déterminer $[Ca_T]_{SR}$.

Les résultats démontrent que 10 μM ISO augmente $[Ca^{2+}]_{SR}$ de 112 % dans le fibres musculaires maintenues à un potentiel membranaire de repos physiologique de -90 mV. Par contre, en l'absence de Ca^{2+} dans la solution externe, l'ISO n'augmente pas de façon significative $[Ca^{2+}]_{SR}$, suggérant que l'ISO induit un flux de Ca^{2+} à travers la membrane plasmique. Cette augmentation de $[Ca^{2+}]_{SR}$ se produit avec un délai exponentiel (τ = 7.0 min) et n'est pas réversible après le retrait de l'ISO de la solution externe. Ces résultats suggèrent donc que l'ISO pourrait stimuler l'expression de certain type de canaux calcique et que ceux-ci demeureraient actifs même après le retrait de l'agoniste β-adrénergique. Puisque l'augmentation de $[Ca^{2+}]_{SR}$ en présence d'ISO se produit au potentiel de repos physiologique, il est peu probable que des canaux calciques dépendant du voltage soient responsables de l'effet observé, même si une phosphorylation de ces canaux puisse modifier leur cinétique et donc augmenter leur probabilité d'ouverture.

De plus, nous avons nous avons observé que l'effet de l'ISO sur l'influx de Ca^{2+} est accru par l'hyperpolarisation des fibres. Cette augmentation survient avec un délai exponentiel (τ = 1.6 min) qui ne peut être expliqué par une simple augmentation de la force motrice pour les ions

calciques ou par le courant rectifiant dans le sens entrant. Ce résultat contredit l'hypothèse selon laquelle ISO activerait une dépendance calcique dépendante du voltage du fait que la probabilité d'ouverture de ce type de canaux augmente avec la dépolarisation membranaire.

En absence d'ISO, nous avons observé que la valeur de fCa demeure la même avec ou sans Ca^{2+} dans la solution externe, suggérant une absence d'influx calcique durant des conditions physiologiques de repos. Lorsque les fibres musculaires sont déplétées de 70 % de leur contenu en Ca^{2+}, la valeur de fCa n'est pas influencée par l'absence ou la présence de Ca^{2+} dans le milieu extracellulaire. Ceci indique que les canaux calciques de la membrane de surface, activé par une diminution du Ca^{2+} dans le RS (canaux SOC), ne sont pas impliqués directement dans la régulation du contenu en Ca^{2+} dans le RS.

L'élimination de l'ISO du milieu extracellulaire produit une diminution transitoire rapide de fCa qui est suivit par une ré-augmentation graduelle à une vitesse similaire de celle obtenue en présence d'ISO. Cet effet peut s'expliquer par une inversion du sens de la pompe calcique ATPase sarco-endoplasmique (SERCA), provoqué par deux facteurs : (1) l'augmentation de $[Ca^{2+}]_{SR}$ et (2) la diminution de la concentration en ATP intracellulaire ($[ATP]_i$), résultant de l'élimination de l'ISO du milieu extracellulaire.

D'autre part, nous avons observé que la stimulation adrénergique augmente le pH myoplasmique. Cette observation peut être expliquée par un effet possible de l'activation des récepteurs α-adrénergiques, lesquels augmentent l'activité des échangeurs Na^+/H^+ via la voie des PLC et de l'IP$_3$. Ceci a pour conséquence de réduire $[H^+]$ dans le myoplasme.

Finalement, nos résultats démontrent que l'ISO augmente $[Ca_T]_{SR}$ au repos ainsi que l'activité des SERCA. Les résultats de cette thèse soulèvent également des questions quant au rôle physiologique des canaux SOC dans la régulation de $[Ca_T]_{SR}$.

Mots clefs :

Tetraméthylmuréxide, muscle squelettique, contenu en calcium, isoprotérénol, réticulum sarcoplasmique.

III. ABSTRACT

Data in this study show the effects of isoproterenol (ISO), a β-adrenergic agonist, on the total calcium content of the sarcoplasmic reticulum (SR), denoted $[Ca_T]_{SR}$. Tetramethyl murexide (TMX), a membrane permeable, low affinity Ca^{2+} indicator was used to monitor SR Ca^{2+} content. The fraction of calcium-bound form of TMX in the SR (fCa) is approximately proportional to the concentration of the free Ca^{2+} in the SR ($[Ca^{2+}]_{SR}$) which in turn can be used to give $[Ca_T]_{SR}$.

Results show that 10 μM ISO increases $[Ca^{2+}]_{SR}$ by 112% in 30 min. in resting frog skeletal muscle. No significant increase was observed with no Ca^{2+} present in the external solution indicating that ISO caused a Ca^{2+} influx across the surface/T-system membrane. This increase in $[Ca^{2+}]_{SR}$ occurred with an exponential delay ($\tau = 7.0$ min.) and failed to reverse after washing out ISO. These results suggest that ISO stimulates the expression of a channel -permeable to calcium during resting potentials- which would remain active or open even after washing out ISO. These results argue against the involvement of most of voltage-dependent Ca^{2+} channels that are gated by depolarization.

Furthermore, we showed that hyperpolarization in ISO further increases Ca^{2+} influx. The increase in rate of influx came on with an exponential delay ($\tau = 1.6$ min.), and couldn't be explained simply by the increased driving force for Ca^{2+} or by inward rectification. This delay also argues against the involvement of hyperpolarization-activated channels. The fact that the rate of Ca^{2+} flux did not decrease during hyperpolarization further supports the idea that the Ca^{2+} influx is not due to depolarization-activated Ca^{2+} channel.

In the absence of ISO, the level of fCa was the same with and without Ca^{2+} in the external solution, indicative of a lack of Ca^{2+} influx under resting physiological conditions. When the level of fCa was reduced to 30% of the physiological level with 20 mM EGTA, the average value of fCa was the same with or without external Ca^{2+}. These results thereby arguing against the involvement of store operated mechanisms in the regulation of SR Ca^{2+} content in the physiological range.

The data show two well distinguished effects when ISO was removed. One is a reversible effect which showed a sudden, transient decrease in SR calcium content (termed "dip"). The "dip" can be described with a single exponential and corresponds with the rate of Ca^{2+} release observed in response to a depolarization to -70 mV. The "dip" appears to require the reversal of the SR calcium pump (SERCA). After the "dip", SR calcium content rose again and reached the same rate as was observed during ISO. This steady rise in SR calcium content appeared to be the other, irreversible effect of ISO.

In addition, during the course of ISO stimulation, we observed an increase in myoplasmic pH. One possible explanation could involve the activation of α-adrenergic receptors by ISO. The receptors activate the PLC-IP3 pathway which, in turn, enhances the Na/H exchanger and thus the removal of H+ ions from the myoplasm.

In summary, the data indicate that adrenergic stimulation increases $[Ca_T]_{SR}$ in resting fibers by activating Ca^{2+} influx across the surface/T-system membrane and is consistent with the expression of an unknown Ca^{2+} channel. Our results also raise doubts about whether store-operated mechanisms are involved in fibers depleted to 30% of their normal $[Ca^{2+}]_{SR}$. The data also suggest that SERCA is directly enhanced by ISO.

Key Words:

Tetramethyl murexide, skeletal muscle, calcium content, isoproterenol, sarcoplasmic reticulum

IV. List of Figures

List of Tables

V. Glossary of Abbreviations

$[Ca^{2+}]_{myo}$	myoplasmic free Ca^{2+} concentration
$[Ca^{2+}]_{SR}$	sarcoplasmic reticulum free Ca^{2+} concentration
$[TMX]_T$	total TMX concentration
"dip"	exponential decrease of fCa after removing ISO
0.1EGTA, NR	internal solution has 0.1 mM EGTA, external solution is NR
20EGTA, NR	internal solution has 20 mM EGTA, external solution is NR
ACh	acetylcholine
AChE	acetylcholinesterase
AKAP	A kinase anchoring protein
ATP	adenosine triphosphate
CaM	calmodulin
CaMK	calmodulin kinase
cAMP	cyclic adenosine monophosphate
CICR	Ca^{2+}-induced Ca^{2+} release
$Cl^-/HCO3^-X$	chloride/bicarbonate exchanger
CRAC	calcium release-activated calcium channel
DAG	diacyl glycerol
D_{APP}	apparent diffusion constant
DHPR	dihydropyridine receptor
ECC	excitation-contraction coupling
EGTA	Ethylene glycol-bis(2-aminoethyl-ether)-N,N,N,N-tetraacetic acid
fCa	fraction of TMX bound with calcium
FKBP12	FK506 binding protein
GDP, GTP	guanosine diphosphate, guanosine triphosphate
GPCR	G-protein coupled receptor
HCN	hyperpolarization-activated cyclic nucleotide-gated channels
HPR	protonated form of phenol red
HTMX	protonated, neutral form of TMX

IP_3	inositol triphosphate
IP_3ROC	IP_3 receptor-operated channel
ISO	isoproterenol
K_d	dissociation constant
K_m	Michaelis constant
LVA	low voltage activated channels
MCT	monocarboxylate transporter
MOPS	3-[N-Morpholino]propanesulfonic acid (pH buffer)
mRNA	messenger RNA
nAChR	nicotinic acetylcholine receptor
NBCe	Na/bicarbonate co-transporter
NR	normal Ringer's solution with 1.7 mM $CaCl_2$
Orai	Transmembrane protein 142A, store-operated regulation by STIM
pH	negative logarithm of hydrogen ion concentration
PIPES	Piperazine-N-N-bis[2-ethanesulfonic acid] (pH buffer)
pK	negative logarithm of the dissociation constant
PKA	protein kinase A
PLB	phospholamban
PLC	phospholipase C
PMCA	plasmalemmal calcium pump
P_o	open probability of a channel
PR	phenol red
RyR	ryanodine receptor
SERCA	sarco/endoplasmic calcium ATP-ase
SLN	sarcolipin
SOC	store-operated channel
SR	sarcoplasmic reticulum
STIM	stromal interaction molecule
TMX	tetramethyl murexide
TRPC	transient receptor potential channel Canonical

1. INTRODUCTION

Adrenaline was isolated and identified in 1895 by Napoleon Cybulski, a Polish physiologist. In 1896, William Bates reported the clinical effects of a substance produced by the adrenal gland in the New York Medical Journal (Bates, 1896). The active principle of suprenal extract that produces its pressor effects was isolated by the joint research of John Abel in 1899 and Jokichi Takamine in 1901. Within a few years (in 1904), it was suggested that this active principle, referred to by British physiologists as "adrenaline", was released from sympathetic nerve terminals to act on smooth muscle cells (Bennett, 1999).

The original observations of adrenaline's effects on the contractions of frog and mammalian muscle were made by Gruber (1914) and Orbeli (1923). Orbeli observed that - when blood adrenaline level increased due to the stimulation of the lumbar sympathetic nerve in the frog - the force of the fatigued skeletal muscle, contracting due to electrical stimulation, recovered from the weakened tension. In the '40s, Brown and co-workers showed that the site of action of adrenaline in fatigued nerve-muscle preparations in the rat and cat is primarily upon the muscle fiber itself (Brown et al., 1948).

In curarized frog skeletal muscle, Hutter & Loevenstein (Hutter and Loewenstein, 1955) and later Oota & Nagai (Oota and Nagai, 1977) reported a positive inotropic effect of adrenaline. This enhancement of twitch tension could be due to catecholamines acting on the actomyosin system, on the sarcoplasmic reticulum (SR) calcium pump or on the

1

release or influx of calcium ions. Rubio and coworkers found that the enhancement of the actomyosin complex observed in heart preparations is not present in skeletal muscle (Rubio et al., 1975).

After the exclusion of the enhancement of actomyosin complex, Gonzalez-Serratos et al, (1981) set out to examine whether adrenaline has a clear positive inotropic effect on frog skeletal muscle, and if so, what mechanisms are responsible for this effect. In split fibers, they showed that the force produced with the release of Ca^{2+} from the SR by caffeine was 60-100% larger when cAMP was added to the solution; simply adding adrenaline to the interior of the cell produced no changes in tension. They speculated that adrenaline acts via cAMP, and in turn, cAMP increases the amount of Ca^{2+} taken up by the SR. Furthermore they suggested that the positive inotropic effect is due to the release of this extra Ca^{2+} accumulated by the stimulation of the SR Ca^{2+} pump and probably by an increase in the capacity of Ca^{2+} binding in the SR. Further investigating with intact fibers, they found that catecholamines produced an increase of twitch tension preferably at lower stimulation frequencies. They also showed that, after bathing the intact fiber in adrenaline for 8 minutes, the first stimulation resulted in an 80% increase of force (Fig. 1). This finding suggests that Ca^{2+} entry and its accumulation in the SR occurred in the resting state.

Partially based on Gonzalez-Serratos et al. (1981) findings, Arrreola and co-workers aimed to answer whether Ca^{2+} channels of frog skeletal muscle are subjected to long-term modulation by adrenaline and whether this modulation could explain twitch potentiation (Arreola et al., 1987). In intact preparation after 27 minutes of exposure to adrenaline, they measured an increased force potentiation, which was greater at high frequency

stimulation. They measured an increased Ca^{2+} current (I_{Ca}) during adrenergic stimulation, and speculated that ISO increased SR calcium content; however, they did not measure sarcoplasmic reticulum free calcium concentration ($[Ca^{2+}]_{SR}$) directly. Since addition of nifedipine, an L-type Ca^{2+} channel inhibitor did not produce a decrease on twitch potentiation, they concluded that these Ca^{2+} channels are probably not involved. They also showed the dependence of enhanced twitch potentiation on the presence of external Ca^{2+}. In addition and opposed to the finding of Gonzalez-Serratos laboratory, they did not measure an increased tension for the first stimulation of the intact fiber after 25 minutes of bathing in adrenaline (Fig. 2). They observed an increase in force potentiation only after five minutes of low frequency stimulation. They concluded that adrenaline is ineffective if no stimulation was applied.
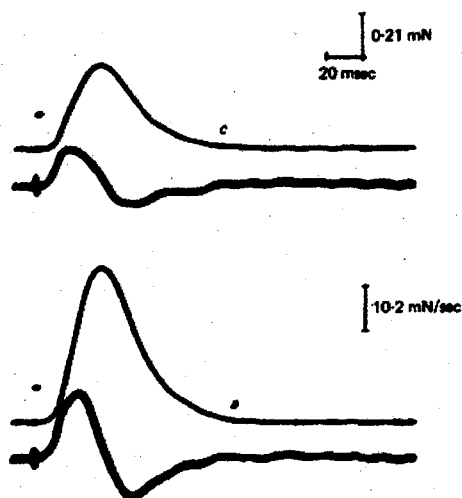
Fig. 1. Effect of L-adrenaline (1 x 10-6 M) on the twitch tension (upper traces) and rate of tension development and decay (lower traces). In c the fiber had not been exposed to adrenaline; in a the fiber had been in a bathing solution containing adrenaline for 8 min before it was stimulated (After Gonzalez-Serratos et al., 1981)

A
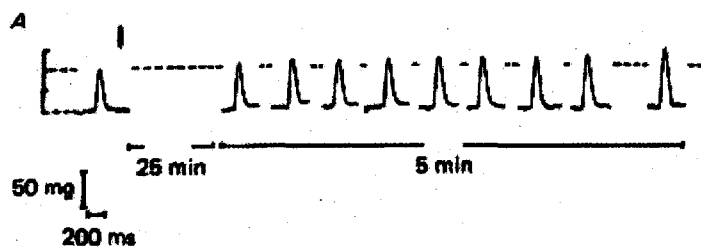
Fig. 2. After a control twitch, adrenaline was added to the external solution and the fiber was bathed for 25 min before the series of twitches elicited at 0.07 Hz. The last twitch is a steady-state potentiation at 5 min (After Arreola et al., 1987)

The motivation for the work of this Ph.D. thesis was based on the controversy between results reported by the above mentioned laboratories: Arreola et al. (1987) reported that twitch potentiation required a train of closely spaced action potentials and attributed this requirement to the build up of voltage activation of some type of voltage-activated Ca^{2+} channels during the train of action potentials; in contrast, Gonzalez-Serratos et al. (1981) reported that adrenaline greatly enhances the first twitch response following adrenergic stimulation which suggests that the enhanced Ca^{2+} entry occurred in the resting state. They both suggested however that the enhanced twitch potentiation is due to an increased $[Ca^{2+}]_{SR}$ resulted by adrenergic stimulation, although they never directly measured it.

1.1 Anatomy of frog skeletal muscle

The primary function of skeletal muscle is to generate force or movement in response to a physiological stimulus. Normally it transduces an electrical command into mechanical response and it has to be able to create a rapid force development and sometimes

maintain its contractile force for relatively long periods (Boron and Boulapep, 2003). To achieve this goal, muscle cells have developed highly specialized anatomical structures and functional mechanisms.

1.1.1 Neuromuscular Junction

At the neuromuscular junction or endplate region, the presynaptic axon transmits an excitatory signal to the postsynaptic muscle. The frog motor endplate in its simplest form consists of an elongated, slender nerve ending embedded in a gutter-like depression of the sarcolemma (Fig. 3, middle image). This nerve terminal contains the usual synaptic organelles, capped by a thin sheath of Schwann cell cytoplasm (Fig. 3, middle image). At the active zone, where vesicles are released from the nerve terminal, these synaptic vesicles containing acetylcholine (ACh) lie adjacent to the presynaptic membrane. The postsynaptic membrane of the muscle cell contains closely packed nicotinic ACh receptors (Fig. 3, bottom image). The extracellular matrix in the synaptic cleft contains the enzyme acetylcholinesterase (AChE) which terminates the action of ACh (Peper et al., 1974).
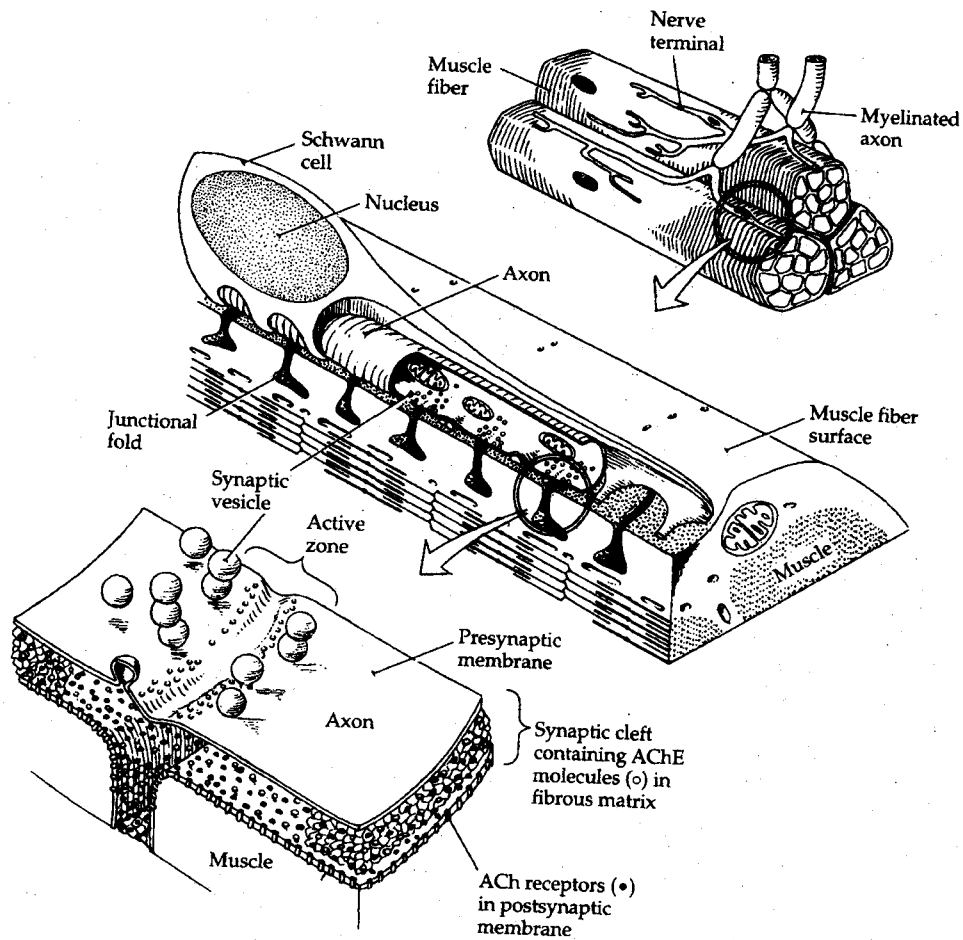
Fig. 3 Anatomy of Frog Neuromuscular Junction. The top image shows the myelinated nerve fibers branching to form the neuromuscular junction. The middle image shows one terminal indenting the muscle surface. The bottom image is a blown up drawing of the active zone of the postsynaptic membrane, with the closely packed ACh receptors, and synaptic vesicles released from the nerve terminal (Peper et al., 1974).

1.1.2 Structure of the muscle fiber

Skeletal muscle fibers are multinucleated cells formed by the fusion of elongated uninucleate cells called myoblasts. Mature fibers may be as long as the muscle of which they form part, and are normally around 50 to 100 μm in diameter in amphibians. Most of

the interior of the fiber consists of the protein filaments which constitute the contractile

apparatus, grouped together in bundles called myofibrils. The myofibrils also contain the

internal membrane systems of the sarcoplasmic reticulum (SR) and the T tubule system.

The myofibrils have characteristic banding patterns, and the bands on adjacent

myofibrils are transversely aligned so that the whole fiber appears striated under the light

microscope (Fig. 4). The two main bands are the dark, strongly birefringent A band and
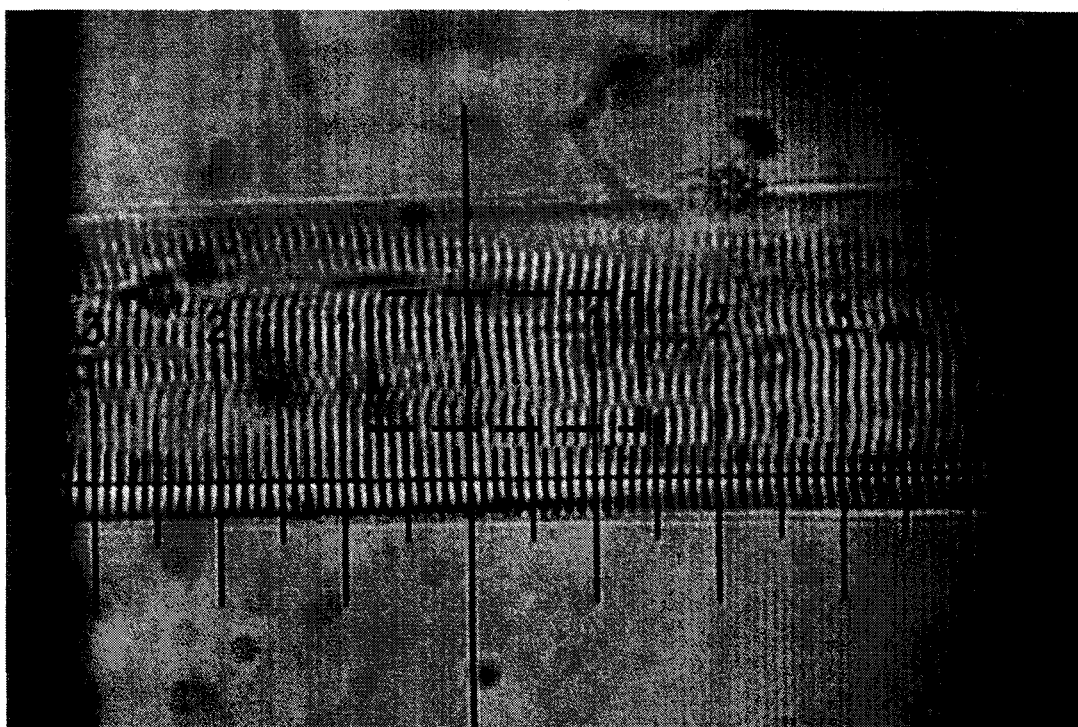
Fig. 4 Light microscope image of the frog semitendinosus muscle. The darker, more birefringent A bands and the lighter, less birefringent I bands are clearly visible. The rectangular area on the figber represents the approximate size of transilluminated spot used for absorbance measurements. Fiber diameter is 85 μM (Photo by the author).

the lighter, less birefringent I band. These bands alternate along the length of the

myofibril. In the middle of the A band is a lighter region, the H zone, which is bisected

by a darker line, the M line. A lighter region in the middle of the H zone, the L zone, can

sometimes be distinguished (Fig 5). Two kinds of protein filaments, called myofilaments, are major components of myofibrils. The thick filaments are called myosin and the thin filaments are called actin. The actin and myosin myofilaments form highly ordered units called sarcomeres, which are joined end to end at the Z line to form the myofibrils (Seeley et al., 2003).
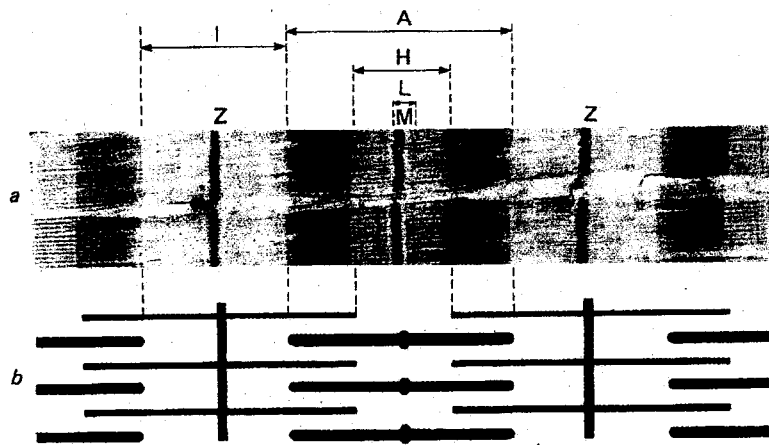
Fig. 5 The striation pattern of a vertebrate skeletal muscle fiber as seen under electron microscope (a), and its interpretation as two sets of filaments (b). Photo by H. E. Huxley. (Keynes and Aidley, 2001)

Muscle contraction is described by the sliding filament theory of Huxley and Niedergerke (Huxley and Niedergerke, 1954), using interference microscopy of living muscle fibers. This theory suggests that contraction is brought about by movement of the thin filaments between the thick filaments. The sliding is caused by a series of cyclic reactions between the projections on the myosin filaments and active sites on the actin filaments. Each projection first attaches itself to the actin filament to form a cross-bridge, then pulls on it and finally releases it, moving back to attach to another site further along the actin filament. The presence of ATP and Ca^{2+} is needed for this process. The increase of myoplasmic calcium concentration ($[Ca^{2+}]_{myo}$) is the activator of muscle contraction. When $[Ca^{2+}]_{myo}$ concentration increases (to about 10^{-6} M), cross bridges are formed

between the two sets of filaments; ATP is split and sliding occurs (Keynes and Aidley, 2001).

An internal membrane system, the sarcoplasmic reticulum supplies Ca^{2+} for contraction upon depolarization. The SR is a series of membrane-bound sacs between the myofibrils. Its major property is that it accumulates Ca^{2+} against a concentration gradient by means of a calcium pump which requires energy from the splitting of ATP for its activity. This pump, called the sarco-endoplasmic calcium ATP-ase (SERCA) serves to maintain the calcium ion concentration in the sarcoplasm of the living muscle at its low resting level (at about 0.1 μM), and to produce relaxation of the muscle after contraction.

The sarcolemma has, along its surface, much regularly arranged, tube-like invaginations called transverse, or T tubules. T tubules project into the muscle fiber and wrap around sarcomeres in the region of Z lines in frog muscle (in mammalian muscle, T tubules run in the region where actin and myosin filaments overlap). Near the T tubules, the SR is enlarged to form terminal cisternae (Peachey, 1965). A T tubule and the two adjacent terminal cisternae together are called a triad (Fig. 6). High-quality electron micrographs by Clara Franzini-Armstrong (1970) showed that, at the triads, the T tubule and its adjacent terminal cisternae are connected by an array of structures called "feet" (Fig. 7). These feet belong to the calcium-release receptor channel (RyR) anchored in the SR membrane. The T tubule membrane, on the other hand, contains particles grouped in fours ("tetrads") that are positioned opposite the feet. These tetrads are groups of four voltage-gated calcium channels, also known as DHP receptors. All the DHP receptor tetrads are closely aligned with ryanodine receptors, but about half of the RyRs have no associated DHP receptors (Franzini-Armstrong, 1970).
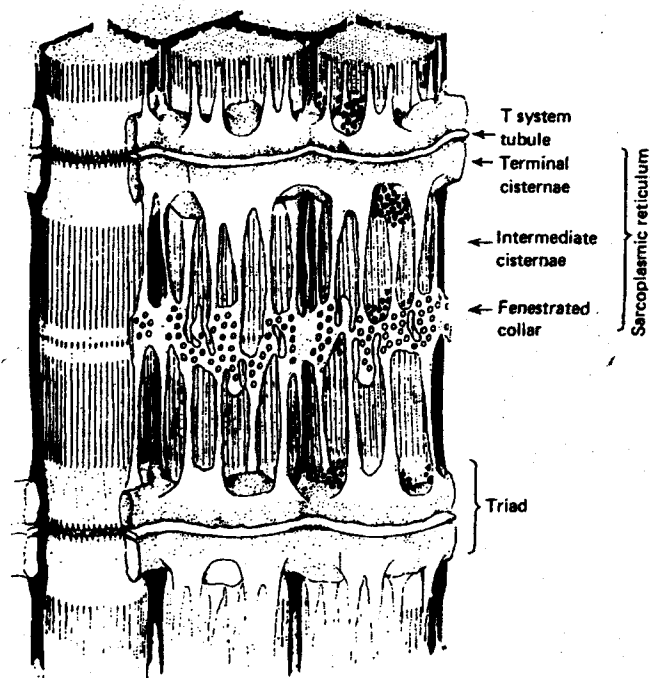
Fig. 6 The internal membrane system of the frog sartorius muscle fiber. In frog, the T tubule system is located at the Z line region. (Peachey, 1965)

Fig. 7 A single triad in frog sartorius muscle. The SR and T-system membranes run parallel and are separated by an empty gap. The SR membrane is scalloped, (marked by "S") with the period of the scallops coinciding with the position of the feet. The periodically repeating feet are well visible. After Franzini-Aramstrong, (1970).

10

1.1.3 Types of skeletal muscle fibers

Some skeletal muscles are resistant to fatigue and are able to maintain tension for a relatively long period, although they don't have to contract rapidly. Examples are muscles that maintain body posture, such as the soleus muscle in the leg. On the other hand, some muscles are capable of contracting very rapidly. However, these "fast-twitch" muscles tend to fatigue quickly. A good example of a fast twitch muscle is the external muscles of the eye, which need to contract rapidly but don't have to maintain contraction for a long period of time. Hence, muscle fibers are generally classified as slow twitch (type I) and fast twitch (type II), depending on their rate of force development. These fibers are also distinguished by their histologic appearance, resistance to fatigue, and biochemical composition (Seeley et al., 2003).

Slow twitch fibers are generally thinner; also appear red because of the abundance of the oxygen-binding protein myoglobin. These muscles rely on oxidative metabolism for energy, hence the high density of mitochondria. In amphibians, these muscles are called tonic muscles. The maximum shortening velocity of these muscles is lower than their fast type counterparts. The slower contraction is due to a different isoform of myosin light chain kinase (MLC), and myosin heavy chain kinase (MHC) present in these fibers, as Lutz an coworkers showed in Rana pipiens anterior tibialis muscle (Lutz et al., 1998).

Fast-twitch fibers differ among themselves with respect to fatigability and maximum velocity of contraction. In mammals, the so called type IIa fast twitch fibers are quite resistant to fatigue. Indeed, their metabolic rate is high; they contain high concentration of myoglobin and mitochondria to compensate for the increased rate of ATP hydrolysis. On the other hand, type IIb fast twitch fibers are not capable of sufficient oxidative

11

metabolism to sustain contraction. These fibers rely on the energy that is stored in glycogen and phosphocreatine, and are more easily fatigable. They have fewer mitochondria and lower concentrations of myoglobin and oxidative enzymes. Because of the low myoglobin content, they appear white (Boron and Boulapep, 2003). In amphibians, fast twitch fibers are classified as type 1, type 2, and type 3 fibers. This classification is based on the differences of maximum shortening velocity (type 1 being the fastest) and the various subunits of myosin molecules (Lannergren, 1987).

1.2 Excitation-contraction coupling in skeletal muscle

Skeletal muscle is excited by an all-or-nothing action potential that is propagated along the whole length of the fiber. This is followed by contraction. The process linking the two events is called the excitation-contraction coupling process.

1.2.1 End-plate potential and action potential

When an action potential arrives at the presynaptic terminal of the motor neuron it causes voltage gated Ca^{2+} channels to open. Calcium ions enter the presynaptic terminal; initiate the release of the neurotransmitter, acetylcholine (ACh) from the synaptic vesicles into the synaptic cleft. Acetylcholine diffuses across the synaptic cleft and binds to nicotinic ACh-receptor channels (nAChR) on the postsynaptic muscle fiber membrane (Seeley et al., 2003). These receptors are nonselective cation channels that open when ACh binds to a specific site on the channel. The result is depolarization, known as the end-plate

potential, is produced. For the first time Fatt and Katz (Fatt and Katz, 1952) showed -in frog muscle using intracellular recording technique- how stimulation of the motor nerve affects the post synaptic membrane potential. If the end-plate potential exceeds the threshold for activating voltage gated Na^+ channels, an action potential results. Generation of an action potential initiates the sequence of processes leading to contraction. (Boron and Boulapep, 2003). Once triggered, the action potential propagates along the sarcolemma and T-tubules. The depolarization of the T-tubule membrane causes the activation of L-type Ca^{2+} channels (also called dihydropyridine receptors or DHPRs). DHPRs are clustered in groups of four called tetrads. DHPRs play a pivotal role in EC-coupling since they serve as the voltage sensor for SR Ca^{2+} release (Rios and Brum, 1987). The coupling mechanism is thought to involve a physical link between the DHPR and the sarcoplasmic reticulum Ca^{2+} release channel (also called as ryanodine receptor or RyR channel).

1.2.2 Central Role of sarcoplasmic reticulum

As depicted in Fig. 6, the sarcoplasmic reticulum consists of a series of membrane-bound sacs between the myofibrils of the skeletal muscle. The volume of the SR is about 16% of that of the volume of the sarcoplasm measured in frog sartorius muscle fibers bathed in isotonic solution (Birks and Davey, 1969). In this relatively small lumen, the SR sequesters the calcium. The release of this sequestered calcium is necessary for initiating contraction upon stimulation. Hence, the SR most important property is that it accumulates Ca^{2+} against its concentration gradient (Keynes and Aidley, 2001). The protein that buffers calcium in the SR is called calsequestrin (CSQ) after the suggestion

of MacLennan. MacLennan and Wong (1971) were the first to purify this protein. Calsequestrin is a very high capacity calcium-binding protein; its molecular weight is between 44 and 65 kD (MacLennan and Wong, 1971; Meissner G et al., 1973; Campbell KP, 1980), and it has a low affinity ($K_d \approx 1$ mM (Pape et al., 2007)) but very high capacity for calcium. CSQ is considered to be responsible for the ability of SR to maintain a high calcium content and also maintain the necessary driving force for calcium release upon stimulation (Franzini-Armstrong et al., 1987; Pape et al., 2007; Pape and Fénelon, 2008). Pape et al. (2007) showed in cut frog muscle fibers that almost all of the calcium in the SR is bound to calsequestrin. They estimated that -upon stimulation- 23 times more released calcium comes from calsequestrin as opposed to from the pool of free Ca^{2+} in the SR indicative of calsequestrin importance as a buffer of $[Ca^{2+}]_{SR}$ during release.

Constantin et al., (1965) observed that calcium accumulated in the terminal sacs of sarcoplasmic reticulum in oxalate treated frog muscle. They identified these regions of the SR as the intracellular calcium sink that controls the relaxation phase of the contraction-relaxation cycle. They also suggested that this area of the SR might also be the regions from which calcium is released to trigger contraction. Indeed, calsequestrin was localized to the terminal cisternae of the SR (MacLennan and Wong, 1971; Meissner, 1975). As shown in sarcoplasmic reticulum vesicles from rabbit leg muscle, calsequestrin has a tendency to aggregate on the junctional side of the membrane (Campbell KP, 1980), suggesting a direct attachment to the junctional membrane (Franzini-Armstrong et al., 1987). Zhang et. al. and other workers later found two proteins in the junctional SR: junctin and triadin (Zhang et al., 1997; Shen et al., 2007).

They suggested that these proteins interact directly to anchor calsequestrin to ryanodine receptor and form a quaternary complex that may be required for normal operation of Ca^{2+} release.

1.2.3 Role of DHPR channels

To release Ca^{2+} upon the arrival of the action potential to the triads, the SR needs a voltage sensor which senses the depolarization of the T tubule membrane. Schneider and Chandler theorized (Schneider and Chandler, 1973) and later Brum and coworkers confirmed (Brum et al., 1988b), that there are voltage sensors present in the T tubule membrane, and their action is necessary for initiating calcium release from the SR. Indeed, one surface membrane protein was located at the junctional domains of the exterior membranes which serves as voltage sensor for the SR: the L-type calcium channel, or DHPR.

Tsien and coworkers (Tsien et al. 1988) classified L-type calcium channels according to their differences in gating, ionic conductance and pharmacology. According to these criteria, they distinguished four different L-type channels: $Ca_v1.1$, 1.2, 1.3, 1.4 (Fig. 8). L-type channels show high sensitivity to dihydropyridines, such as nifedipine and BAY K 8644. The responsiveness to these drugs is one of the defining criteria for separating them from the other voltage gated Ca^{2+} channels. Hence they are named dihydropyridine receptor channels (DHPR). In skeletal muscle, excitation-contraction coupling $Ca_v1.1$ channels play a major role as the voltage sensor. These channels are primarily voltage gated but can be modified by intracellular protein-protein interactions as well.

	Slow, persistent
	HVA
Tsien type[a]	L
Snutch gene class[b]	S, C, D, F
Structural nomenclature[c]	$Ca_v1.1, 1.2, 1.3, 1.4$
Activation range[d]	Positive to −30 mV
Inactivation range	−60 to −10 mV
Inactivation[e]	Very slow ($\tau > 500$ ms)
Deactivation rate[f]	Rapid
Single-channel conductance[g]	25 pS
Single-channel openings	Continual reopening
Relative conductance	$Ba^{2+} > Ca^{2+}$
Divalent block	$Cd^{2+} > Ni^{2+}$
ω-CTX GVIA block[h]	No
Dihydropyridine sensitivity[i]	Sensitive

Fig. 8 Types of L-type Ca^{2+} channels
Lower case letters in index refer to the following references from where the results were taken:
[a](Tsien et al., 1988), [b](Snutch et al., 1990; Birnbaumer et al., 1994), [c](Ertel et al., 2000),
[d] In 10 mM calcium
[e]Inactivation rate at 0 mV, 10 mM Ca or 10 mM Ba extracellular, EGTA in cell, 21 °C.
[f]Rate of turn-off tail current at -80 to -50 mV.
[g]Maximum slope conductance in 110 mM Ba.
[h]ω-Conotoxin GVIA from Conus geographus
[i]Enhancement by BAY K 8644 and inhibition by nifedipine
(after Tsien et al., 1988)

L-type calcium channels were first purified using ion-exchange chromatography by Curtis and Catterall (Curtis and Catterall, 1984) from the transverse tubule membranes of skeletal muscle. Analysis of the biochemical properties revealed that the protein has five distinct subunits α_1, α_2, β, δ, and γ. Takahashi et al. (1987) demonstrated in purified

dihydropyridine-sensitive calcium channels -from rabbit skeletal muscle- that these subunits are located in close proximity to each other with the principal transmembrane subunit α_1 in association with the disulfide-linked $\alpha_2\delta$ subunit, an intracellular phosphorylated β subunit, and a transmembrane γ subunit (Fig. 9).
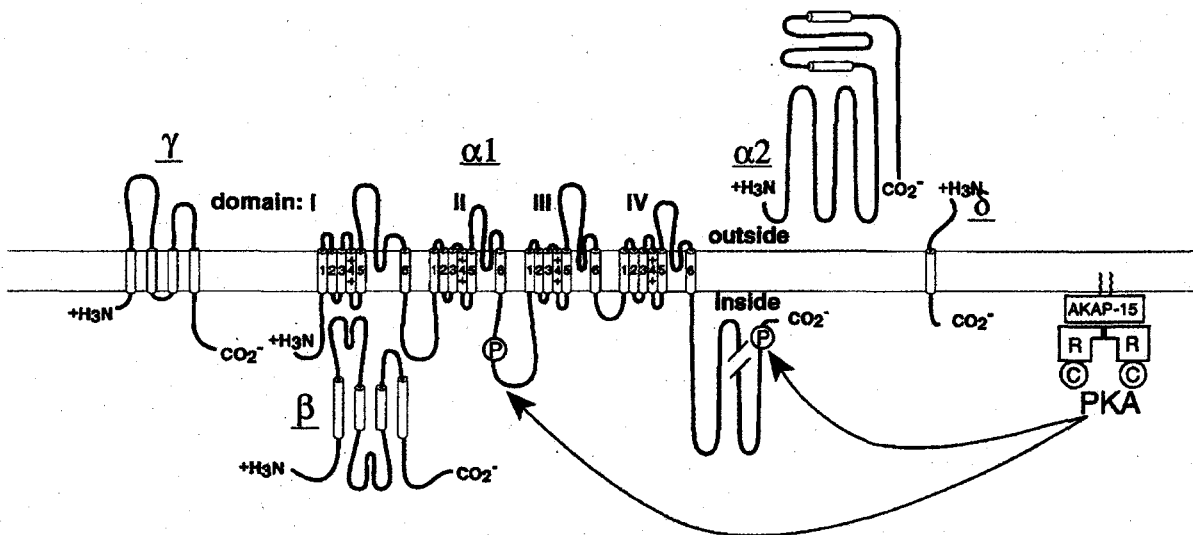
Fig. 9 Subunit structure and regulations of Cav1 channels.
The subunit composition and structure of Ca^{2+} channels purified from skeletal muscle are illustrated. The model is updated from the original description of the subunit structure of skeletal muscle Ca^{2+} channels (Takahashi et al 1987). P, sites of phosphorylation by cAMP-dependent protein kinase that have been demonstrated in intact cells. The actual disulfide linkage between the α_2 and δ subunits are not shown. (Catterall, 2000).

In skeletal muscle, single twitches do not require Ca^{2+} from the extracellular space (Armstrong et al., 1972). It has been proposed that excitation-contraction coupling occurs via direct mechanical coupling – protein-protein interaction – between the voltage sensitive Ca^{2+} channel (DHPR) and the RyR1 or α-RyR channels in mammals and amphibians respectively (Franzini-Armstrong, 1970; Adams and Beam, 1990). During EC coupling there are voltage-driven conformational changes occurring in the DHPR that

are recorded as intramembranous charge movement that precede the channel opening (Schneider and Chandler, 1973; Garcia et al., 1994). These voltage-driven charge movements are thought to reflect of movement of the voltage sensors (DHPRs) as they change to a conformation. This change in conformation presumably gates the opening of skeletal muscle RyRs (RyR1) in the SR via a mechanical, possibly direct link between the two proteins (Brum et al., 1988a). In frog skeletal muscle, intramembranous charge movements show two well distinguishable components (Schneider and Chandler, 1973; Adrian and Peres, 1977; Hui and Chandler, 1991). The early component, Q_β, which decays exponentially, and the late "hump", $Q\gamma$ (see Fig. 10). Pharmacological studies suggested that $Q\gamma$ might be closely associated with Ca^{2+} release from sarcoplasmic reticulum (Huang, 1982). Using voltage clamp technique, Hui (1983) also speculated that $Q\gamma$ is linked to Ca^{2+} release from the SR. This idea that $Q\gamma$ charge is caused by movement of voltage sensors in the T tubular membrane that activate Ca^{2+} release channels in the closely apposed SR membrane, presumably via mechanical coupling was supported by the results from other labs (Hui, 1983; Vergara and Caputo, 1983; Hui and Chandler, 1991; Pape and Carrier, 2002). Nifedipine, a substance that binds to DHPRs and inhibits L-type I_{Ca} inhibits $Q\gamma$ and in addition it inhibits SR Ca^{2+} release (Huang, 1990). Using nifedipine during adrenergic stimulation however, did not change the enhanced force potentiation in frog fast twitch and rat soleus muscles (Arreola et al. 1987, Cairns and Dulhunty 1993). This result suggests that catecholamines enhance a pathway other than DHPR channels for Ca^{2+} entry.

18
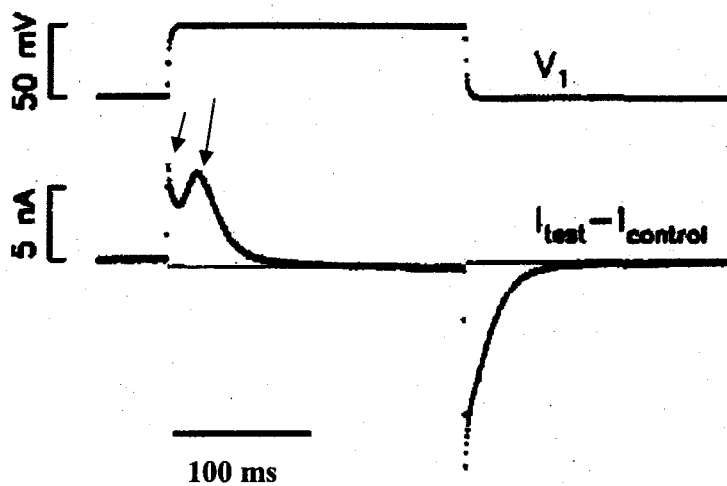
Fig. 10 Intramembranous charge movement.
The top trace shows the voltage pulse from -90 mV to -40 mV. The next trace shows the corresponding $I_{test} - I_{control}$ signal. The arrows indicate the early component Q_β (left), and the late "hump" Q_γ (right) (Jong et al., 1995).

Phosphorylation sites for cAMP-dependent protein kinase (PKA) are found on the α_1 and β subunits of DHPR in skeletal muscle cells (Curtis and Catterall, 1985; Jahn et al., 1988). Ca^{2+} flux through the channel is regulated by cAMP-dependent protein phosphorylation, (Flockerzi et al., 1986; Catterall, 2000). Ion flux studies in phospholipid vesicles showed that phosphorylation of the $\alpha 1$ and β subunits can greatly increase the number of functional Ca^{2+} channels in purified preparations (Nunoki et al., 1989; Mundina-Weilenmann et al., 1991); furthermore, single-channel recordings in planar bilayer membranes show increases in open probability after phosphorylation by PKA (Flockerzi et al., 1986). As biochemical studies revealed, PKA is anchored to DHPR channel by an A kinase anchoring protein (AKAP) (Rubin CS, 1994; Gray et al., 1998). The specific anchoring molecule in skeletal muscle is AKAP15, a 15 kD protein that binds to the regulatory subunit of PKA (Fig. 9) (Gray et al., 1997). This close proximity

makes the cAMP-dependent protein kinase regulation very rapid, with observable effects within 50 ms (Johnson et al., 1994; Catterall, 2000).

In cultured skeletal muscle cells, repetitive depolarization causes a dramatic enhancement of Ca^{2+} currents (Fleig and Penner, 1996) in the critical membrane potential range near to -20 mV. This potentiation is strongly voltage dependent and also is dependent on the cAMP - PKA cascade (Sculptoreanu et al., 1993). This may result from interaction between voltage-dependent gating and phosphorylation of the Ca^{2+} channel itself (Catterall, 2000). This mechanism may greatly increase Ca^{2+} channel activity during tetanic stimulation and may play a critical role in regulation of contractile force of skeletal muscle in response to adrenaline and to the frequency of stimulation of the motor nerve (Sculptoreanu et al., 1993) . Also, Arreola et al. (1987) showed an increase of L-type I_{Ca} in adrenaline in response to low frequency stimulations.

1.2.4 Role of RyR channels

When DHPRs in the T tubular membrane activate the Ca^{2+} release channels of the SR membrane (RyR channels), these channels open and Ca^{2+} will be released into the sarcoplasm. Ca^{2+} release channels in the SR membrane were named after the plant alkaloid called ryanodine. Ryanodine has a potent paralytic action on skeletal muscle. It was shown to inhibit SR Ca^{2+} release by binding with high affinity to a protein present in the SR membrane (Fleischer et al., 1985). Incorporating heavy SR proteins into planar lipid bilayer, Smith et al. (Smith et al., 1985) reported single channel recordings of Ca^{2+} release channels. Based on their results, Meissner and co-workers (Meissner et al., 1986) suggested that heavy SR vesicles indeed contain Ca^{2+} release channels.

The RyR channel consists of four polypeptide subunits of 560 kDa, normally arranged in a homo-tetrametric structure, which contains a carboxyl (C) – terminal transmembrane domain, and a large amino (N) – terminal cytoplasmic domain, the foot region (Block et al., 1988; Bhat et al., 1997).

In amphibian skeletal muscle, there are two isoforms of ryanodine receptor channels present: α-RyR and β-RyR (these isoforms are homologous with the mammalian RyR1 and RyR3). Using freeze-fracture method, α-RyR isoforms were localized in the junctional region, and β-RyR isoforms were localized at the parajunctional region of the terminal cisternae (Felder and Franzini-Armstrong, 2002). By examining micrographs from frog sartorius muscle, Franzini-Armstrong (1970) showed small projections of the SR membrane whose tips were joined to the T system membrane by some amorphous material. She called these projections and the amorphous material SR feet. It has been proposed that these feet portions of RyR channels are in mechanical contact with DHPRs (Franzini-Armstrong, 1970) and as noted above, the latter serves as voltage sensor for these coupled RyRs (Schneider and Chandler, 1973). Bianchi and Bolton (1966) first proposed then supported by Ford and Podolsky (1968) and Endo et al. (1968) that Ca^{2+} itself can actually trigger Ca^{2+} release from the SR in frog skeletal muscle. Later, Fabiato (Fabiato, 1983) observed in cardiac muscle that cardiac RyR2 isoforms can be activated by the local rise (to $1 - 10$ μM) of myoplasmic calcium, a phenomenon termed Ca^{2+}-induced Ca^{2+} release (CICR). Rios and Pizarro proposed that in amphibians, via their voltage sensors, the depolarization-induced Ca^{2+} release from α-RyRs activates nearby β-RyRs through Ca^{2+} -induced Ca^{2+} release (Rios and Pizarro, 1988; Rios and Pizarro, 1991). According to this idea, calcium for CICR in skeletal muscle (in opposed to in

21

cardiac muscle where the source of calcium is extracellular as well) comes from the SR through the junctionally located α-RyR.

Besides the alkaloid ryanodine and calcium, RyR channels can be modulated with other substances. Ogawa and Ebashi (Ogawa and Ebashi, 1976) showed an increase of Ca^{2+} release from the SR in the presence of ATP on fragmented bullfrog SR. Smith et al. (1989) using radioisotope efflux measurements also in fragmented SR vesicles observed that Mg^{2+} in millimolar range blocked calcium release. In lipid bilayers, they demonstrated that calmodulin inhibits RyR channel by reducing the mean duration of channel opening, without having an effect on single-channel conductance (Smith et al., 1989).

Analysis of the RyR protein sequence in skeletal muscle revealed that it contains phosphorylation sites (Suko et al., 1993) and that protein kinase A in fact phosphorylates RyR1 channels (Reiken et al., 2003). Jayaraman et al. (1992) found that in lipid bilayers FK506 binding protein (FKBP12) co-purifies with the RYR1. By co-expressing RyR and FKBP12 in insect cells, Brillantes and coworkers (1994) demonstrated that FKBP12 modulates channel gating by increasing channels with full conductance levels, decreasing open probability (P_o) after caffeine activation, and increasing mean open time. Marx et al., 1998, found, that in lipid bilayers, addition of FKBP12 to RYR1 induced a process, they termed as coupled gating. They hypothesized that coupled gating provides a mechanism by which RyR1 channels that are not associated with voltage-dependent Ca^{2+} channels can be regulated (Marx et al., 1998). The hypothesis suggests that the binding of four FKBP12 molecules stabilizes a conformation of the RyR that favors channel opening to the maximum conductance (Ahern et al., 1997).

22

Further investigating in skeletal muscle of dogs with heart failure (HF), Marks and

coworkers (Reiken et al., 2003) found that long term sympathetic over-stimulation (e.g.

stress that caused heart failure in their experimental animals) resulted in weakened

skeletal muscle contractions. In microsomes, they identified PKA phosphorylation sites

on RYR1 at Ser^{2843}, and that phosphorylation causes the dissociation of FKBP12 from

RyR1. Dissociation of FKBP12 increases P_o of the channel (Brillantes et al., 1994;

Gaburjakova et al., 2001), increases its Ca^{2+} sensitivity (Ahern et al., 1997), and in

addition, inhibits coupled gating (Marx et al., 1998). They suggested that skeletal muscle

contractions in HF animals become weaker because their RyR1 channels with the

released FKBP12 by PKA phosphorylation becomes "leaky" causing decrease in SR

$[Ca^{2+}]$ (Reiken et al., 2003). However, this idea was not supported with the more

physiological skinned (EDL) and intact (FDL) preparations of rat and mouse muscle

(Blazev et al., 2001). These researchers did not measure any noticeable effect of 1-3 μM

PKA inhibitor H-89 on action potential-mediated Ca^{2+} transients.

Taken together, there are contradicting evidences of whether or not phosphorylation

can cause "leaky" SR at rest.

1.2.5 Role of SERCA1 Pump

In order to produce movements, skeletal muscle has to be able to both rapidly contract

and relax. During relaxation, elevated $[Ca^{2+}]_{myo}$ has to decrease. In skeletal muscle, this

occurs by the SR by the Sarco-Endoplamic Reticulum Calcium ATP-ase (SERCA).

Sarco-Endoplasmic Reticulum Calcium ATP-ase is located in the membrane of SR in

skeletal muscle. This protein has a total of seven known isoforms which show great

variability in sequence and tissue expression (Andersen JP and B., 1998). SERCA1a is expressed exclusively in adult skeletal muscle, whereas the SERCA1b variant is found in the same fibers in the fetus only (Brandl et al., 1987). SERCA2a is expressed in both cardiac and slow twitch skeletal muscles and its function is similar to that of SERCA1a in fast twitch muscle. (Brandl et al., 1987), SERCA2b is a housekeeping protein involved in basal $[Ca^{2+}]_{myo}$ regulation in β-cells of the pancreas (Armstrong et al., 1972; Carafoli, 2000; Arredouani et al., 2002). The expression of SERCA3 is mostly restricted to some tissues like pancreatic β-cells (Andersen JP and B., 1998; Arredouani et al., 2002), and is weakly expressed in muscle (Carafoli, 2000).

The SERCA pump is a protein with a hydrophobic region located in the lipid bilayer, and a hydrophilic region reaching into the cytoplasm (Fig. 11) (Herbette et al., 1977). The hydrophobic region has ten transmembrane segments (M1-M10) (MacLennan et al., 1985), these segments form a cavity that has high affinity for Ca^{2+} and which is responsible for the translocation of the calcium ion (MacLennan et al., 1997).

The SERCA1a is the predominant form of the pump in fast twitch skeletal muscle (Brandl et al., 1987) Its major function is to control cytosolic Ca^{2+} concentration (Arredouani, 2004). Its Michaelis constant for calcium ($K_m = 0.4$ μM) makes this protein ideal to efficiently respond to elevated $[Ca^{2+}]_{myo}$ after Ca^{2+} release from the SR (Lytton et al., 1992), and restore the elevated myoplasmic calcium concentration to resting levels, around 0.1 μM.
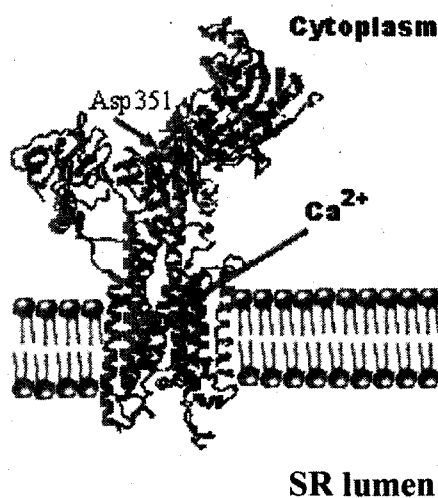
Fig. 11 Structure and predicted topology of the SERCA
Ca^{2+} indicates the high affinity transmembrane segments (M4, M5, M6, M8) which form a cavity for calcium translocation. ASP 351 is located on the long loop connecting the cytosolic hydrophilic and the hydrophobic region in the bilayer and involved in the hydrolysis of ATP (Arredouani, 2004).

The SERCA1 pump co-purifies with sarcolipin (SLN), a 31 amino acid protein (Odermatt et al., 1998). SLN decreases Ca^{2+} affinity of SERCA1, but increases its maximal uptake rate (Fig. 12). As Fig. 12 shows, when present at low $[Ca^{2+}]_{myo}$, SLN inhibits Ca^{2+} uptake but at high $[Ca^{2+}]_{myo}$ it has a stimulatory effect on uptake rates of the pump (Odermatt et al., 1998).

As opposed to phospholamban (PLB), a cardiac muscle SERCA2 regulator which can be phosphorylated during β-adrenergic stimulation which leads to an increase in SERCA2 activity (Slack et al., 1997), SLN does not appear to be modulated by phosphorylation (Odermatt et al., 1998). Another modulator, calmodulin kinase (CaMK) can directly phosphorylate SERCA2 (Toyofuku et al., 1994), but has no effect on SERCA1 since the latter isoform does not have the Serine 38, the phosphorylation site for CaMK (Dode et al., 1996).

25

200

o SERCA1
● SERCA1 + Ra-SLN

Ca^{2+} uptake (% of V_{max} of SERCA1 control)

150

100

50

0

8.0   7.5   7.0   6.5   6.0   5.5   5.0

pCa
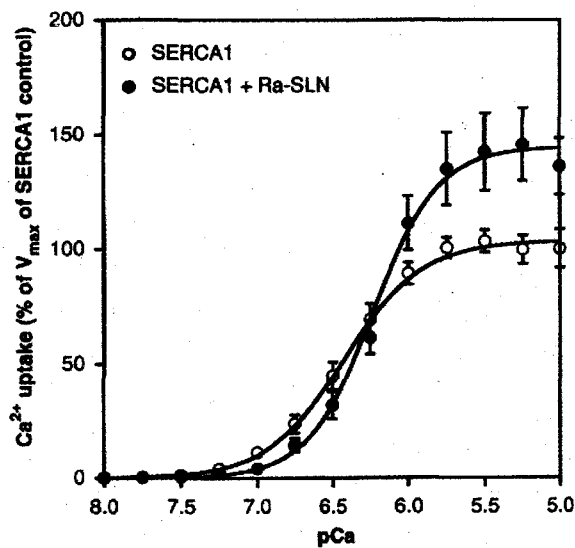
Fig. 12 Effects of SLN on Ca^{2+} uptake activity by SERCA1
SLN decreases apparent Ca^{2+} affinity, thereby lowering Ca^{2+} uptake rates at low Ca^{2+} concentrations, but, at saturating Ca^{2+} concentrations, V_{max} is stimulated. (Odermatt et al., 1998).

The lack of phosphorylation by CaMK (Dode et al., 1996), or through the cAMP-PKA pathway (Odermatt et al., 1998) on SLN-SERCA1 complex, distinguishes clearly the response of skeletal muscle from that of cardiac muscle during adrenergic stimulation. However, the phosphorylation of an unknown Ca^{2+} channel inhibitor or an alternate, unknown enhancing effect of adrenergic stimulation via the increased [Ca^{2+}]$_{myo}$ can not be ruled out (see Discussion).

1.3 Effects of adrenergic stimulation on excitation-contraction coupling

The effects of different adrenergic agonists on EC coupling have been extensively studied (for review: Tasken and Aandahl, 2004). It has been shown that adrenergic stimulation

increases force potentiation (Gonzalez-Serratos et al., 1981; Arreola et al., 1987; Cairns SP, 1993; Sculptoreanu et al., 1993), peak tension, and sustained tension (Huerta, 1991) in frog skeletal muscle. When the muscle is incubated in ISO, it develops a greater force during contractions (Gonzalez-Serratos et al., 1981; Arreola et al., 1987). Studies with skinned skeletal muscle fibers revealed, that as opposed to cardiac cells, adrenergic stimulation has no effect on the contractile mechanism of skeletal muscle (Rubio et al., 1975; Fabiato A, 1978). Adrenaline's positive inotropic effects on frog skeletal muscle as proposed by Gonzales et al. (1981), may be caused by 1.) increased surface Ca^{2+} influx (Schmid et al., 1985; Huerta, 1991), 2.) decreased surface Ca^{2+} efflux (Gonzalez-Serratos et al., 1981), 3.) faster recycling of Ca^{2+} within the cell (Gonzalez-Serratos et al., 1981), 4.) enhanced Ca^{2+} release from the SR (Cairns SP, 1993; Ruehr et al., 2003), or 5.) enhanced SERCA1 pump (Gonzalez-Serratos et al., 1981; Rudolf et al., 2006). Since adrenaline does not enhance the contractile mechanism in skeletal muscle (Rubio et al., 1975), these effects may eventually result in a greater Ca^{2+} release from the SR upon stimulation. The next five paragraphs briefly review the main research related to these five effects.

1.3.1 Increased Ca^{2+} influx

In cultured skeletal muscle using $^{45}Ca^{2+}$, Schmid et. al. (1985) showed that isoproterenol (ISO) increased the nitredipine-sensitive L-type $^{45}Ca^{2+}$ influx under depolarizing conditions (K^+ contractions). They also found that the effects of ISO on increased $^{45}Ca^{2+}$ influx was additive to those of depolarization in the absence of ISO (Schmid et al., 1985). Indeed, L-type Ca^{2+} channels can be phosphorylated by PKA (Sculptoreanu et al., 1993;

27

Johnson et al., 1994) and phosphorylation increased Ca^{2+} transport across the sarcolemma again in response to depolarization (Johnson et al., 1994). However, the significance of these channels in the activation of skeletal muscle has been questioned, since blocking of these channels did not diminish the enhancement of contractile force of the intact EDL or soleus muscle (Arreola et al., 1987; Cairns SP, 1993; Reading SA, 2003). It is also noted that this thesis is concerned with possible ISO-induced Ca^{2+} influx in resting fibers (i.e. held at the holding potential).

1.3.2 Decreased surface Ca^{2+} efflux

Curtis (1966) demonstrated Ca^{2+} efflux in resting intact fast-twitch fibers from frog using $^{45}Ca^{2+}$. Thereby, he established the presence of both Ca^{2+} influx and efflux in the resting steady-state condition. Gonzalez-Serratos et al. (1981) hypothesized that one of adrenaline's effects on skeletal muscle is to decrease Ca^{2+} efflux across the plasmalemma. In perfused rat heart, Patten and Clark (1983) showed that adrenergic stimulation increases $[Ca^{2+}]_{myo}$. They speculated that Ca^{2+} efflux was inhibited, and Ca^{2+} influx was probably enhanced by adrenergic mechanisms (Patten and Clark, 1983). In summary, there is no data for or against the idea that adrenergic stimulation can decrease Ca^{2+} efflux.

1.3.3 Faster Ca^{2+} recycling within the cell

Gonzalez-Serratos et al. (1981) also suggested that extra calcium release from the SR which results in faster and stronger contractions may be the result of faster recycling of Ca^{2+} within the cell. Faster recycling of Ca^{2+} is -according to their suggestion- briefer

Ca^{2+} release and/or enhanced rate of pumping Ca^{2+} back to the SR by the SERCA and/or faster recovery from calcium inactivation. In intact skeletal muscle fibers, Rudolf, et al. (2006) monitored the dynamics of $[Ca^{2+}]_{SR}$ in the tibialis anterior muscle of the living mouse during adrenergic simulation while stimulating the muscle through its motor nerve. Their results did not show any difference in the kinetics of release/reuptake in the presence or absence of isoproterenol; however they demonstrated an increased efficacy of the cycle in ISO for motor nerve stimulation (e.g. more Ca^{2+} release and faster reuptake of Ca^{2+} in ISO during the same time period; Rudolf et al., 2006).

1.3.4 Enhanced Ca^{2+} release from the SR

Ruehr et al. (2003) showed that the caffeine-induced Ca^{2+} efflux of RyR1 -expressed in CHO (Chinese hamster ovary) cells- is enhanced by β-adrenergic stimulation via cAMP-PKA phosphorylation. They speculated that PKA phosphorylation of RyR1 channels in skeletal muscle may play a role in muscle contractility. In their study from Marks' laboratory, Wehrens et al. (2005) exposed their specimens to cardiac and respiratory stress for 21 days before examining these long term effects. "Hyperphosphorylation", as they termed this long term effect of adrenergic stimulation, caused cardiac FKBP12.6 to detach from RyR2 and these channels become leaky. They speculated that leakiness causes the drop of resting SR $[Ca^{2+}]$, with this, results in less Ca^{2+} release upon stimulation, and weaker contractions, causing heart failure in their specimens (Wehrens et al., 2005; Andrew M. Bellinger, 2008). They observed that skeletal muscle contractions in these animals are more fatigable, and speculated that this was caused by hyperphosphorylation of skeletal RyR1 channels and lower $[Ca^{2+}]_{SR}$. On the other hand,

Rudolf et al. (2006), using yellow cameleon (D1ER), -a genetically encoded ratiometric fluorescent Ca^{2+} indicator which is expressed in the SR- measured a greater drop in $[Ca^{2+}]_{SR}$ in ISO than in control experiments during single twitches and higher frequency stimulations. In contrast to the speculation above of a drop in the $[Ca^{2+}]_{SR}$, they also estimated a small increase in $[Ca^{2+}]_{SR}$ in ISO. However, their study can be criticized by the fact that their dye has a very high affinity ($K_{d(D1ER)}$ = 60 µM, Palmer et al., 2004). This fact probably prevented them from reliably monitoring the changes in $[Ca^{2+}]_{SR}$ at physiological level (~0.6 mM at rest). Based on their results they suggested that adrenergic stimulation results in a greater Ca^{2+} release from the SR which in turn causes a greater force in muscle contraction.

1.3.5 Enhanced Ca^{2+} uptake into the SR

As described in section 1.2.5, the absence of PLB in fast twitch skeletal muscle makes phosphorylation of SERCA1a less likely (Brillantes et al., 1994; Marx et al., 1998; Gaburjakova et al., 2001; Marx et al., 2001). In studies in vivo and intact preparations Rudolf et al., (2006) experienced that during the same time period more Ca^{2+} is taken up by the SR in fibers stimulated by isoproterenol compared with controls. They suggest that cAMP/PKA may have an indirect effect on SERCA activity, mediated by PKA activation of glycogen metabolism which increases the availability of ATP (Rudolf et al., 2006). This effect may explain a higher Ca^{2+} loading of the SR upon β-adrenergic stimulation.

1.3.6 Other ways to enhance the force of twitch tension by adrenaline

It is important to note that besides increased $[Ca^{2+}]_{SR}$ there are other possibilities for ISO to enhance the force of twitch tension. Adrenergic stimulation can increase the force of twitch tension by modifying SR Ca^{2+} release feedback mechanisms, without actually increasing $[Ca^{2+}]_{SR}$. I will shortly discuss the four most common sites where ISO could influence these mechanisms.

The first-discovered mechanism is calcium inactivation of Ca^{2+} release, a negative feedback mechanism which rapidly inactivates the SR Ca^{2+} release channel. This mechanism was first described by Baylor et al. (1983) and also showed by Schneider and Simon (1988) in voltage clamped intact frog muscle fiber. Jong et al. (1995a) further characterized this mechanism in frog cut fibers

Jong et al. (1995b) also in frog cut skeletal muscle found a positive feedback mechanism of Ca^{2+} release on the kinetics of Iγ, the late component of intramembranous charge movement which is thought to be in close association with Ca^{2+} release from the SR. They suggested that the acceleration of the ON kinetics of Iγ is produced by SR Ca^{2+} release and the accompanying increase in free $[Ca^{2+}]$ that is expected to occur at myoplasmic sites near open RyR channels. They showed maximal effect when $[Ca_T]_{SR}$ neared 300 μM, about a 1/10th of the physiological value.

Pape et al. (1996) found a strong negative feedback mechanism of Ca^{2+} release on Iγ that first slows then essentially shuts down Iγ. This mechanism becomes apparent when the rate of Ca^{2+} release from the SR increases above a certain level.

Pape & Carrier (1998) found Ca-induced Ca^{2+} release (CICR) evidenced by a decrease in release permeabition when $[Ca^{2+}]_{SR}$ decreases from 300 μM to near zero.

31

Results of Fenelon & Pape (2002) with depolarization to -60 mV indicated that activation of neighboring Ca^{2+} release channels are not involved so that Ca^{2+} released from an SR Ca^{2+} release channel increases Ca^{2+} release through an "autoregulatory process". Pape, Fenelon & Carrier (2002) found a CICR mechanism consistent with recruitment of neighboring channels at more depolarized potentials (they studied -45 mV) when $[Ca^{2+}]_{SR}$ is near physiological levels. This mechanism enhances Ca^{2+} release by 7-fold or greater.

If adrenergic stimulation decreased the effect of one or both negative feedback mechanisms or enhanced one or both of the positive feedback processes the resulting greater Ca^{2+} release from the SR would cause a greater twitch tension. Since it appears that the DHPRs and RyRs might be phosphorylated by adrenergic stimulation, it seems likely that one or more of these feedback mechanisms might be affected. These effects could be additive to the increase of $[Ca^{2+}]_{SR}$ showed in this study. They also highlight the need for caution when interpreting the effects of ISO or other agents on the tension response. Namely, a change in Ca^{2+} release associated with ISO stimulation -or some other agent or condition- does not necessarily mean a change in $[Ca^{2+}]_{SR}$ as is often proposed. Also a change in $[Ca^{2+}]_{SR}$ would be not necessarily mean a corresponding change in SR Ca^{2+} release owing to the tight feed back control on Ca^{2+} release.

1.4 Effects of adrenergic stimulation on resting muscle

1.4.1 Adrenergic stimulation appears to enhance SERCA1 activity

The resting level of myoplasmic calcium in skeletal muscle is maintained by two pump

proteins. These are the SERCA1 pump, and the plasmalemmal calcium pump (PMCA1)

(Michalak et al., 1984; Shannon et al., 2000). These pump proteins are the most likely

candidates for this job because they affinities are very close to the resting free calcium

concentration in the sarcoplasm ($K_m = 0.4$ μM, for SERCA1 (Lytton et al., 1992), and K_m

$\approx$ 0.2-1.0 μM for PMCA1 (Balnave and Allen, 1998)). The surface sodium-calcium

exchanger (Na/CaE) is also responsible for restoring the resting levels of myoplasmic

Ca^{2+}, but because of its low affinity for $[Ca^{2+}]_{myo}$ ($K_m = 3\mu$M), its major function is most

likely the removal of Ca^{2+} from the myoplasm at higher than resting concentration, e. g.

during high frequency contractions (Balnave and Allen, 1998).

1.4.2 PMCA is phosphorylated by PKC

Zurini et al. (1984) showed that the Plasma-Membrane Calcium ATP-ase (PMCA)

possesses an autoinhibitory domain. They demonstrated that PMCA pump can be

phosphorylated by PKC in the middle of its calmodulin- (CaM) binding domain. This

phosphorylation completely prevents CaM binding and lowers the affinity for Ca^{2+} of the

the active site (K_d increased from 0.2 μM to one around 30 μM), keeping the pump

essentially inhibited (James et al., 1995). Gonzales-Serratos et al. (1981) speculated that

inhibited Ca^{2+} efflux will cause an increase in $[Ca^{2+}]_{myo}$, and this extra calcium will be removed from the myoplasm by SERCA1 and, as a result, $[Ca^{2+}]_{SR}$ will increase.

Martin et al. (1990) using light microscopic autoradiography on rat soleus and gastrocnemius muscles demonstrated the presence of $\alpha 1$ adrenoreceptors in slow and fast twitch skeletal muscles. Activating $\alpha 1$ receptors with ISO increases [PKC] through the IP3 – DAG pathway (Leeb-Lundberg et al., 1985). It is possible, they speculated that increased PKC level through adrenergic stimulation of $\alpha 1$ receptors (Leeb-Lundberg et al., 1985) autophosphorylates the PMCA pump causing its inhibition (James et al., 1995). This supports the possible mechanism of increasing fiber Ca^{2+} content by delaying Ca^{2+} efflux through the PMCA surface Ca^{2+} pump.

1.4.3 ISO increases myoplasmic pH

Owen (1986) showed a 0.06 pH unit alkalinization in ISO with cultured smooth muscle cells. She proposed that $\alpha 1$ receptor stimulation increases the IP3 level (thereby stimulating surface $Na-H^+$-exchanger (Na/HE)). Also, in frog cut skeletal muscle fibers using EGTA, Pirouzi measured a 0.05 pH unit increase of myoplasmic pH during 10-minute ISO exposure (Pirouzi, 1999).

1.5 Objectives of the study

1.5.1 Goal

Our goal was to determine if adrenergic stimulation -as previously speculated- does indeed increase $[Ca^{2+}]_{SR}$. Also, we wanted to answer the question as to whether such an increase in calcium content can occur in resting fibers (as suggested by the results of Gonzalez-Serratos et al. 1981) or whether it requires stimulation in order to activate voltage-dependent Ca^{2+} channels (as suggested by the results of Arreola et al. 1987).

1.5.2 Working hypothesis

Our working hypothesis was based on early studies with frog fast twitch skeletal muscle that showed catecholamines' positive inotropic effect on twitch tension (Oota and Nagai, 1977; Gonzalez-Serratos et al., 1981; Arreola et al., 1987). Researchers speculated, but never directly measured, that these enhancing effects are due to enhanced SR Ca^{2+} pump and thereby the increased concentration of Ca^{2+} within the SR (Gonzalez-Serratos et al., 1981), or simply the enhanced Ca^{2+} influx into the sarcoplasm from the extracellular space via a Ca^{2+} channel other than L-type (Arreola et al., 1987).

We hypothesized that adrenergic stimulation increases resting $[Ca^{2+}]_{SR}$ by increasing surface Ca^{2+} influx and in addition, it enhances SERCA. Also, we hypothesized that these enhancing effects can occur at rest.

35

1.5.3 Specific objectives

The objective of this thesis was to answer the following questions:

1.) Is $[Ca^{2+}]_{SR}$ increased by ISO?

It was anticipated that the answer for this objective would resolve the contradiction of possible explanations for the observed tension response of Gonzalez-Serratos et al. (1981) and Arreola et al. (1987). The former results were connected with an increase in Ca^{2+} content in the resting state (enhanced tension response with 1st action potential) whereas the latter indicated that the enhanced tension response required multiple action potentials.

2.) Is $[Ca^{2+}]_{SR}$ (in the absence of ISO) influenced by whether or not Ca^{2+} is present in the external solution?

If yes, this would indicate the presence of a significant Ca^{2+} influx at rest. (N.B. that a net-zero surface Ca^{2+} flux can occur with influx balanced by efflux. Eliminating influx by removing external Ca^{2+} would reveal a resting efflux, if present).

3.) With partial reduction of calcium load, is $[Ca^{2+}]_{SR}$ influenced by whether or not Ca^{2+} is present in the external solution?

If a store-operated mechanism –like that revealed by total depletion- is involved in regulating $[Ca^{2+}]_{SR}$ at physiological levels of $[Ca^{2+}]_{SR}$, then a Ca^{2+} influx should be activated with partial depletion. This would be indicated by a greater value of $[Ca^{2+}]_{SR}$ with external Ca^{2+} present.

36

4.) If an increase in $[Ca^{2+}]_{SR}$ by ISO is involved, is the rate of this increase influenced by hyperpolarizing the fiber (from a holding potential of -90 mV to -110 mV)?

In case if ISO increases $[Ca^{2+}]_{SR}$, are voltage-dependent Ca^{2+} channels involved?

5.) Determine whether ISO effects on $[Ca^{2+}]_{SR}$ are reversible or not?

6.) Confirm whether ISO increases myoplasmic pH.

2. MATERIALS AND METHODS

2.1 Isolation and preparation of single muscle fiber obtained from the frog

In this study, we used fast twitch skeletal muscle fibers (semitendinosus) from the hind leg of the American Bullfrog (Rana catesbeiana). Bull frogs were kept at room temperature in partially water filled large terrarium containers and were fed regularly. Bull frogs were killed by decapitation and spinal cord destruction with protocols approved by the Comite d'ethique de l'experimentation animale at the Universite de Sherbrooke (protocol 126-08). Fast twitch semitendinosus and iliofibularis muscles were removed from the hind leg of the frog and then placed in isotonic, 245 mOsm Ringer's solution and kept at -2.2°C until further processing. Muscles were not used after 48 hours.

Semitendinosus or iliofibularis muscles were lightly stretched and pinned in an agar filled Petri dish under Ringer's solution. After securely pinning the muscles, the Ringer's were changed to a high-potassium, calcium-free solution (relaxing solution), which caused a transient contraction of the muscle followed by relaxation. Before isolating muscle fibers, the muscle was left for about 60 minutes until it completely relaxed.

2.2 The double Vaseline gap chamber

With the aid of a dissecting stereo microscope, a cut section of a single fiber was mechanically isolated and, after careful examination to verify visual damage, it was stretched to a sarcomere length of $3.5 - 4.0$ μm and mounted on a double Vaseline-gap chamber (Fig. 13, 14) (Hille and Campbell, 1976; Pape et al., 1995; Pape et al., 2002). The cut ends of the fiber were fixed with delrin clips and the clips were held to the bottom of the end pools with Vaseline, holding the fiber at its stretched length. Vaseline seals provided electrical isolation between the central pool and the two end pools. Two Lucite covers, applied partially over the central and end pools, provided nominally complete isolation of the central and end pool solutions (Irving et al., 1987). Soon after mounting, the membrane of the fiber in the end pools were permeabilized to small molecules and ions by a 2 minute exposure to a detergent (0.01% saponin) dissolved the in internal solution similar to that used for the experiment (Pape et al., 1995). The end pools were then rinsed thoroughly with the same internal solution not containing saponin. The central pool solution was changed to Ringer's solution or 0 Ca 1 EGTA Ringer's solution (for control experiments).

The chamber was then transferred to the experimental apparatus where electrical connections were made between the electrical apparatus and the solutions in the two end pools and in the central pool (Fig. 13, 14) with the use of agar bridges. One of the end pools, denoted by EP1, was used to measure potential (V1) and the other end pool denoted by EP2, was used to inject current (I2). The central pool (CP) was maintained at earth potential by a bath-clamp amplifier. The potential in end pool 1 was maintained at

-90 mV (V1), by passing a small holding current into end pool 2 and collecting it in the central pool. Unless indicated, V1 was always held at -90 mV. V1 was controlled by the command voltage across a 26 MΩ resistor in series with the fiber. Once on the stage of the experimental apparatus, the chamber's temperature was maintained at 14 - 16°C by its contact with a copper block cooled by circulating water from a temperature-regulated water bath (Pape and Carrier, 1998).
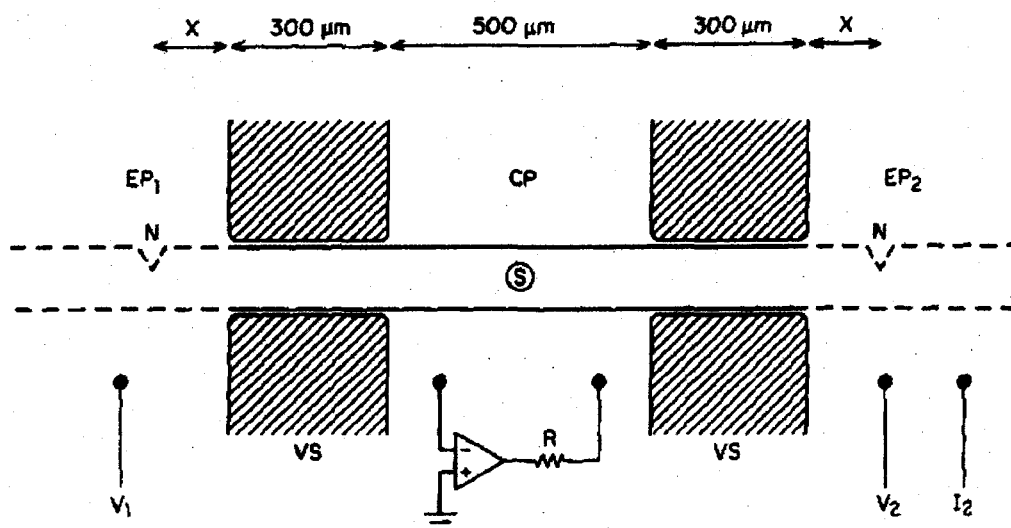
Fig. 13 Double Vaseline gap chamber. The solution that bathes the fiber is separated into three compartments by two ~300μm long Vaseline seals (VS). EP1, the left-hand end pool used for measuring voltage V1, and EP2 the right hand end pool used for passing current I2, as well as monitoring voltage V2. CP denotes the 500 μm long central pool, which was held at earth potential. S denotes the spot also referred to as optical recording site. The dashed lines in both end pools represent the saponin permeabilized fiber segments. The elctrophysiological device is described in section 2.3.
(Figure after Irving et. al, 1987)
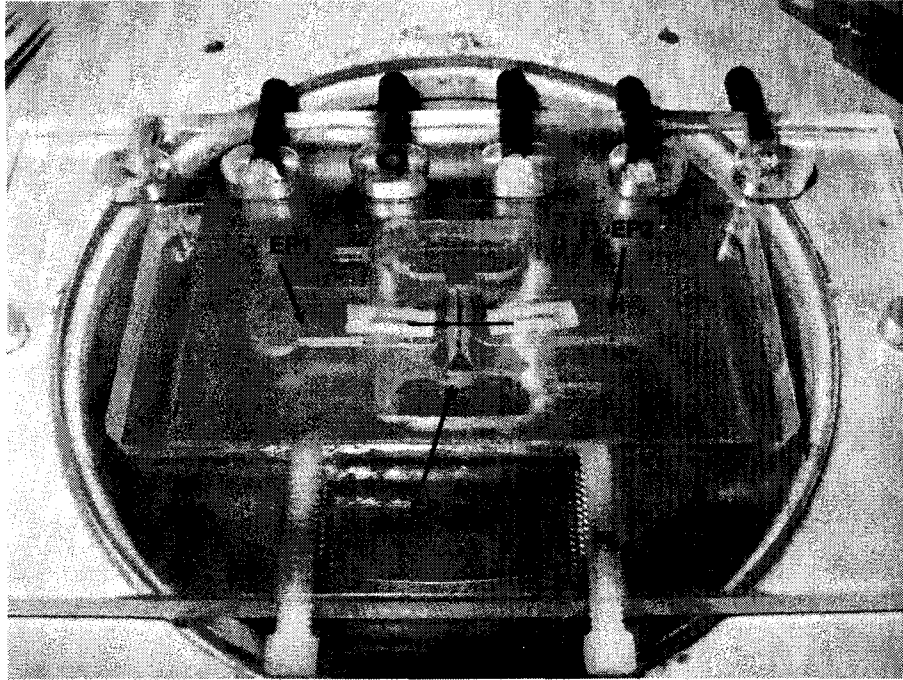
Fig. 14 Photograph of the double Vaseline gap chamber used for the experiments.
The thin black line between the white clips indicates the position of the fiber. The plastic clips are for holding the fiber in place. The clips are in the end pools (EP); the fiber reaches from one end pool into the other across the central pool (CP) (Photo by the author).

2.3 Instruments for data acquisition

During the course of an experiment a maximum of eight signals were monitored: four or six optical signals (0 – 5), and two electrical signals V1 in EP1, and I2, the current injected to the fiber in EP2 to maintain the holding potential. I2 current is the injected current that maintains a steady resting potential of the membrane (denoted I_h). I_h was used to indicate the quality of the Vaseline seals and surface/T system membrane.

41

2.3.1 Current clamp recording

Agar bridges, filled with the appropriate end-pool or central-pool solution, provided electrical connections between the three compartments and five small side pools (one for each electrode of V1, V0, I0, I2, V2) filled with 3 M KCl. These side pools were fitted with Ag/AgCl pellets. These pellets served as electrodes.

Before each experiment, the Ag/AgCl pellets still fitted in the side pools were bathed in 3-6% sodium hypochlorite (NaOCl – bleach) for 15 minutes. This procedure rechloridized the pellets and virtually eliminated the junction potential between the Ag/AgCl pellets and the side pool solution (3 M KCl). At the beginning of each experiment, we measured the voltage between the side pools that were connected to EP1 and CP, with a 3 M KCl agar bridge. In rare cases when the voltage was 1 mV or greater, the 3 M KCl was removed from the side pools and the rechlorization process was repeated. At the end of the experiment the measurement was repeated, so that electrode drift could be assessed. The electrode drift was generally within 1 mV.

Monitored through the left-hand end pool (EP1), fibers were held at their resting potential of -90 mV (V1, Fig. 13, 14). Currents were collected by the bath clamp in the central pool. The electrical apparatus has been described in section 2.3. Briefly, signals were filtered by a four-pole Bessel filter with a switch-selectable amplifier before and after the filter. The signals then were multiplexed and sampled by an A/D converter in an ITC16-MAC computer interface device which was connected to a MAC computer.

Since there was no action potential stimulation during these experiments, the major goal of electrical recording was to maintain the fiber at the resting potential.

2.3.2 Zeiss Axiovert 100 Inverted microscope setup

Optical measurements were performed using a Zeiss Axiovert 100 inverted microscope (Carl Zeiss Inc., Oberkochen, Germany). As Fig 15 shows, the chamber with the cut fiber was placed on the stage of the inverted microscope. When the shutter (S) was opened, the fiber was trans-illuminated by white light from a tungsten-halogen bulb (400 – 1100nm, TH). The light beam was focused on an area of the fiber (see spot S in Fig. 13, and MF) in Fig. 15) by a 20X water immersion condenser (CON) objective (ICS Acroplan Infinity-corrected objective NA 0.4; Carl Zeiss, Inc., Thornwood, NY), and the emerging light was collected by a 32X infinity-corrected (OBJ) objective (NA 0.4; Carl Zeiss Inc.), and passed through two dichroic mirrors and two beam splitters. The first dichroic mirror (505 DRLP) reflects light below 505 nm and transmits longer wavelengths. The reflected shorter wavelengths were sent through a 485(22), 470(30), or 480(30) nm band filter, focused by a lens (L1) on a photodiode (PD1). (Band filters pass light through within a range of wavelengths. For example, the 480(30) filter passes light from 465 to 495 nm). The transmitted light then passed through the second dichroic mirror (505 DRLPXR) which reflects light above 650 nm and transmits the lower wavelengths. The reflected beam passed through a 675(40) or a 690(30) band filter, and then a lens (L2), which focused the light on a photodiode (PD2). Since neither of the dyes used in our experiments absorb light at these wavelengths, this channel was used for monitoring the intrinsic change of the fiber during the experiment. The remaining light that is transmitted through the second dichroic mirror was then split by a 40/60 beam splitter and was sent through a 530(30) and a 555(50) or 560(30) band filters respectively, and picked up by two photodiodes (PD3, PD4 respectively).

Each photodiode was connected to an operational amplifier circuit, which had a 10 MΩ feedback resistor. The V2 and I2 signals passed through separate voltage followers (VF-4, World Precision Instruments, Sarasota, FL), and together with the photodiode signals, passed through separate instrumentation amplifier/filter channels. Each of the signals was filtered by a four-pole Bessel filter (824L8L-4; Frequency Devices Inc., Haverhill, MA) with its cutoff frequency set to 1 kHz. Separate switch-selectable amplifiers were placed before (gain of 1, 10, or 100) and after (gain of 1, 2, 5, or 10) the filter in each channel. The signals were multiplexed and sampled by a nominal 16-bit A/D converter in an ITC16-MAC computer interface device (Instrutech Corp., Great Neck, NY), which was connected to a Power Macintosh 7100 computer. D/A ports of the interface were also used to control the shutter and the voltage command. Stimulation and sampling protocols written in C were downloaded into the ITC-16 MAC interface, which then controlled the data acquisition during the experiment.

2.3.2.1 Calibration of the setup

This section describes how the effective extinction coefficients (ε) were determined on our setup.

The interference filters used in the experiments were calibrated for their extinction coefficients with TMX and CaTMX solutions in the above described Zeiss Axiovert 100 setup. The solutions we used for the calibration protocol were "Blank" with 150 mM KCl, 2 mM $MgCl_2$, 10 PIPES, pH 7.0; "0" solution with 2 mM TMX added to "Blank"; and "1" with 10 mM $CaCl_2$ added to the 2 mM "TMX" solution.

PM HF L TH SM

S

MF

OBJ

PD1 PD2 PD3

L1 L2 L3
F1 F2 F3

L4

PM PD4

40/60 F4

505DRLP 505DRLPXR
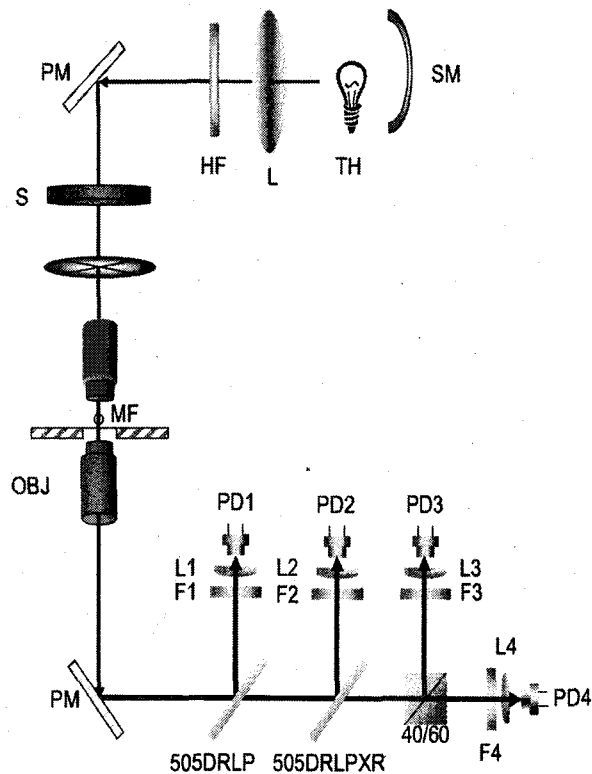
Fig. 15 Schematic diagram of Zeiss Axiovert 100 optical apparatus
The apparatus simultaneously measures four wavelengths (PD1 – PD4). SM, spherical mirror; TH 100W tungsten halogen lamp powered by a regulated constant-current power supply; L, collecting lens; HF, heat filter; PM, plane mirror; S, computer controlled shutter; FD, field diaphragm; CON, water immersion condenser objective; MF, fiber in the experimental chamber with glass coverslip bottom; OBJ, objective, L1 – L4 lenses focusing light onto the photodiodes PD1 – PD4; F1 – F4, bandwidth filters; 40/60 beam splitter; 505DRLP, dichroic mirror reflecting wavelengths from 449 nm - 515 nm, transmitting light with wavelengths below and above the transmitting range; 505 DRLXPR; dichroic mirror transmitting light between 530 and 670 nm, reflecting light with wavelengths below and above the transmitting range (see more details in text). Position of filters: PD1 480(30) nm, PD2 675(40) or 690(30) nm, PD3: 530(30) nm, PD4: 555(50) or 560(30) nm.

Light intensities at each wavelength ($I(\lambda)$) were recorded in "Blank", "0", and "1" solutions. From these data we calculated the absorbance ($A(\lambda)$) of the interference filters in TMX and CaTMX as follows:

$$A_0(\lambda) = \log \frac{I_{Blank}(\lambda)}{I_0(\lambda)} \tag{2.1}$$

$$A_1(\lambda) = \log \frac{I(\lambda)_{Blank}}{I_1(\lambda)}. \tag{2.2}$$

Beer's law is given by

$$A = \varepsilon * \ell * c \tag{2.3}$$

where A: absorbance, ε: extinction coefficients, l: path length of the light across the fluid, c: concentration of the dye. Combining the Beer's equation for two filters, λ and 520 gives:

$$\frac{A_0(\lambda)}{A(520)} = \frac{\varepsilon_{TMX}(\lambda) * \ell * c}{\varepsilon(520) * \ell * c}. \tag{2.4}$$

46

Since the path length (l) and dye concentration (c) are the same, they cancel, and by rearranging:

$$\varepsilon(\lambda)_{TMX} = \frac{A_0(\lambda) * \varepsilon(520)}{A(520)}$$ (2.5)

which gives the extinction coefficient in TMX of the filter of (λ) wavelength.

520 nm is the isosbestic wavelength of TMX solution. At the isosbestic wavelength the absorbance of the calcium-free and calcium-bonded forms of TMX are the same (see Fig. 16, where the two spectra intersect). The extinction coefficient at this wavelength is 15,800 $M^{-1}cm^{-1}$(Maylie et al., 1987).

In cases when Ca^{2+} is added to the solution, concentrations in eqn. 2.4 won't cancel since different TMX species in different concentrations are present: free TMX ([TMX]), and TMX with Ca^{2+} bound to it ([CaTMX]). This corresponding equation is:

$$\frac{A_1(\lambda)}{A(520)} = \frac{\varepsilon_{CaTMX}(\lambda) * l * [CaTMX]}{\varepsilon(520) * l * [TMX]_T} + \frac{\varepsilon_{TMX}(\lambda) * l * [TMX]}{\varepsilon(520) * l * [TMX]_T}.$$ (2.6)

The extinction coefficient at wavelength λ in CaTMX calculated by the following steps:

$$R_1 \equiv \frac{A_1(\lambda)}{A(520)}$$ (2.7)

from eqn 2.6, and

$$R_0 \equiv \frac{A_0(\lambda)}{A(520)} = \frac{\varepsilon_{TMX}(\lambda)}{\varepsilon(520)}$$ (2.8)

from eqn (2.4), and

$$f \equiv \frac{[CaTMX]}{[TMX]_T};$$ (2.9)

then substituting eqns. 2.7, 2.8, 2.9 into eqn. 2.6, and rearranging:

$$R_1 = R_0 * (1-f) + \frac{\varepsilon_{CaTMX}(\lambda)}{\varepsilon(520)} * f$$ (2.10)

and by rearranging,

$$\varepsilon_{CaTMX}(\lambda) = \frac{(R_1 - R_0(1-f)) * \varepsilon(520)}{f}.$$ (2.11)

The concentrations of total TMX and TMX with calcium ([TMX]$_T$ and [CaTMX], respectively) are needed for obtaining their ratio (f) in order to solve eqn. 2.11. The concentrations of these TMX species were determined by fitting (using the least squares fit method) the absorbance spectrum of CaTMX solution done on spectrophotometer.

Fig. 16 shows a TMX-CaTMX spectrum which was used for the fitting process. The isosbestic wavelength is at 520 nm, where the two spectra intersect. Absorbance values are normalized to the absorbance at the isosbestic wavelength (520 nm). The spectrum

48

was plotted by using absorbance data measured in every 5 nm in the range of 400 – 700

nm on the spectrophotometer.
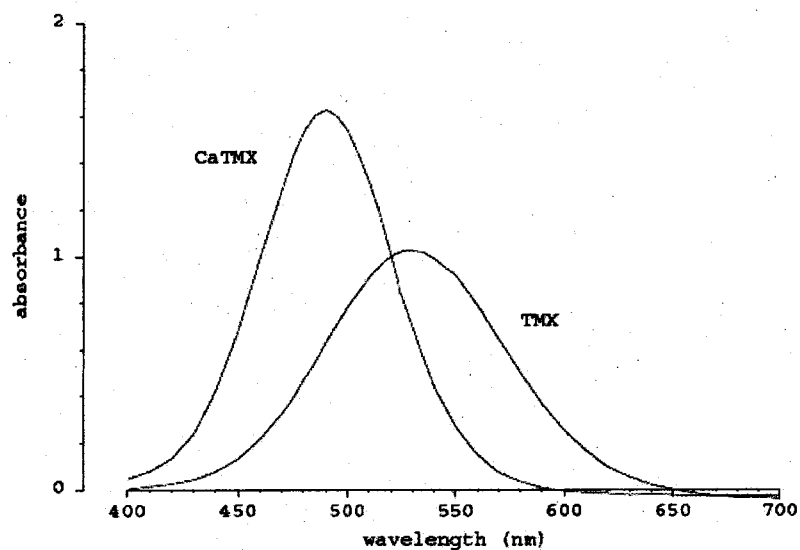
Fig. 16 TMX absorbance spectra.
CaTMX: TMX with calcium, TMX calcium free TMX. Absorbance values are corrected for ∞Ca and
normalized to the isosbestic absorbance, which is at 520 nm, where the two spectra intersect.. Exp: 9 mars
2001.

For the calibration on the setup, the 520(10) filter was assumed (and verified) to be

isosbestic. Its extinction coefficient was assumed to be 15,800 $M^{-1}cm^{-1}$, the value

determined from spectrophotometer measurements for the isosbestic wavelength of 520

nm (Maylie et.al., 1987a).. Absorbances with the 520(10) filter thereby served as

references for the other filters (see eqn's 2.7 and 2.8 to give R_1 and R_0, respectively).

(

49

The first column in Table 2.1 shows the bandwidth filters calibrated on the setup. The second and third columns show the calculated effective extinction coefficients, specific to the setup.

Filters (λ)	εTMX	εCaTMX
nm	$M^{-1} cm^{-1}$	$M^{-1} cm^{-1}$
(1)	(2)	(3
480(30)	7931	26711
485(22)	8071	27439
520(10)	15800	15800
530(30)	15419	10437
555(50)	11683	3324
560(10)	12495	2955
570(30)	10110	2406
675(40)	0	0

Table 2.1 Extinction coefficients of the different interference filters used in the experiments
Data from filter calibration experiments: 319071, 319073. Column 1 shows the wavelengths monitored during the calibration, columns 2, 3 indicate the extinction coefficients calculated with eqns 2.1 – 2.11. $[Ca]_T$=6.7 mM, $[TMX]_T$=2.21 mM, [CaTMX]=1.47, fCa=0.6674, $[Ca^{2+}]$=5.22 mM,

Calculations shown in APPENDIX – C show how information about the concentrations of Ca-bound and Ca-free TMX ([CaTMX] and [TMX], respectively) is derived from the measurement-derived A_{TMX} signals during an experiment using the least-squares method and the value for the extinction coefficients determined above.

2.4 Method for estimating $[Ca^{2+}]_{SR}$ with TMX

2.4.1 TMX is a reliable calcium indicator in the SR

This section explains the advantages of using TMX as calcium indicator in the SR of resting muscle. 1.) TMX has a finite but slow rate of permeability through membranes so

that it is sequestered in the SR. 2.) The K_d value of TMX of 2.6 mM is significantly greater than $[Ca^{2+}]_{SR}$ (~1 mM) so that saturation is avoided thus TMX is responsive to changes in $[Ca^{2+}]_{SR}$. On the other hand, K_d of TMX is not so great, that [CaTMX] is reduced to an extent that it becomes difficult to measure. 3.) TMX shows little if any binding to fixed sites in the sarcoplasm (Maylie et al., 1987), also results of Pape et al. (2007) indicate a lack of binding of TMX to fixed sites in the SR. It is noted that almost all dyes do display a large degree of binding to fixed sites 4.) Essentially no CaTMX is present in the myoplasm so that all of the CaTMX signal would be from the SR. The virtually zero $[CaTMX]_{myo}$ is due to the K_d of TMX and the low $[Ca^{2+}]_{myo}$: fCa_{myo}, the fraction of Ca^{2+}-bound TMX in the sarcoplasm = $[Ca^{2+}]_{myo} / ([Ca^{2+}]_{myo} + K_d)$. If $[Ca^{2+}]_{myo}$ is 10^{-4} mM which results the fCa_{myo} to be 4×10^{-5}, which is negligible. Moreover, no Ca^{2+} was present in the internal solution or added to the end pools so that there should be essentially no CaTMX in the sarcoplasm.

TMX, however, does have one disadvantage namely that it freely crosses SR membrane so information about the concentration of TMX in the SR ($[TMX]_{SR}$) is not readily available. One approach to deal with this problem is described in section 2.4.4.

2.4.2 Calculating $A_D(\lambda)$, the dye-related absorbance at different wavelengths

As described in Pape et. al. (2007), intrinsic absorbances were subtracted from raw absorbance (A_{raw}) measurements to yield the dye-related absorbances (A_D).

To calculate A_D at a given wavelength (λ), first A_{raw} was calculated:

$$A_{raw}(\lambda) = \log_{10} \frac{I_{spot\_off}(\lambda)}{I(\lambda)} \qquad (2.12)$$

51

where I is the intensity of the light passing through a rectangular area (spot), focused on the center of the fiber, and I_{spot_off} is the intensity of light when the fiber is moved out of the field.

I_{spot_off} measurements were performed at the beginning and at the end of the experiment and the value of I_{spot_off} for each run were determined by linear interpolation. There was generally little change in light intensity in I_{spot_off} between the beginning and the end of the experiment, so that the error due to the changing light intensity from the lamp was generally small compared to the errors discussed below.

The spot-on corrected absorbance (A_{SOC}) was calculated with the following formula:

$$A_{SOC}(\lambda) = A_{raw}(\lambda) - A_{spot\_on}(\lambda) \tag{2.13}$$

where

$$A_{spot\_on}(\lambda) = \log_{10} \frac{I_{spot\_off}(\lambda)}{I_{no\_dye}(\lambda)} \tag{2.14}$$

$A_{spot\_on}(\lambda)$ is the value of the intrinsic absorbance of the fiber. I_{no_dye} is the light intensity measured just before adding dye to the end pools.

Finally, the dye-related absorbance is calculated by

$$A_D(\lambda) = A_{SOC}(\lambda) - A_{SOC}(\lambda_{long}) \tag{2.15}$$

where $A_{SOC}(\lambda_{long})$ is the spot-on corrected absorbance at long wavelength where the dye does not have detectable absorbance (675(40) nm in the majority of the experiments). (It

is important to note that the I_{spot_off} values in eqns 2.12 and 2.14 are for different times, so they do not necessarily cancel when eqns 2.12 and 2.14 are substituted into eqn 2.15). The method used to obtain A_D (eqn. 2.15), assumes, that any changes in intrinsic absorbance are independent of wavelength. This was verified as shown by Fig. 20 in Results.

2.4.3 Determining fCa during an experiment

In this study, we monitored the absolute values of absorbances of the dye TMX at different wavelengths in order to determine the fraction of TMX complexed with Ca^{2+}, given by fCa:

$$fCa = \frac{[CaTMX]}{[TMX_T]},$$

(2.16)

The following calculation shows how fCa in the following equations was determined during an experiment from the measured absorbances at wavelength λ and at the isosbestic wavelength of 520 nm.

$$A(\lambda) = \varepsilon_{TMX}(\lambda) * l * [TMX] + fCa(\lambda) * l * [CaTMX],$$

(2.17)

$$A(520) = \varepsilon(520) * l * [TMX]_T.$$

(2.18)

The ratio R is calculated by:

$$R = \frac{A(\lambda)}{A(520)} = \frac{\varepsilon_{TMX}(\lambda)}{\varepsilon(520)}(1 - fCa) + \frac{\varepsilon_{CaTMX}}{\varepsilon(520)}fCa \qquad (2.19)$$

and by rearranging,

$$fCa = \frac{\varepsilon(520)\frac{A(\lambda)}{A(520)} - \varepsilon_{TMX}(\lambda)}{\varepsilon_{CaTMX} - \varepsilon_{TMX}(\lambda)}. \qquad (2.20)$$

2.4.4 TMX gives an estimation of total resting SR calcium $[Ca_T]_{SR}$

The first step towards determining $[Ca_T]_{SR}$ was to calculate the fraction of total TMX in a fiber that is complexed with Ca^{2+}, denoted by fCa as described in the previous section (eqn's 2.17 – 2.20).

As the following steps show, fCa gives information about $[Ca^{2+}]_{SR}$ and $[Ca_T]_{SR}$. These steps are illustrated by the following scheme:

$$fCa \rightarrow fCa_{SR} \rightarrow [Ca^{2+}]_{SR} \rightarrow [Ca_T]_{SR}$$
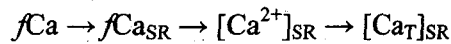
The first step used the relationship between fCa of the whole fiber given by eqn. 2.16, and the fraction of total TMX in the SR complexed with Ca^{2+} (denoted fCa_{SR}), determined by Lamboley and Pape (2008). In their study, cut muscle fibers were equilibrated with TMX and relaxing solution internally and relaxing solution externally. After the dye diffusion period ($\sim$ 60 minutes), optical measurements were performed to determine fCa (Fig. 17, abscissa). 0.01% (v/v) saponin then was added to the central pool to permeabilize the sarcolemma but leave the SR membrane intact. TMX quickly diffused out of the myoplasm across the permeabilized sarcolemma into the central pool,

decreasing it's concentration to virtually zero. Optical measurements were then performed to determine $f\text{Ca}_{SR}$ (left-side ordinate in Fig. 17), plotted as filled circles. The right-side ordinate indicates the free Ca^{2+} in the SR ($[\text{Ca}^{2+}]_{SR}$) obtained by eqn.2.21 using $f\text{Ca}_{SR}$. This gives the relationship between $f\text{Ca}$ and $f\text{Ca}_{SR}$. Once $f\text{Ca}_{SR}$ is determined, the following function was used for calculating $[\text{Ca}^{2+}]_{SR}$:

$$[Ca^{2+}]_{SR} = \frac{fCa_{SR} * K_d}{1 - fCa_{SR}}. \tag{2.21}$$

The curve in Fig 17 is the least squares best fit of eqn B6 in Appendix B to the $f\text{Ca}_{SR}$ vs. $f\text{Ca}$ data. This best fit curve can be used to estimate $[\text{Ca}^{2+}]_{SR}$ from $f\text{Ca}$ for the whole fiber.
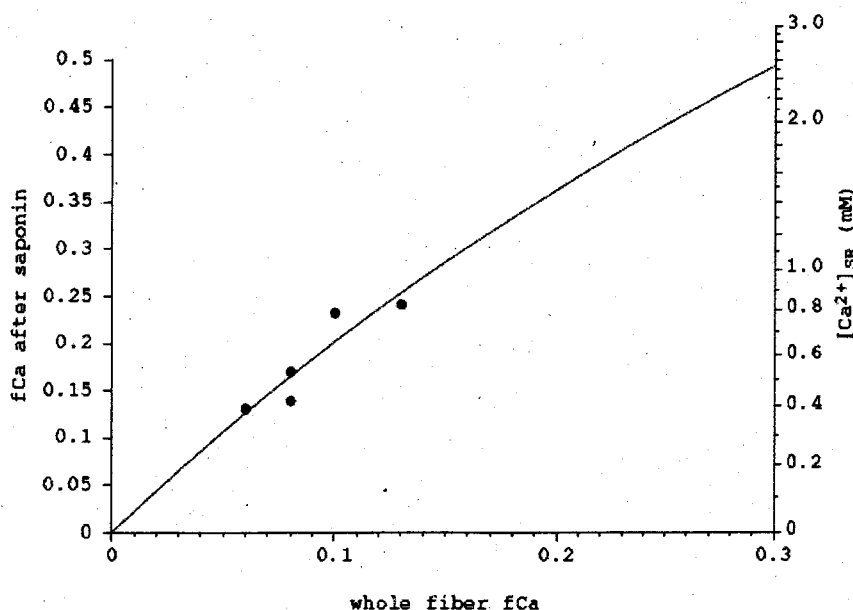
Fig. 17 $[\text{Ca}^{2+}]_{SR}$ **obtained with TMX by calculating** $f\text{Ca}$ **from the whole fiber, vs. that from the SR only**
The abscissa shows $f\text{Ca}$ values measured in the whole fiber. The left-side ordinate shows values from the same fiber after permeabilizing the sarcolemma with saponin. Data points are the results of individual experiments. The curve is the best fit to the measured values. The right-side ordinate shows the corresponding $[\text{Ca}^{2+}]_{SR}$ values (modified after Lamboley and Pape, 2008).

55

Using the value of $[Ca^{2+}]_{SR}$ obtained with eqn. 2.21, f_{CSQ} the fraction of calcium-binding sites occupied by Ca^{2+} on calsequestrin from Pape et al., 2007, defined as follows:

$$f_{CSQ} = \frac{[Ca^{2+}]_{SR}{}^{n}}{[Ca^{2+}]_{SR}{}^{n} + k_{d,CSQ}{}^{n}},$$

(2.22)

where the value of Hill coefficient n = 2.9, $k_{d,CSQ}$, the dissociation coefficient of CSQ for Ca^{2+} is 1 mM.

The next step was to determine the total calcium content of SR ($[Ca_T]_{SR}$). Using the values of $[Ca^{2+}]_{SR}$ and f_{CSQ} (obtained with eqn. 2.21 and 2.23, respectively) and substituting them into eqn. 2.23 below taken from Pape et al. (2007), we can calculate the total calcium content in the SR.

$$[Ca_T]_{SR} = [Ca^{2+}]_{SR} + f_{CSQ} \cdot Q_T + [CaTMX]_{SR}.$$

(2.23)

where Q_T is the concentration of Ca^{2+}-binding sites on calsequestrin referred to SR volume. For more details and explanation of the relationship between fCa, $[Ca^{2+}]_{SR}$ and $[Ca_T]_{SR}$ see Fig. 23 in section 3.4 in Results.

2.5 Solutions used

2.5.1 Relaxing solution

Relaxing solution was used in Petri dish for isolating single fibers, and for mounting the cut fiber into the chamber.

Composition of Relaxing solution (in mM):

Solution	K-glutamate	PIPES	EGTA	$MgSO_4x7H_2O$
Relaxing	120	5	0.1	1.0

The pH of the solution was adjusted to 7.0 with KOH, and the osmolality to 245 mOsm.

2.5.2 Internal Solutions

For the majority of the experiments we used two different internal solutions. In one we used potassium-glutamate internal solution with no calcium added (0.1 EGTA, 0Ca). In experiments where we lowered the calcium content of the fiber, the internal solutions included 20 mM EGTA (20 EGTA, 0Ca):

Composition of internal solutions (in mM):

Solution	K-glutamate	EGTA	$MgSO_4x7H_2O$	MOPS	$Na_2ATPx3H_2O$	K_2-CPx2H$_2$O	K-PEP	Ca(OH)$_2$
K-internal	45	20	6.8	5	5.5	20	5	1.76
0 Ca 20 EGTA	48	20	6.8	5	5.5	20	5	--
0 Ca 0.1 EGTA	76	0.1	6.7	5	5.0	20	5	--

(K-PEP: Potasium Phopho-enol Pyruvate)

The pH was adjusted to 7.0 with KOH and the osmolality to 490 mOsm. The purpose of double osmolality was to be able to add different dyes (TMX or phenol red) to the same batch of solution. Just before the experiment, 2 mM of TMX was added and the osmolality was adjusted to 245 mOsm with water. For the experiments, where the myoplasmic pH was monitored during ISO, 1 mM phenol red was added and the osmolality was adjusted to 245 mOsm with water. For osmolality measurements Fiske osmometer (Fiske Instruments Inc.) was used.

2.5.3 External Solutions

The external solution in the center pool was Ringer's. Depending on the type of the experiment, we used either 0 Ca Ringer's (0 Ca Ringer's), or normal Ringer's (NR).

Composition of the external solutions (in mM):

Solution	NaCl	KCl	Na_2HPO_4	NaH_2PO_4xH2O	CaCl	$MgCl_2$	EGTA-Na
NR	120	2.5	2.15	0.85	1.7	--	--
0 Ca Ringer's	105.5	2.5	2.15	0.85	--	10	1.0

The pH of the external solutions was adjusted to 7.0 with NaOH, and the osmolality to 245 mOsm.

The external solution in the center pool (1.5 ml in volume) was circulated with a speed of 3.2 ml/min using a peristaltic pump (Cole Parmer Masterflex L/S; Cole Parmer

58

Instrument Co., Barrington, IL, USA), exchanging the entire volume approximately 2 times per minute. The temperature of the circulating fluid was maintained at 14 - 16°C, by sending it through a hollow coil of stainless steel tubing, which was bathed in a temperature-regulated water bath directly connected to the temperature regulating system for the chamber. This approach prevents changes in fluid flux and temperature.

2.5.4 External solution change to ISO

After about 60 minutes, -the time necessary for $[TMX]_T$ to approach a leveled value at the optical recording site (see Fig. 21 in Results)- the external solution in the center pool was exchanged to one containing 10 µM isoproterenol (ISO). Five minutes before the solution change, a small amount of 100 mM ISO stock solution was made from isoproterenol-hydrochloride powder (Sigma), and then it was further diluted with external solution to the concentration of 10 µM. During the solution change the pump was switched to exchange mode. There was approximately 20 ml external solution pumped through the central pool until the pump was set back to recycling mode. The time of the exchange period was 6.5 – 7 min.

The following experiment, shown in Fig. 18, was performed to evaluate the time from the addition of the dye to the equilibration in the central pool during solution change. Due to the dead space caused by the length (160 cm) of tubing from the stopcock to the chamber (stainless steel coil and Intramedic Polyethylene Tubing, PE 205, by Becton, Dickinson and Company, Parsippany, NJ), it took 60 seconds after switching the pump to exchange mode (the beginning of the horizontal bar) for the external solution with ISO to

reach the fiber. The dye concentration reached its half maximum in approximately 80 seconds, and the near maximum, equilibrated value was measured in 2 minutes.
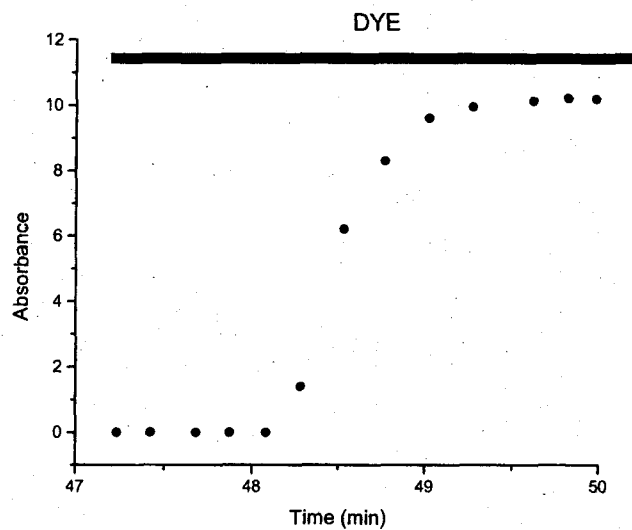
Fig. 18 Time needed for ISO to reach the fiber in the center pool
Calibration of the peristaltic pump. Ringer's solution was used for blank; Ringer's with 2 mM TMX added was the solution denoted as DYE. The pump was switched to exchange position at the beginning of the horizontal bar. DYE reached the fiber in 60 s, reached its half maximum concentration in the central pool in 62 s, and approached its maximum concentration in 107s. Exp: 407081.

2.6 Method for estimating myoplasmic pH with phenol red

The value of pH was determined by the absorbance of phenol red at the optical recording site. Fig. 22 shows the spectrum of phenol red (PR) and its protonated form (HPR). The isosbestic wavelength for phenol red is 480 nm. On the setup, this was monitored with a 480(30) interference filter.

The same dichroic mirror and filter setup of Zeiss Axiovert 100 was used as in the above mentioned experiments with TMX (see chapter 2.3.1, Fig. 15), except that the 555(50) nm filter was replaced with the 560(10) filter. The reason for this replacement is that phenol red is more sensitive to pH at this wavelength, and by using a narrower band filter we could monitor a narrow range close to the peak absorbance of unprotonated phenol red. The 675(40) nm interference filter was used to monitor the intrinsic changes of the fiber since phenol red does not absorb light at this wavelength (Fig. 19).

For determining dye related absorbances for phenol red, we used the same equations as for determining dye related TMX absorbances (eqns (2.14 – 2.15)).
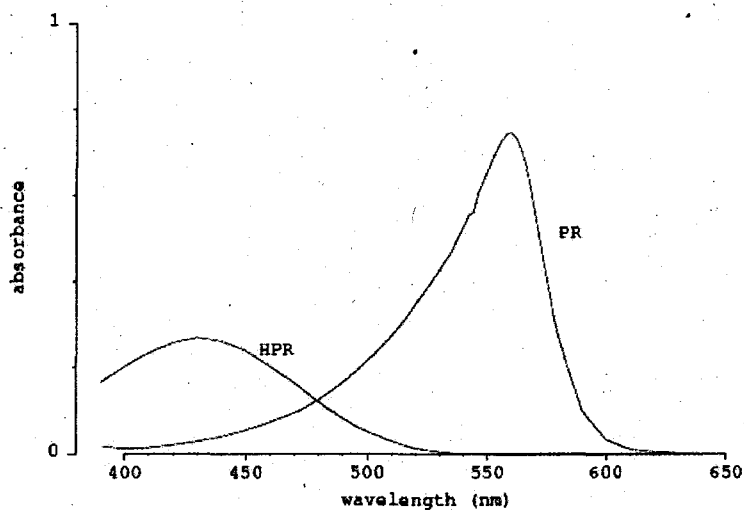
Fig. 19 Phenol red spectrums, protonated (HPR, pH = 6), and unprotonated (PR, pH = 9.5).
The isosbestic wavelength for phenol red is 480 nm, where the two waveforms intersect. This wavelength was used for monitoring phenol red concentration. The peak absorbance of PR spectrum is ~ 560 nm. Exp: Jan. 11, 2005, [HPR] = 13 µM, [PR] = 12.9 µM, in 120 mM KCl and 1 mM MOPS.

The concentration of phenol red at the optical site was estimated with Beer's law (eqn. 2.3) from the value of dye related absorbance of 480(30) (A_{D480}), and the extinction

61

coefficient for phenol red at 480 was taken to be 11,000 $M^{-1}cm^{-1}$ (Lisman and Strong, 1979). The fractional amount of phenol red in the unprotonated form, f, was estimated from

$$f = \frac{r - r_{min}}{r_{max} - r_{min}},$$ (2.24)

where $r = A_{D(560)} / A_{D(480)}$. The values of r_{max} and r_{min} were determined with cuvettes mounted on the setup, their values were 3.21 and 0.0541, respectively (Pape and Carrier, 1998).

The value of pH was calculated then from the expression,

$$pH = pK + \log\frac{f}{1 - f}$$ (2.25)

where the value of pK is 7.7 (Lisman and Strong, 1979).

2.7 Statistical analyses

Student's two-tailed t test and was used to determine the statistical significance of the difference between two sets of results. The difference was considered to be significant if $P < 0.05$.

3. RESULTS

3.1 Intrinsic wavelength dependence

Fig. 20, panel A shows experiments carried out to evaluate whether there is wavelength dependence in the change in intrinsic absorbances during the course of experiments. In this study, the fiber was prepared, mounted, and clamped the same way as it was during a regular experiment, except there was no dye added. Upper traces (A_{Raw}) show the raw absorbances at different wavelengths vs. time after saponin. Raw absorbances were determined by using eqn. 2.12. Lower traces (A_D) show nominal dye-related absorbances from the same experiment. These were determined by eqn. 2.15. During the course of this experiment from 61 – 151 minutes, absorbance changes in the shorter wavelengths were $A_D(480)$ = -0.0080, $A_D(520)$ = -0.0115, $A_D(570)$ = -0.0062. Table 3.1 summarizes the changes in raw absorbances of the different wavelengths between 60 and 150 minutes. Column (a) gives the fiber reference; columns (1 – 4) indicate the changes in absorbance during the above given time period at the wavelengths indicated. The mean values are not significantly different from zero and not significantly different from one another. These data indicate that during the course of an experiment, there is no significant change in absorbance at the monitored wavelengths which would be caused by the change in intrinsic properties of the fiber.

Fig. 20, panel B shows an experiment which evaluates whether the addition of 10 μM ISO causes any systematic offset in intrinsic absorbances (again, as monitored by dye-related absorbance with no dye present). The conditions in this study were the same

A

0.10

0.05

0.00

-0.05

A_D and A_{Raw}

60   80   100   120   140   160

Time after saponin (min)

▲ 480_{Raw}
☆ 570_{Raw}
○ 520_{Raw}
● 690_{Raw}

690_D
$570_D, 480_D$
520_D

B

0.10

0.05

0.00

-0.05

A_D and A_{Raw}

20   40   60   80   100

Time after saponin (min)

▲ 450_{Raw}

570_{Raw}
530_{Raw}

690_{Raw}

450_D
$530_D 570_D$
690_D

ISO
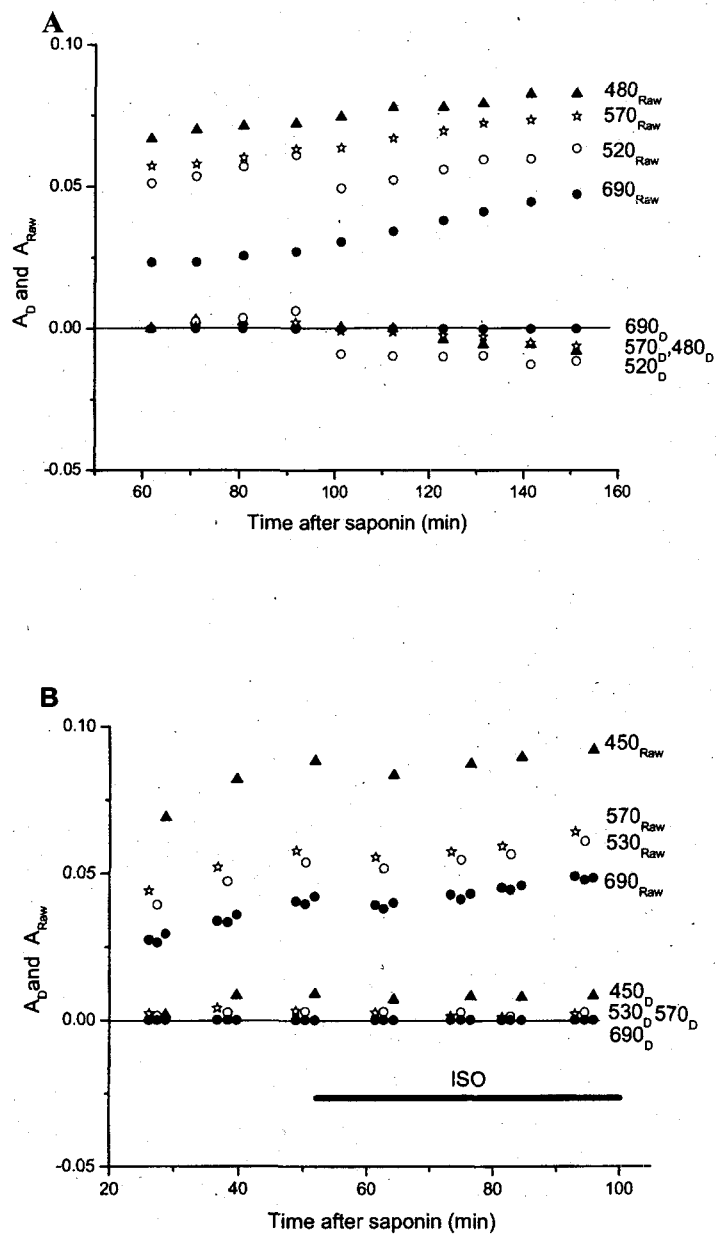
Fig. 20 Raw and intrinsic-corrected absorbances (A_D) in time without adding Dye, with ISO (B) and without ISO (A)

Panel A, B: Upper traces ($A_{Raw}(\lambda)$): absorbances in four wavelengths as calculated by eqn. 2.14. Lower traces ($A_D(\lambda)$): intrinsic corrected absorbances of the same wavelengths (A_D) as calculated by eqn. 2.15. External solution Ringer's, internal solution 0 Ca K-internal.

Panel A: Exp: N14062

Panel B: the horizontal bar indicates the presence of 10 μM ISO in the external solution. Exp: N15062

described above, except that 10 μM ISO was added to the external solution 52 minutes after saponin treatment, indicated by the horizontal bar. Upper traces (A_{Raw}) show the raw absorbances at different wavelengths vs. time after saponin. Raw and dye related absorbances were determined as described in the previous section. Dye related absorbances -before adding ISO, and at 30 minutes in ISO- were $A_D(450)$ = 0.0882 and 0.0896, $A_D(530)$ = 0.0538 and 0.0565, $A_D(570)$ = 0.0577 and 0.0593, respectively. These data do not show a significant ISO related difference in dye related absorbances. Since there is no dye present in these experiments, the non-zero A_D values in both panels are due to errors in the intrinsic correction. As will be seen later, these errors are small, - though not negligible- compared to the TMX-related absorbance values of interest.

A

Exp	$\Delta A_D 480$	$\Delta A_D 520$	$\Delta A_D 570$	$\Delta A_{RAW} 690$
(a)	(1)	(2)	(3)	(4)
N14062	-0.0080	-0.0115	-0.0062	0.0240
N01062	0.0046	0.0051	0.0053	0.0011
110071	-0.0071	-0.0039	-0.0087	-0.0048
109073	-0.0348	-	-0.0213	0.0213
103071	0.0059	-	0.0061	-0.0114
Mean	-0.0079	-0.0034	-0.0050	0.0060
SEM	0.0065	0.0039	0.0045	0.0063

B

Exp	$\Delta A_D 450$	$\Delta A_D 530$	$\Delta A_D 570$	$\Delta A_{RAW} 690$
N15062	0.0014	0.0027	0.0016	0.0063

Table 3.1 Changes in raw absorbance by ISO (B) and without ISO (A) at different wavelengths during the course of experiments
Column (a) gives the fiber reference, columns (1 -3) give the change of dye-related absorbances at the indicated wavelengths and column 4 gives the changes in raw absorbance at 690 nm, between 60 and 160 minutes. The means are not significantly different from zero and from one another.

3.2 Diffusion of TMX in the fiber from the end pools to the optical measuring site

The most accurate measurements with TMX can be achieved when its concentration is equilibrated in the fiber's myoplasm at the optical measuring site. After equilibration, any changes in $[TMX]_T$, $[CaTMX]$ and $[TMX]$ should be due to another controlled variable – in our case- the effect of ISO. The purpose of this experiment was to determine the time necessary for the dye to reach this steady concentration.
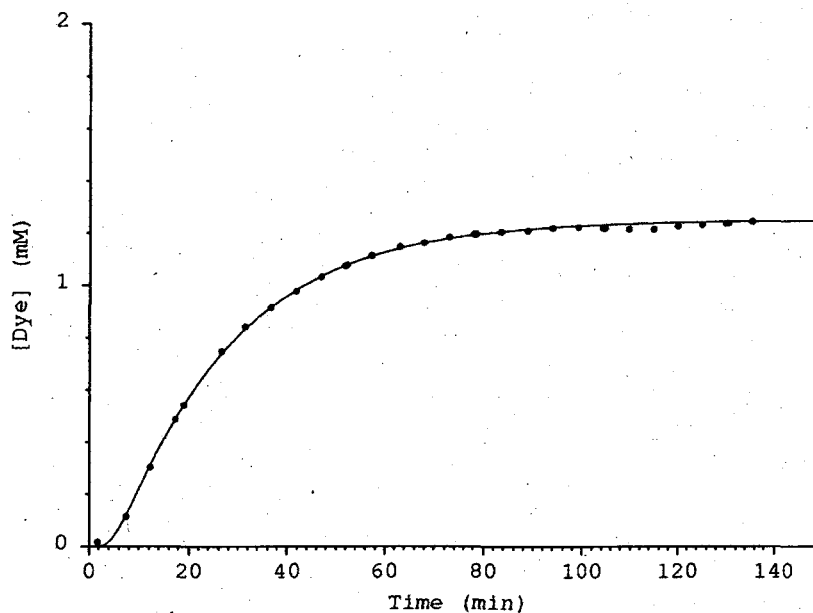
Fig. 21 Dye diffusion curve of TMX in the fiber
Dye was added to the end pools 28 minutes after saponin treatment at t = 0. The curve shows a least square fit of eqn. 6 and 8 in Maylie et. al., 1987a, derived from free diffusion plus linear reversible binding (Maylie et al., 1987a; Maylie et al., 1987b). Total TMX concentration: 1.22 mM, $D_{APP} = 0.871 * 10^{-6}$ cm^2/s, Exp: 331061.

After adding the internal solution containing TMX to the end pools, TMX began to diffuse in the fiber towards the optical recording site in the center of the central pool. Fig. 21 shows an example of the time course of dye concentration at the optical recording site

66

vs. time from the addition of the dye: t = 0. The continuous curve is the least squares fit of eqn. 6 and 8 in Maylie et al., (1987a), derived from free diffusion plus linear reversible binding and/or sequestration from Maylie et al., (1987b). As indicated by the close fit of the curve to the data points, the dye diffusion within the fiber is well described by the one-dimensional diffusion equation used by Maylie et al. (1987a, eqn. 4 and 5). The path length the dye has to travel within the fiber to the optical recording site is approximately 550 μm (300 μm under the seal and 250 μm to the center of the central pool). The equilibration process between the optical site and the end pools takes about 60 minutes (Fig 21).

The multiple effects described with Fig. 22 and 23 are covered in detail in separate sections below. These sections include the increase in fCa by ISO (section 3.3), the evaluation of the involvement of store-operated mechanisms in partially depleted fibers (section 3.4) and the effects of ISO on $[Ca^{2+}]_{SR}$ and $[Ca_T]_{SR}$ (section 3.5).

3.3 There is an ISO-dependent Ca^{2+} influx in the steady resting fiber

To address the problem of whether calcium enters the cell in ISO at rest, two sets of conditions were prepared: one with NR and another with 0 Ca Ringer's as external solution. In both cases, the internal solution contained 0.1 mM EGTA. Fig. 22, panel A and B show individual experiments with these conditions. The horizontal bar indicates the time period when 10 μM ISO was present in the external solution. The points clearly

67

show an increase in *fCa* while in ISO when external calcium was present (Fig 22, panel A), and there is no apparent change in *fCa* in the absence of external Ca^{2+} (panel B). The thin lines in all panels in Fig. 22 are line fits to *fCa* data points in the last 15 minutes before adding ISO and from 15 to 30 minutes in ISO. The slopes of these line fits indicate the rate of change of *fCa* (d*fCa*/dt). The significance of these slopes will be discussed later in this chapter. After the removal of ISO, *fCa* quickly drops and then recovers to about the same rate of rise it had before removing ISO. Analysis and possible explanation of this "dip" in *fCa* and subsequent recovery will be shown in section 3.8.

Table 3.2 summarizes the results from all of the experiments like that in Fig. 22. Blocks A and B show the two pairs of different experimental conditions used: with or without external calcium, respectively. In these experiments the internal solution contained 0.1 mM EGTA -resulting in normal resting $[Ca^{2+}]_{SR}$ (corresponds with Fig. 22, panel A and B). Columns 2 and 3 give the mean values of *fCa* measured 5 minutes before adding ISO and between 28 -30 minutes in ISO, respectively. Column 4 gives the value of the percent increase from before ISO to 28 – 30 min in ISO (% increase from column 2 to 3). The mean value of percent increase is 121% (SEM = 37%, n = 6) in fibers that contained external calcium (Block A). Panel B in Fig. 22 shows results from an experiment where no external calcium was present. There was no apparent change in ISO in this case. Similarly, the mean value of percent increase in Table 3.2 Block B, column 4 indicates no significant increase in *fCa* with no Ca^{2+} in the external solution. These results indicate that ISO causes a net influx of Ca^{2+} into the fiber across the outer surface/T-system membranes.

A. 0.1 mM EGTA, NR

B. 0.1 mM EGTA, 0 Ca
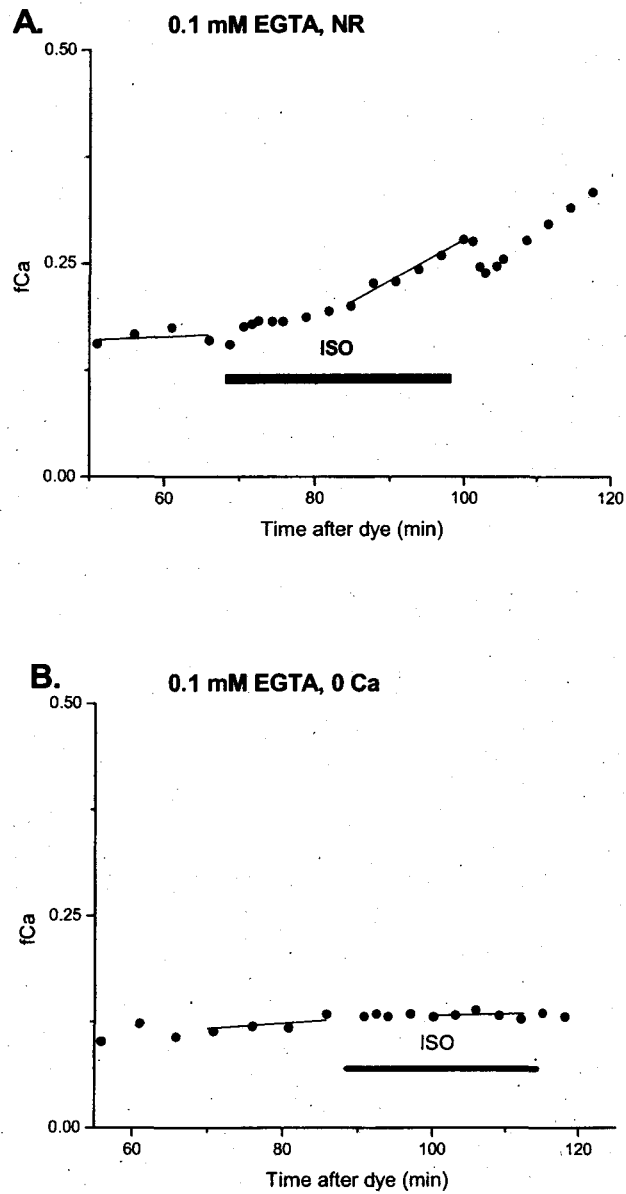
Fig. 22 panel A, B Effects of ISO on fCa in fibers with normal $[Ca^{2+}]_{SR}$ with NR (A) and 0 Ca Ringer's (B) external solutions. The internal solution contained 0.1 mM EGTA and 0 Ca.

The horizontal bar marks the period, when 10 µM ISO was added to the external solution. The thin lines are the least square fits to data points of the last 15 minutes before and in ISO.

A. The external solution is NR, fCa before adding ISO: 0.1600, before removing ISO: 0.2780, Exp: 006061. B. The external solution is 0 Ca Ringer's, fCa before adding ISO: 0.1390, before removing ISO: 0.1380, fractional increase: -0.0072, Exp: 423071.

69

C. **20 mM EGTA, NR**
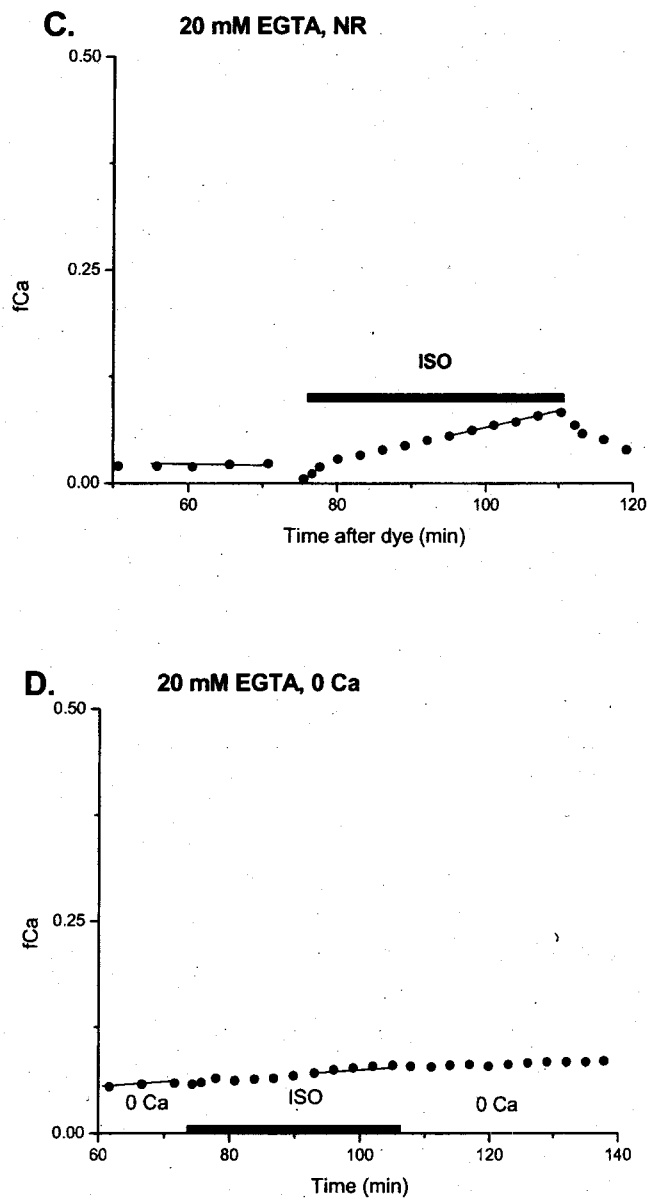
D. **20 mM EGTA, 0 Ca**

Fig. 22 panel C, D Effects of ISO on *fCa* in fibers with depleted [Ca^{2+}]$_{SR}$ with NR (C) and 0 Ca Ringer's (D) external solutions
The internal solution contained 20 mM EGTA and 0 Ca to decrease Ca content to the minimum. The horizontal bar marks the period when the fiber was exposed to ISO. C. the external solution is NR; during the period of ISO *fCa* increased more then three fold, *fCa*, last before adding and last before removing ISO: 0.0230 and 0.0830, respectively, the fractional increase is 2.6087, Exp: 226073. **D.** the external solution is 0 Ca Ringer's; *fCa*, last before adding and last before removing ISO: 0.0590 and 0.0793, respectively, the fractional increase is 0.3446, Exp: D11062.

70

A

0.1 mM EGTA/ NR

Exp (1)	Last Before fCa_{Bef} (2)	End ISO fCa_{End} (3)	%increase % (4)	$dfCa_{Bef}/dt$ min^{-1} (5)	$dfCa_{Iso}/dt$ min^{-1} (6)
O10061	0.0240	0.0960	300.00	0.0001	0.0016
O06061	0.1600	0.2780	73.75	0.0004	0.0048
912061	0.0174	0.0387	122.51	0.0001	0.0011
627061	0.1685	0.3584	112.71	0.0012	0.0064
909051	0.0810	0.1340	65.43	-0.0002	0.0040
913051	0.1050	0.1610	53.33	-0.0012	0.0044
mean	0.0926	0.1777	121.29*	0.0001	0.0037*
SEM	0.0264	0.0486	37.42	0.0003	0.0008

B

0.1 mM EGTA/ 0 Ca Ring.

Exp (1)	Last Before fCa_{Bef} (2)	End ISO fCa_{End} (3)	%increase % (4)	$dfCa_{Bef}/dt$ min^{-1} (5)	$dfCa_{Iso}/dt$ min^{-1} (6)
720062	0.0420	0.0520	23.81	-0.0014	0.0000
O11061	0.1310	0.1910	45.80	0.0005	0.0026
404071	0.1090	0.1260	15.60	-0.0002	0.0010
406071	0.0480	0.0633	31.94	0.0003	0.0006
423071	0.1390	0.1380	-0.72	0.0015	0.0003
mean	0.0938	0.1141	23.29	0.0002	0.0009
SEM	0.0205	0.0256	7.80	0.0005	0.0005

C

20 mM EGTA/ NR

Exp (1)	Last Before fCa_{Bef} (2)	End ISO fCa_{End} (3)	%increase % (4)	$dfCa_{Bef}/dt$ min^{-1} (5)	$dfCa_{Iso}/dt$ min^{-1} (6)
226073	0.0230	0.0830	260.87	-0.0005	0.0018
307071	0.0160	0.1490	831.25	0.0006	0.0042
213071	0.0650	0.1130	73.85	0.0003	0.0047
D19071	0.0130	0.0320	146.15	-0.0002	0.0017
mean	0.0293	0.0943	328.03*	0.0001	0.0031*
SEM	0.0121	0.0248	172.10	0.0003	0.0008

D

20 mM EGTA/ 0 Ca Ring.

Exp (1)	Last Before fCa_{Bef} (2)	End ISO fCa_{End} (3)	%increase % (4)	$dfCa_{Bef}/dt$ min^{-1} (5)	$dfCa_{Iso}/dt$ min^{-1} (6)
226071	0.0140	0.0210	50.00	0.0000	0.0001
D11062	0.0590	0.0793	34.46	0.0002	0.0007
D05062	0.0040	0.0090	125.00	0.0007	0.0006
mean	0.0257	0.0364	69.82	0.0003	0.0005
SEM	0.0120	0.0154	19.76	0.0001	0.0001

Table 3.2 Summary of experiments with normal $[Ca^{2+}]_{SR}$ (Blocks A and B) and depleted $[Ca^{2+}]_{SR}$ (Blocks C and D) with and without external Ca^{2+} (A, C and B, D, respectively).
Column 1 shows individual experiments, columns 2 and 3 show values of fCa measured 5 minutes before adding ISO and between 28 – 30 minutes in ISO, respectively. Column 4 shows the % increase from columns 3 to 4. Columns 5 and 6 show the slope of the line fit on fCa data points 15 minute before and the last 15 minutes in ISO, respectively. (* significantly different, P < 0.05)

Columns 5 and 6 give dfCa/dt, the rate of change of fCa in the last 15 minutes before adding ISO and between 15-30 minutes in ISO, respectively. The values were obtained by fitting a line on the data points of fCa in the time periods indicated above, and shown on individual experiments in Fig. 22, panels A-D. These values will be discussed later.

For easy comparison, the mean values of fCa from Table 3.2, column 2 and 3 are illustrated in Fig. 23, in front row (5 min before ISO) and in back row (30 min in ISO), respectively. The sagittal rows A-D correspond with experiments shown in Table 3.2, rows of means A-D; yellow hue indicates fibers with normal $[Ca^{2+}]_{SR}$ (A, B), blue hue depicts fibers with depleted (C, D) $[Ca^{2+}]_{SR}$. In this section only rows A and B will be discussed. The main thing to note is that there is a significant increase in fCa after ~30 min in ISO when Ca^{2+} was present (row A). This is about a 2-fold increase (121%, Table 3.1, Block A, column 5). These results indicate an ISO-dependent Ca^{2+} influx in the steady resting fiber. This is one of the main experimental findings in this study.

The similar values of means of fCa in Table 3.1, Blocks A and B, column 2 also indicate that, in the absence of ISO, there is no net Ca^{2+} influx across the sarcolemma and no net Ca^{2+} leak from the SR at rest. This similarity is well represented by Fig. 23 sagittal rows A and B in the first row.
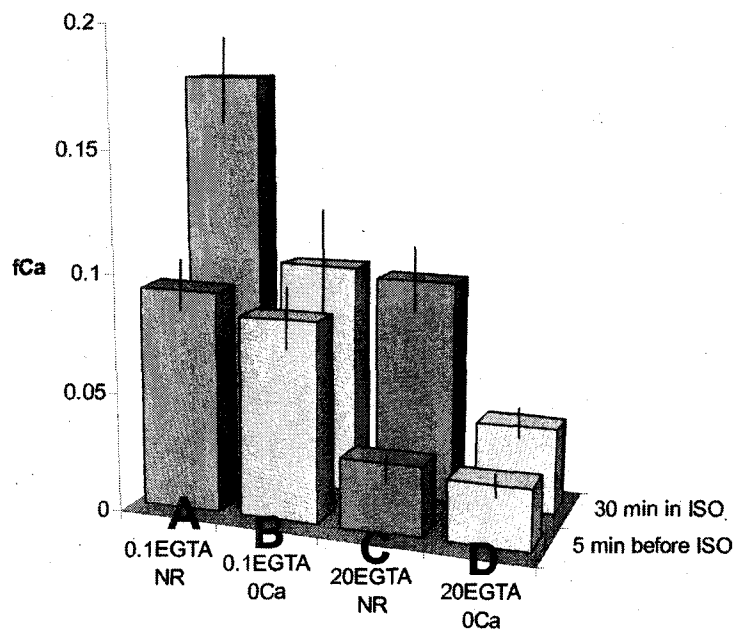
Fig. 23 Means of *f*Ca values in fibers with close to physiological $[Ca^{2+}]_{SR}$ (sagittal rows A, B, yellow hue) and in depleted fibers (sagittal rows C, D, blue hue) The front and second rows represent data taken 5 minute before adding ISO and 28 – 30 min in ISO.

3.4 Store-operated mechanisms are not involved in regulating fiber Ca^{2+} content at about 30% of its physiological $[Ca^{2+}]_{SR}$ level

This section evaluates the involvement of store-operated mechanisms in partially depleted fibers depicted in Fig 22 and 23, panels C, D and sagittal rows C, D, respectively. Also, Table 3.2, Blocks C and D summarize data obtained from individual experiments.

To lower SR calcium content below physiological levels we added 20 mM EGTA to the calcium free internal solution. The presence of 20 mM EGTA in the internal solution decreased *f*Ca values to about 30% of values measured in fibers with 0.1 mM EGTA

(Fig. 23, front row C and D vs. A and B; see also in Table 3.2, Blocks C and D, column 2 vs. A and B, column 2).

The fact that the means of fCa values are similar in both fibers with and without external Ca^{2+} (fCa = 0.0293, 0.0257; SEM = 0.0121, 0.0120; n = 4, 3, respectively; see Table 3.2, Blocks C, D, column 2) indicates that this level of partial depletion does not result in the involvement of store-operated mechanisms. If store- operated mechanisms were stimulated, as one might expect, fCa values should be higher in fibers with external Ca^{2+} present compared to those without external Ca^{2+}.

Data obtained by the analysis of the rate of change of fCa before the addition of ISO (Table 3.2, Blocks C and D, column 5) also indicate the absence of net Ca^{2+} influx in partially depleted fibers ($d f$Ca/dt = 0.0001, 0.0003; SEM = 0.0003, 0.0001; n = 4, 3 with and without external calcium, respectively – $d f$Ca/dt values are not significantly different from zero). If Ca^{2+} influx were present, it would be indicated by slopes that are significantly different from zero (see Table 3.2 Blocks A, B, column 6).

3.5 Effects of ISO on $[Ca^{2+}]_{SR}$ and $[Ca_T]_{SR}$

The effects of ISO on $[Ca^{2+}]_{SR}$ and on $[Ca_T]_{SR}$ determined from the mean values of fCa data from Table 3.2, columns 2 and 3 above. The relationship between fCa and $[Ca^{2+}]_{SR}$ and detailed explanation is shown in Materials and Methods, in section 2.4.4. The relationship between fCa and $[Ca_T]_{SR}$ is determined by eqns 2.20 - 2.23 shown in Materials and Methods (Pape et al., 2007). Fig. 24 depicts this relationship using data

from experiments from this study. The abscissa shows values of fCa, monitored during the experiments. The ordinate shows the corresponding $[Ca_T]_{SR}$ values. The line is the best fit to the values represented by data points. The means of these values are tabulated in Table 3.3, columns 5 and 6. In this Table, column 1 gives experiments with the two different pairs of experimental conditions described in the previous section. Briefly: the first two rows A, B have 0.1 EGTA in the internal solution, the first row (A) has NR, the second (B) has 0 Ca Ringer's in the external solution. The last two rows (C, D) contain 20 mM EGTA in the internal solution, the third row (C) has NR, and the fourth (D) has 0 Ca Ringer's as external solution. Columns 2 and 3 are the means of $[Ca^{2+}]_{SR}$ values before adding ISO and the last value at 28 -30 min in ISO, respectively. These values were calculated by using the method of Pape et al. (2007), and described in the Materials and Methods section (see section 2.4.4). Columns 5 and 6 are the corresponding total
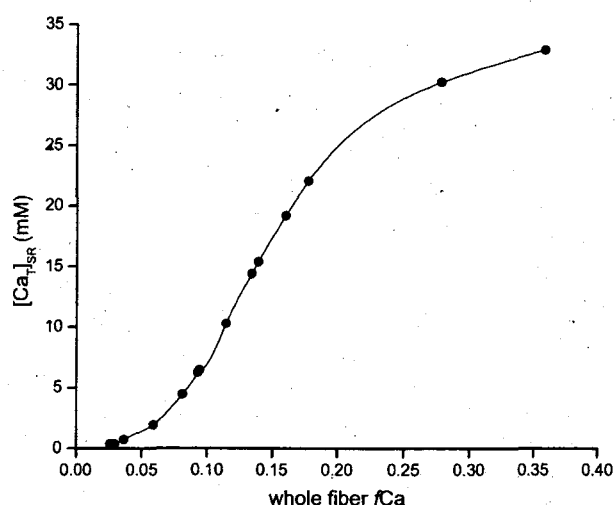
Fig. 24 Relationship between fCa and [CaT]SR.
The lowest values are obtained from fibers depleted from Ca^{2+} with 20 mM EGTA in the internal solution. The highest values obtained from fibers -with 0.1 mM EGTA in the internal solution- at ~30 minutes in ISO.

	[Ca^{2+}]$_{SR}$ Last Before mM	[Ca^{2+}]$_{SR}$ end ISO mM	% increase of [Ca^{2+}]$_{SR}$ %	[Ca$_T$]$_{SR}$ Last Before mM	[Ca$_T$]$_{SR}$ end ISO mM	Δ[Ca$_T$]$_{SR}$ mM	% increase of [Ca$_T$]$_{SR}$ %
(1)	(2)	(3)	(4)	(5)	(6)	(7)	(8)
A 0.1 mM EGTA/ NR (n = 6)	0.6094	1.2936	112.29	6.2265	22.0095	15.78	253.48
B 0.1 mM EGTA/ 0 Ca Ring. (n = 5)	0.6178	0.7695	24.55	6.4171	10.2609	3.84	59.90
C 20 mM EGTA/ NR (n = 4)	0.1787	0.6211	247.52	0.3490	6.4192	6.07	1739.39
D 20 mM EGTA/ 0 Ca Ring. (n = 3)	0.1562	0.2245	43.76	0.3480	0.7396	0.39	112.52

Table 3.3 Means of [Ca^{2+}]$_{SR}$ and [Ca$_T$]$_{SR}$ values and their percent increase in ISO
Each row indicates a specific type of experiment: rows A and B are experiments with 0.1 EGTA in the internal solution; experiment in the first row was done with calcium present (NR) in the external solution; experiments in the second row was for control, with Ca removed from the external solution (0 Ca Ringer's). Row C and D indicate the same type of experiments indicated in the first two rows, except the internal solution contained 20 mM EGTA for decreasing SR calcium.
Columns (2, 3, 4 and 5, 6,) are the means of [Ca^{2+}]$_{SR}$ and [Ca$_T$]$_{SR}$ before adding ISO, the last point in ISO, and the percent increase, respectively.

calcium concentrations in the SR, calculated from the means of [Ca^{2+}]$_{SR}$ in column 3 (Last Before) and column 4 (End ISO). For calculating the [Ca^{2+}]$_{SR}$ values, eqns. B1 – B6 were used (see Appendix – B). Column 4 shows the percent increase of means of [Ca^{2+}]$_{SR}$. For calculations to obtain [Ca$_T$]$_{SR}$, we used eqn 2.23 in Materials and Methods.

One thing to note is that the % increase of [Ca2+]SR was more than two times that of [CaT]SR (253.5% vs. 112.3%). The explanation for this increase lies in the nature of the CSQ binding curve (Fig. 25).
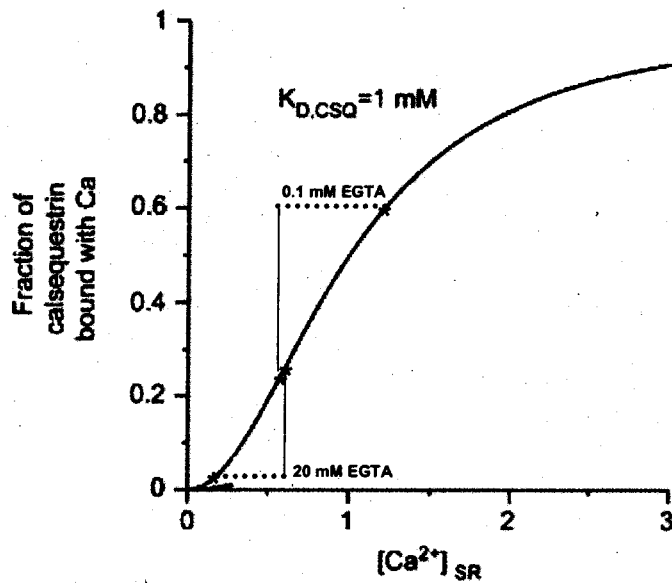
Fig. 25 Ca-calsequestrin binding curve.
The upper dotted horizontal bar marks the range of $[Ca^{2+}]_{SR}$ in normal (containing 0.1 mM EGTA in the internal solution, condition A and B), the lower dotted line in depleted (with 20 mM EGTA, conditions C and D) fibers in this study (normal $[Ca^{2+}]_{SR}$ fibers: 0.6094 mM – 1.2936 mM, depleted: 0.1562 mM – 0.6211 mM; before ISO and at ~30 min. in ISO, respectively). Modified after Fig. 5 in Pape et al. 2007.

Fig. 25 depicts the CSQ binding curve, the fraction of CSQ bound with Ca^{2+} vs. $[Ca^{2+}]_{SR}$, modified from Pape et al., 2007. The upper dotted line indicates the range of $[Ca^{2+}]_{SR}$ in experiments represented by row A in Table 3.3, CSQ binding curve is the steepest in this range, indicating a greater buffering power for Ca^{2+}, which increases the concentration of Ca^{2+}-bound CSQ ([Ca-CSQ]), for smaller increase in $[Ca^{2+}]_{SR}$ in the SR.

The greater buffering power of CSQ in the physiological $[Ca^{2+}]_{SR}$ range seen in Fig. 25 also explaines why $\Delta[Ca_T]_{SR}$ is greater in ISO in the physiological range of $[Ca^{2+}]_{SR}$ than in depleted fibers (15.78 mM and 6.07 mM in Table 3.3 A, column 7, and C, column 7, respectively).

3.6 The rate of change of fCa while in ISO

Thin lines in Fig. 22 above (described with the figure) show $dfCa/dt$ in those individual experiments. The means of these values in all experiments are shown in Table 3.2, columns 5 and 6 The fits were calculated by the best least squares fit method. A steeper slope indicates a greater Ca^{2+} influx into the SR and thereby into the fiber. Fig. 26 below summarizes the individual experiments and gives the means of the slopes of line fits in both experimental conditions with and without external calcium in both normal and reduced $[Ca^{2+}]_{SR}$ fibers (see values in Table 3.2, columns 5 and 6). The solid lines represent the rate of change of fCa with Ca^{2+} present and the dashed lines show values with no external calcium. The lines in ISO represent the means of slopes reached in the last 15 minutes while in ISO, they do not intend to represent the pattern of the increase of fCa (which will be considered later). Since the lines in ISO are shifted, this figure is only for illustrating the slopes.
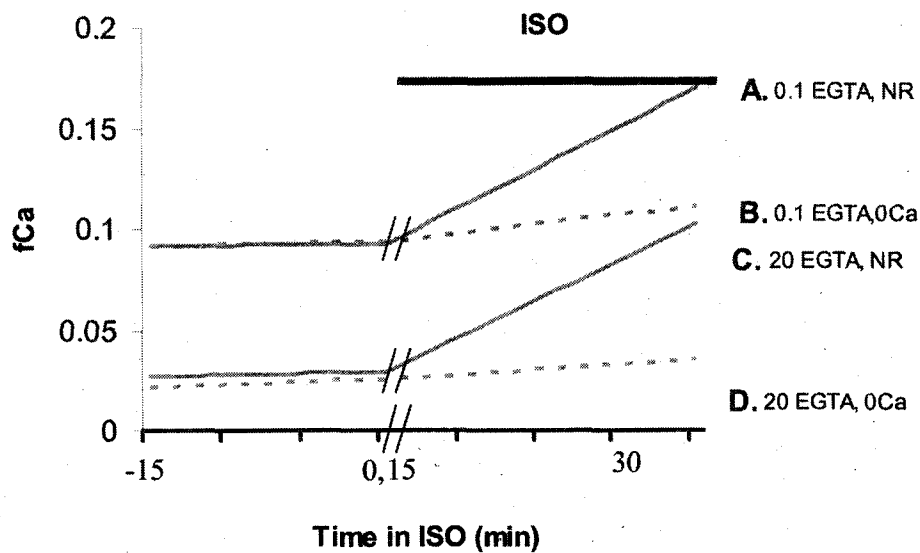
Fig. 26 Means of change of *fCa* values before and in ISO in fibers with 0.1 mM (upper traces) and 20 mM (lower traces) EGTA in the internal solution.
$t_{(0)}$ indicates the time of addition of ISO. The slopes were determined by the best least squares fit to the last 15 minutes of *fCa* values before adding ISO ($t_{(-15)} - t_{(0)}$), and the last 15 minutes in ISO ($t_{(15)} - t_{(30)}$). **Solid line**: NR external solution; **dashed line**: 0 Ca external solution.
Data is given in Table 3.1, columns 6 and 7.

The x axis indicates the time the fiber was exposed to ISO. The "0" on the time scale is the time of ISO addition. Negative values on the x axis indicate the time until the addition of ISO. In ISO, the rate of change of *f*Ca increases significantly in experiments which contained Ca^{2+} in the external solution (Table 3.2, A, C, column 6). In fibers, where external Ca^{2+} was removed there was no significant change in slope while in ISO. The increased slope in ISO in fibers with NR implies an increased Ca^{2+} influx. The

interesting result with this figure is that the slope was similar in ISO with NR in both fibers with physiological and reduced $[Ca^{2+}]_{SR}$.

In summary, these results indicate that if stimulated with β-adrenergic agonists, Ca^{2+} enters the cell from the extracellular space and $[Ca^{2+}]_{SR}$ increases. This Ca^{2+} influx is most likely via ion channels that can open at resting potential.

3.7 The increase of *f*Ca in ISO reaches its steady rate after a delay

This section evaluates the changes of *f*Ca during the period of ISO exposure. After the addition of ISO to the NR external solution, there was a delay before the rate of increase of *f*Ca reached its final steady slope.

The data after addition of ISO in Fig. 27 A is well described by an exponential and sloping line function (0.1 mM EGTA internal solution). However, the functional form of the data was not always this clear (Fig. 22 A), so that the following approach was adapted to estimate the delay. The first step was to fit a line to the *f*Ca data points of the last 15 minutes before adding ISO. In Fig. 27, panel A the arrow indicates the extrapolation of this line to the time when ISO reached the fiber (Time = 0, ~65 - 70 min after dye). This point gave the value of *f*Ca0. *f*Ca0 is the predicted value of *f*Ca at the time ISO was added. The second step was to extrapolate the line fit to *f*Ca values during the last 15 minutes in ISO back to Time 0, when ISO was added (same as the time of *f*Ca0). In Fig. 27, the dotted line shows this extrapolation back to the time of addition of ISO. The

A

fCa

0.50

0.25

0.00

ISO

fCa$_0$

m$_0$

m*τ

-20   0   20

Time in ISO (min)

B

fCa

0.2

0.1

0.0

ISO

0 Ca Ringer's   NR

-10   0   10   20

Time in ISO (min)
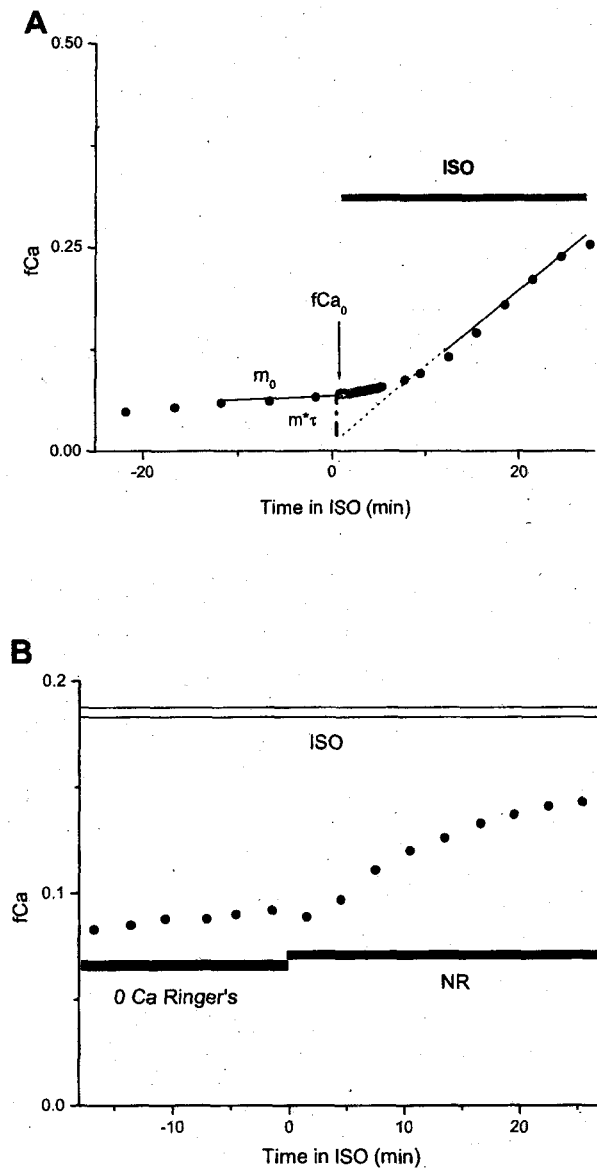
Fig. 27 A. *fCa* **increases in the presence of 10 µM ISO** in the external solution when Ca is present. Addition of ISO to the external solution that contains Ca^{2+} (NR), will show an exponential delay with tau = 6.52 min. until it reaches its steady slope. fCa_0 = 0.0660, m_0 = 0.0007, m_∞ = 0.0095, shift = 0.0079, tau = 6.52 min; Exp: 913061 (internal solution: 0.1 EGTA).

B. Addition of Ca^{2+} to the prebathed fiber in ISO causes an instant increase in *fCa*. The empty horizontal bar on the top indicates that 10 µM ISO was constantly present in the external solution. The addition of external calcium begins at the beginning of the filled horizontal line marked as "NR", at Time = 0 min. Exp: 331081

vertical dotted-dashed line marks the difference between this latter extrapolated value and *f*Ca0. This difference is referred to as the "shift".

The time constant associated with the delay (τ) given by the following equation:

$$\tau = \frac{shift}{m_\infty - m_0}.$$

(3.1)

where m_∞ is the slope of the fit when $t \gg \tau$, m_0 is the slope of the line fit before adding ISO. The derivation of eqn 3.1 is given in Appendix D.

In the experiment shown in Fig. 27, panel A the shift, *f*Ca0, m_∞, and m_0 values were 0.0776, 0.105, 0.0012 min^{-1}, and 0.0050 min^{-1}, respectively. These values substituted into eqn 3.1 gave the value of τ of 6.5 min. Table 3.4 summarizes the results for the time constant of the delay in experiments with NR external solution with and 0.1 mM or 20 mM EGTA in the internal solution. Columns (a) in both parts of the table give the fiber reference. Columns 1 give the shift, the difference in the extrapolated value (from the fit of a sloping line) and predicted value (from line fit to data before adding ISO) of *f*Ca at the time, ISO was added. Columns 2 give the extrapolated values of *f*Ca at the time of addition of ISO (*f*Ca0). Columns 3 give tau, the time constant of the delay of increase of *f*Ca in ISO, calculated by eqn. 3.1.

In summary, there is a delay with the average time constant of ~7 minutes from the time of addition of ISO until the development of a steady rise of *f*Ca, and this delay is not affected by lowered $[Ca^{2+}]_{SR}$. This delay corresponds with Gonzalez-Serratos et al., (1981) observation that inotropic effect takes 8 minutes to reach its maximum level (see Discussion).

82

A. 0.1 EGTA internal, NR external

(a)	$fCa(t0) - fCa_{extra}$ shift (1)	$fCa(t0)$ ISO (2)	Tau τ=shift/slope (3)
			min
O10061	0.0299	0.0410	6.5670
O06061	0.1236	0.1550	6.5913
913061	0.0079	0.0660	6.5176
912061	0.0031	0.0116	7.4692
627061	0.1559	0.1927	5.7749
909051	0.0234	0.0660	10.7250
913051	0.0776	0.1050	6.2241
mean	0.0618	0.1000	7.0076
SEM	0.0222	0.0207	0.630

B. 20 EGTA internal, NR external

(a)	$fCa(t0) - fCa_{extra}$ shift (1)	$fCa(t0)$ ISO (2)	Tau τ=shift/slope (3)
			min
226073	0.0023	0.0110	4.7454
307071	0.0085	0.0130	1.0676
213071	0.0295	0.0500	4.3089
D19071	-0.0085	0.0170	15.4236
mean	0.0079	0.0228	6.3864
SEM	0.0080	0.0092	3.1221

Table 3.4 Values of delay of increase of *fCa* in ISO with NR external solution in normal and depleted fibers
In both parts column (a) is the fiber reference, column (1) gives the difference in the extrapolated value (from exp. + slope fit) and predicted value (from line fit to data before adding ISO) of *fCa* at the time, ISO was added; column (2) gives *fCa* values at the time ISO was added, predicted from the line fit on valued before adding ISO, and finally, column (3) gives the tau of the delay in ISO.

3.7.1 Prebathing the fiber in ISO eliminates the delay in *fCa* increase

Another approach to investigate ISO's effect is to expose the fiber to 0 Ca external solution with 10 μM ISO, then add Ca^{2+}, and monitor the change of *fCa*. We hypothesized, that if the delayed increase of *f*Ca in ISO was caused by the time necessary

83

for the onset of enhancing mechanisms, this delay could be eliminated if ISO was already present in the external solution in advance of the addition of Ca^{2+}.

As we showed earlier, there is no Ca^{2+} influx and increase of fCa when the external solution is Ca^{2+} free. Fig. 27, panel B shows a typical experiment where Ca^{2+} was added to the external solution that has already contained ISO (empty bar). Ca^{2+} was added twenty minutes after the addition of ISO. The minimum of 20 minutes was chosen by using the mean of tau of delay from table 3.4, part A, column 3 of ~7 min. After 20 minutes the effect of ISO is expected to reach 95% of its maximum. The upper solid horizontal bar marks the time period when Ca^{2+} was present in the external solution. The results indicate a rapid rise in fCa. This relationship suggests that after ISO had prepared the pathways for calcium –either by phosphorylation or channel expression- without the presence of the Ca^{2+} itself; the moment Ca^{2+} was added, it entered the fiber across the plasma membrane and was pumped into the SR.

3.8 Removing ISO results in a sudden, transient decrease in fCa

This section addresses the change of values of fCa after removing ISO from the external solution.

Fig. 28 shows fCa values vs. time in a typical experiment when ISO was removed from the central pool. The horizontal bar marks the period of ISO presence in the external solution, and time zero on the time scale marks the time ISO was washed out. Filled and empty circles mark fCa values in ISO or after ISO, respectively. When ISO was washed

out of the solution, *fCa* drops suddenly, then after this transient decrease, it reaches a

steady positive slope similar to that measured in the last 15 minutes in ISO.
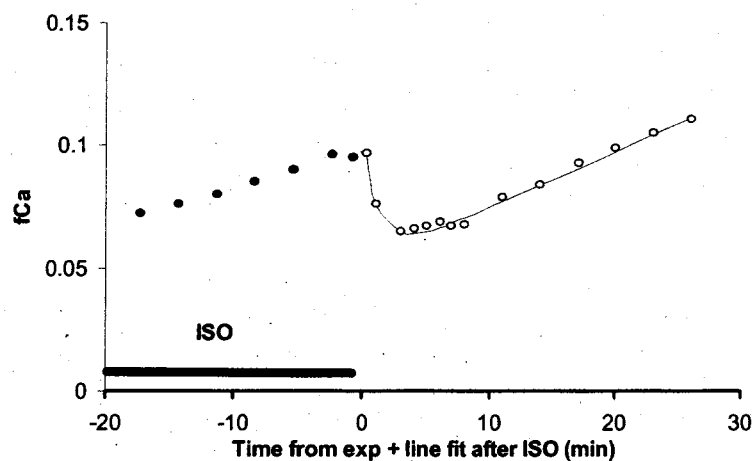
Fig. 28 *fCa* transiently "dips" after removing ISO, then recovers its slope
The horizontal bar marks the period until ISO was present in the NR external solution. At the end of the bar, ISO was removed. *fCa* values decreased exponentially, then reached a steady slope, which is very similar to that in ISO (filled circles). The line marks the function least-square fitted to the data points (see text and eqn 3.3; empty circles). Slopes in ISO and after removing ISO: 0.0016 min^{-1} and 0.0023 min^{-1}; *fCa* at the beginning of fit: 0.0989; tau of "dip": 1.47 min; Exp: O10061.

Each experiment, with NR as external solution, showed this pattern of "dip" after the

removal of ISO. In cases when calcium was removed from the external solution, the

phenomenon of "dip" never occurred (see Fig. 22, panel B, and D).

To evaluate this finding, we first fit a function to *fCa* data points after the removal of

ISO. The function was an exponential plus a line given by:

$$f_{FIT} - fCa_0 = mt - C\left(1 - e^{\frac{-t}{\tau}}\right),$$ (3.2)

85

where C is a constant, gives the magnitude of the decrease, m is the steady slope of the fit

at $t = \infty$, and t is time after the removal of ISO (see Appendix A for detailed information).

(1)	m_{ISO} (2)	m_{after} (3)	fCa(t-ref) (4)	fCaLow. After (5)	C (6)	C/ ($fCa_{(t\text{-}ref)}$- $fCa_{(bef)}$) (7)	τ_{after} (8)
	min^{-1}	min^{-1}					min
010061	0.0016	0.0023	0.0989	0.0650	-0.0462	-0.6169	1.47
006061	0.0048	0.0067	0.2810	0.2390	-0.0550	-0.4543	0.64
912061	0.0011	0.0019	0.0405	0.0389	-0.0044	-0.1896	1.86
627061	0.0064	0.0035	0.4027	0.3718	-0.0711	-0.3038	0.18
909051	0.0040	0.0055	0.1452	0.1360	-0.0215	-0.3345	0.95
913051	0.0044	0.0045	0.1657	0.1520	-0.0261	-0.4305	0.38
mean	0.0037	0.0041	0.1890	0.1671	-0.0374	-0.3882	0.9133
SEM	0.0008	0.0008	0.0538	0.0500	0.0100	0.0600	0.2648
	P > 0.05						

Table 3.5 Values of fCa change in ISO and after removing ISO
Values obtained by an exponential and line fit to fCa data in ISO and after removal of ISO (eqn. 3.3).
Column (1) gives the fiber reference. For easy comparison column (2) is shown from Table 3.2, part A, are
the constants obtained by the fit on fCa data explained in the caption of the original table. Columns (3) and
(8) are constants obtained by fitting an exponential and line to fCa data after removing ISO. Column (4) is
the extrapolated fCa value at the time of the start of exponential decrease, column (5) is the lowest fCa
value after removing ISO, just before fCa begun to rise again to reach a constant slope. Column (6) is the
constant for the exponential fit, column (7) is the ratio of column 6 and the absolute fCa gain in ISO. Note,
that the slopes in ISO and after the removal of ISO are not significantly different. Also note, that in column
5, the lowest value of fCa is in average 12% less, than the last value in ISO, which means a 39% loss off
the gained fCa while in ISO (column 7).

The function was least-squares best fitted to the points after ISO. Table 3.5 gives values

of the fits. Column (1) gives the fiber reference, column 2 gives the final slope of fCa in

ISO taken from Fig. 26, and explained there; column 3 gives the slope of the fit after

removing ISO (value of m in eqn. 3.2). The mean values of the two slopes are very

similar, 0.0037 min^{-1} and 0.0041 min^{-1}, respectively and not significantly different from

each other. Column 4 shows the extrapolated values of fCa after the removal of ISO, at

the moment fCa began to decrease. This value was calculated by the intersection of line

before removing ISO in column 2 and the exponential fit described by eqn 3.2. Column

5 shows the lowest values of fCa at the trough of the "dip". Column 6 is the magnitude of

the exponential decrease of fCa after the removal of ISO. This value gives the absolute decrease in fCa. (N.B. that C is more negative than the values of $fCa_{Low\ After} - fCa_{(t-ref)}$, the minimum value, since the latter is superimposed on constant rate of increase in fCa.) Column 7 gives the ratio of the absolute decrease in fCa to the value of gained fCa in ISO. From this column, the mean decrease in fCa associated with the dip was 39% of the gain of fCa associated with ISO. Column 8 shows the time constant of the exponential decrease obtained by fitting an exponential and a sloping line to fCa data after removing ISO. The mean value of 0.9133 min indicates a very rapid drop of fCa in a short time. This rapid decrease reaches its minimum value about two minutes after removing ISO then it is reverses and reaches a steady increase, m_{after} (Table 3.5, column 5 and 3, respectively).

In summary, the observed "dip" and subsequent recovery indicate at least two effects of ISO, one irreversible and the other rapidly reversed. The main effect of increased Ca^{2+} influx is irreversible at least in the short term of tens of minutes. This is shown by the similarity of slopes of fCa in and after ISO (0.0037 and 0.0041 min^{-1}, respectively) in columns 2 and 3 in table 3.5. It is important to note that the "dip" involves a significant net efflux of Ca^{2+} across the SR membrane following the removal of ISO. The latter effect indicates the reversal of some effects of ISO on probably the SERCA pump (see detailed argument in Discussion).

3.9 Hyperpolarization increases Ca^{2+} influx from the interstitium

To partially test whether L-type Ca^{2+} channels or some other voltage dependent Ca^{2+} channel is involved in the Ca^{2+} influx during adrenergic stimulation, fibers were hyperpolarized for a five-minute period from the resting -90 mV to -110 mV. Fig. 29 panel A shows the plot of fCa vs. time in such an experiment with no Ca^{2+} in the external solution. During the five minute hyperpolarization period, marked by the horizontal bar and the two vertical lines, fCa values did not change. Restoring the resting potential had no effect either. This result however, was expected, since it was shown in Fig. 22 panel B and D that external calcium is necessary for the increase of fCa in ISO. In the case with ISO and Ca^{2+} in the external solution, the five-minute hyperpolarization resulted a large increase in fCa. This increase appeared to be exponential with an average time constant of $\tau = 1.6$ min (Table 3.6, column 4). After restoring the potential, the rate of increase gradually decreased until it reached a steady positive slope. This slope was not significantly different from that before hyperpolarization. These data suggest that increased Ca^{2+} influx during adrenergic stimulation is further enhanced by hyperpolarization.
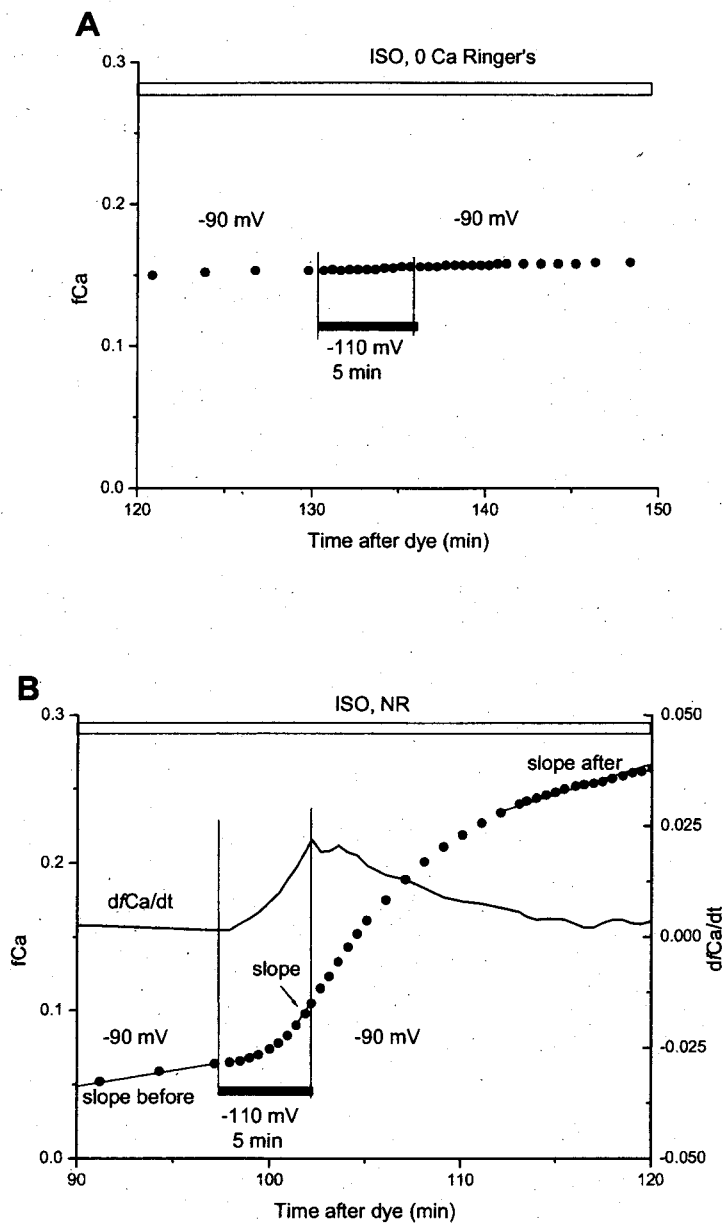
Fig. 29 Effect of hyperpolarization in ISO in absence and presence of external Ca^{2+}

The horizontal bars and the two vertical lines mark the 5-minute time period of hyperpolarization. In case when calcium was removed from the external solution (panel **A**) fCa did not change during hyperpolarization. Adding calcium (panel **B**) caused a steady slope of increase of fCa in ISO (mean: 0.0026 min-1,SEM = 0.008, n = 4). During the 5-minute hyperpolarization fCa increased with an exponentional delay (mean: τ = 1.60 min, SEM = 0.27, n = 4), reaching a slope (slope). By restoring resting potential, increase in fCa decreased gradually until reaching a close to similar slope (slope after) than that before hyperpolarization (slope before) dfCa/dt is the time derivative of fCa traces. Panel A: Exp: 310081, panel B: Exp: 303083.

(1)	-- -90 mV -- Slope Bef (2)	--- -110 mV --- Slope (3)	 Tau (4)	-- -90 mV -- Slope Aft (5)
	min^{-1}	min^{-1}	min	min^{-1}
227081	0.0008	0.0043	1.8956	0.0019
227081b	0.0035	0.0075	0.8041	0.0040
222081	0.0043	0.0156	1.6960	0.0032
303083	0.0019	0.0172	1.9960	0.0030
mean	0.0026	0.0112	1.5980	0.0030
SEM	0.0008	0.0031	0.2718	0.0004
	*	*		

Table 3.6 Effect of hyperpolarization on fCa increase in ISO
The mean steady slope of fCa increase during hyperpolarization is significantly greater then before or after at -90 mV (columns 3 and 2, 5, respectively). Tau (4) was obtained by fCa values determined by fitting a line and extrapolated back to the time of the beginning of hyperpolarization, and the actual fCa values measured at tat time, and using eqns. 3.7 – 3.9.
* $P < 0.05$

The solid line in Fig. 29 panel B shows the time derivative of fCa values. An important thing to note is that there was no decrease in $dfCa/dt$ at the start of the hyperpolarization which would have been indicative of the involvement of a voltage-dependent Ca^{2+} channel. On the other hand, when the holding potential was restored to -90 mV, $dfCa/dt$ changed direction, began to decrease with a close to similar rate as that of its increase during hyperpolarization. Thin lines are the line fits to the data points 15 minutes before (slope before), the last three data points during hyperpolarization (slope) and between 10 – 20 minutes after restoring the holding potential to -90 mV (slope after).

Table 3.6 shows the means of slopes of lines fitted on fCa values (see the slopes also in Fig. 29) in a 15-minute period before, last 3 data points during, and between 10 – 20 min. after hyperpolarization, when it reached the steady slope (columns 2,3 and 5, respectively), also the average of time constants (column 4). The time constant was calculated by using eqn 3.1.

Since fCa values do not show a step change, either at the beginning or after the end of hyperpolarization, the results argue against the involvement of hyperpolarization-activated channels or some type of inward rectifier channel. Another possibility would be that hyperpolarization increases the driving force for Ca^{2+}, which in turn would increase Ca^{2+} through channels that are already open. Such an effect, however, should also be instantaneous. Furthermore, such an effect would only increase driving force by 10%, which could not explain the two-fold increase in dfCa/dt.

A possible explanation could be that hyperpolarization causes the recruitment of more channels for Ca^{2+} influx.

3.10 Isoproterenol increases sarcoplasmic pH

Besides increasing the calcium content of the SR, adrenergic stimulation of a resting fiber influences the pH of the sarcoplasm as well. Fig. 30 illustrates the effect of ISO on the pH of the sarcoplasm during a 40-minute exposure. (N.B. earlier work indicated that the pK for phenol red is 0.1 – 0.4 pH units lower than the value used here of 7.7 based on in vitro measurements. The actual pH is greater by 0.1 – 0.4 pH units then indicated in Fig. 30). The preparation contained 0 Ca internal solution with 0.1 mM EGTA, the external solution was NR. Shortly after the addition of ISO myoplasmic pH increased, then after 6 minutes it decreased to a steady level, which is, on average, 0.05 pH units higher then that before ISO.

After removing ISO, there was a gradual decrease in pH, until it reached a steady level about 10 minutes later. Similar results, also with ISO and with cut fibers but 1.8 mM Ca^{2+} and 20 mM EGTA in the internal solution, were obtained (unpublished).

Owen (1986) demonstrated in vascular smooth muscle that adrenergic stimulation enhances the surface Na/H exchanger via α-adrenergic receptor pathway. She showed that ISO, though primarily a β-adrenergic receptor, stimulates α-receptors. She found an increase in myoplasmic pH of 0.06 units, when using 10 μM ISO as agonist. This value is very close to our result in the frog skeletal muscle.
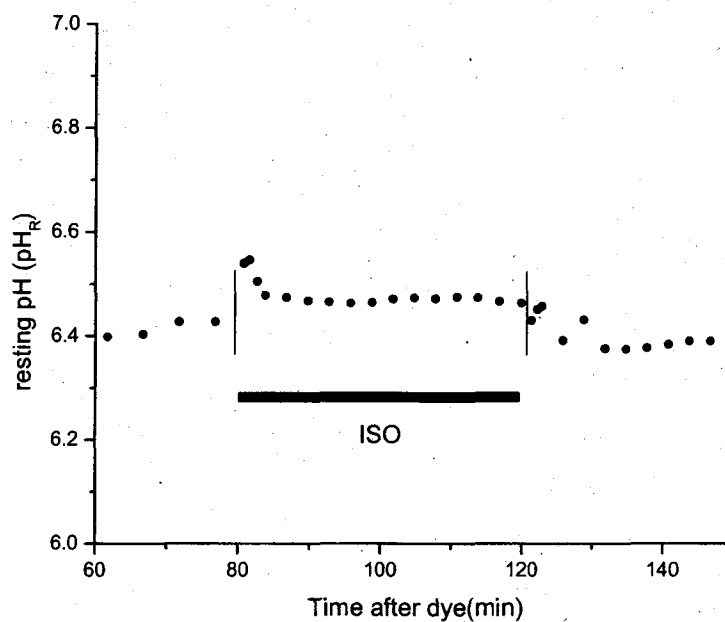
Fig. 30 Effect of ISO on myoplasmic pH
The horizontal bar and the vertical lines mark the period when 10 μM ISO was present in the external solution. Sarcoplasmic pH increased in ISO with 0.05 pH unit, and recovered to similar values after removing the drug. Internal solution contained 0 Ca and 0.1 mM EGTA; the external solution was NR. Last value of pH before ISO: 6.43, average value in ISO: 6.48, value 5 minutes after removing ISO: 6.39. Exp: 312071.

Although the literature to date lacks studies demonstrating the α-adrenergic receptor – IP_3 cascade enhancing effect on the Na/H exchanger in fast twitch skeletal muscle, it seems likely that ISO influences myoplasmic pH via this pathway.

4. DISCUSSION

4.1 Adrenergic stimulation increases $[Ca^{2+}]_{SR}$ at rest

One of the major findings of this study is that in cut fibers at rest, adrenergic stimulation increases fCa, indicative of an increase in the sarcoplasmic free calcium concentration ($[Ca^{2+}]_{SR}$) and thereby total SR and fiber calcium content. With normal Ringer's external solution, ~30min adrenergic stimulation with 10 μM ISO increased fCa, $[Ca^{2+}]_{SR}$, and $[Ca_T]_{SR}$ (average increase in fCa, $[Ca^{2+}]_{SR}$, $[Ca_T]_{SR}$ were 121%, 112%, 253%, respectively). In the control experiments neither the values of fCa nor those of $[Ca^{2+}]_{SR}$ and $[Ca_T]_{SR}$ showed any significant increase (Table 3.2, rows A, B, columns 2, 3 and Table 3.3, rows A, B, columns 2, 3 and 5, 6). Since the increase in fCa required external calcium (Fig. 23 sagittal rows A and B), the results also indicate that ISO stimulates Ca^{2+} influx across the surface/T system membrane.

These findings provide at least a partial explanation for the observations of many researchers that adrenergic stimulation increases twitch tension in frog and/or mammalian skeletal muscle (among others: Gonzalez-Serratos et al.1981, Arreola et al. 1987).

Our findings, described above, support the results of Gonzalez-Serratos and co-workers who measured an increased twitch tension for the first twitch after incubating the fiber in adrenaline without previous stimulations. They also support Rudolf et al. (2006) suggestion that stimulation with ISO results in a small increase in $[Ca^{2+}]_{SR}$. However, we are the first to show that calcium content in the SR, thereby $[Ca_T]_{SR}$ increases at rest for

adrenergic stimulation. This fact most likely leads to a greater and stronger contraction for the first stimulation measured by Gonzalez-Serratos et al. (1981).

4.2 Hyperpolarization increases Ca^{2+} influx in ISO

Our major finding explained in the previous section points out that ISO stimulates Ca^{2+} influx across the surface/T system membrane at rest. To evaluate whether L-type channels or some other voltage-gated Ca^{2+} channels were responsible, fibers were hyperpolarized to -110 mV. Hyperpolarization to -110 mV should immediately increase the driving force for Ca^{2+} by about 10%. Ca^{2+} influx mediated by increased driving force would show a step change in the slope of fCa that was established before hyperpolarization (Table 3.6 column 2 and Fig. 29, panel B). This slope, however remains apparently steady for about 90 – 120s after the beginning of hyperpolarization. On the other hand, this steady slope at the beginning also indicates that voltage gated channels were not activated by ISO before hyperpolarization. If they were, we would have expected a sudden decrease of the slope of fCa values, indicative of closing of these channels. The increase in rate of fCa however, was coming on with a delay of $\tau = 1.6$ min (Table 3.6, column 4), until it reached its maximum final slope which is about 4-fold greater than the one established before hyperpolarization. This magnitude of increase is too great to be caused only by the increased driving force for Ca^{2+} at -110 mV (Table 3.6. columns 2 and 3).

Another possibility for the increased rate of Ca^{2+} entry would be the hyperpolarization-activated cyclic nucleotide-gated channels (HCN). However, the lack of step change in the rate of fCa at the beginning of hyperpolarization period argues against their role in this process.

One interesting possible candidate is the transient receptor potential channel – Canonical (TRPC), a Ca^{2+} channel without a clearly demonstrated function at this time. These channels have recently been linked to store-operated calcium entry mechanisms, but it has been suggested, that they can be activated by other unknown mechanisms (Yuan et al., 2007). In any case, the main finding in this section is that ISO stimulates some, as yet unknown, voltage-insensitive Ca^{2+} channel that significantly increases the SR calcium content.

4.3 Store –operated channels are not activated at physiologically depleted $[Ca^{2+}]_{SR}$

This section considers the implications of the effects of external Ca^{2+} on fCa values in fibers with depleted $[Ca^{2+}]_{SR}$ before adding ISO.

In the experiments in this study, in which 20 mM EGTA was added to the internal solution, the average of initial fCa values were ~30% of those where 0.1 EGTA was present (Fig. 23 front row columns C, D vs. A, B). The average level of fCa with 20 mM EGTA in the internal solution is the same in the presence and absence of external calcium. If surface Ca^{2+} flux were significant, the values of fCa in fibers with NR would be expected to be greater then those measured in fibers with no external Ca^{2+} present. The

fact that essentially the same steady level of low *fCa* was measured in preparations with Ca^{2+} absent or present in the external solution indicate that store-operated Ca^{2+} entry (SOCE) is not activated at ~30% of normal resting $[Ca^{2+}]_{SR}$.

Store-operated calcium entry was demonstrated among others by Yuan et al. (2007) in transfected HEK cells, by Roos et al. (2005), in Jurkat cells, and by Stiber et al. (2008), in myotubes and adult mouse skeletal muscle cells. In the above mentioned studies, the authors depleted the SR of Ca^{2+}, using thapsigargin (TG), an inhibitor of the SERCA pump. In skeletal muscle, in response to store depletion, the Ca^{2+} sensor STIM1 clusters into punctae at SR/T tubule membrane, activates ORAI1 and TRPC channels which in turn open for SOC-mediated Ca^{2+} influx (Shin and Muallem, 2008). In these preparations, SOCE was activated with near total depletion, so that it is unknown at what level of depletion gets SOCE activated.

Our study is the first to indicate that store operated mechanisms are not recruited when the calcium content changes from the physiological level as low as 30% of the physiological level. Since SOCE is not activated in this range, the question remains as to how the physiological SR calcium content is determined.

4.4 Lowered $[Ca^{2+}]_{SR}$ does not increase the rate of store filling in ISO

This section considers the implications of the effects of ISO on *fCa* values in fibers with normal and depleted $[Ca^{2+}]_{SR}$.

Experiments, carried out with normal $[Ca^{2+}]_{SR}$ (0.1 mM EGTA in the internal solution), showed increased rate of fCa increase in ISO when calcium was available. We made the same observation with depleted (20 mM EGTA internal) fibers. The absolute rates of increase of fCa surprisingly, were very similar in both cases (Fig. 26A, C).

It is important to note, however, that the similar rate of change of fCa in these two different preparations results in a different rate of change in $[Ca_T]_{SR}$. The difference is due to the non-linearity of the binding curve of Ca-Calsequestrin (CaCSQ) in this range. As Fig. 25 illustrates, the Ca-Calsequestrin binding curve is sigmoidal; its Hill coefficient is around 3, and its $K_d = 1$ mM (Pape et al., 2007). The figure plots the binding curve of Ca-Calsequestrin the fraction of CSQ bound to Ca^{2+} ($fCaCSQ$, ordinate) vs. $[Ca^{2+}]_{SR}$ (abscissa). The range of $[Ca^{2+}]_{SR}$ at ~30 min. in ISO in our study is from 0.2245 mM (in depleted fibers Table 3.3, row D, column 3) to 1.2936 mM (in normal $[Ca^{2+}]_{SR}$ fibers, row A). The total length of both dotted lines in Fig 25 illustrates this entire range of $[Ca^{2+}]_{SR}$. CSQ buffering power is greater in the normal $[Ca^{2+}]_{SR}$ range, -as indicated by the steeper slope of the binding curve under the upper dotted line- than in the $[Ca^{2+}]_{SR}$ range of depleted fibers, indicated by the somewhat less steep curve at the lower dotted line. This results in a greater increase in $[Ca_T]_{SR}$ for the expense of the increase in $[Ca^{2+}]_{SR}$. Indeed, the average increase in $[Ca_T]_{SR}$ in ISO was 15.78 mM in fibers with normal $[Ca^{2+}]_{SR}$ vs. 6.07 mM in depleted fibers (Table 3.3, rows A, C, column 7).These values give an average $d[Ca_T]_{SR}/dt$ of 0.5260 mM/min vs. 0.2023 mM/min in normal $[Ca^{2+}]_{SR}$ and depleted fibers, respectively. These data indicate that the Ca^{2+} influx is about 2.5 times greater in fibers with normal $[Ca^{2+}]_{SR}$.

This result is consistent with our previous finding, that store-operated mechanisms are not stimulated by ISO at this level of depletion of the SR (e.g. ~30% of normal). If ISO somehow activated the SOC-mediated Ca^{2+} entry, we would have expected a greater Ca^{2+} influx in the partially depleted fibers. This is because if SOCE was involved, one might expect the double activation to be additive i.e. ISO + store depletion.

4.5 Delay in reaching the steady rate of increase of *fCa* in ISO

A delay in the increase of *fCa* with an average time constant of 7.0 minutes (Fig. 27 panel A and table 3.4 part A) was seen, when ISO was added to the external solution. The time constant of the delay is consistent with the 8-minute delay in maximum force development shown by Gonzalez-Serratos et al. (1981). Interestingly, prebathing the fiber in ISO before adding Ca^{2+} eliminated the delay and caused an immediate rapid increase of *fCa*. These results together highlight that ISO does have a latent period until its effects on Ca^{2+} influx take place. It seems reasonable to hypothesize that ISO stimulates the expression of some type of channel that conducts Ca^{2+} at -90 mV.

The presence of delay in both the maximum force development and the reaching of steady rate of *fCa* pretty much rules out the possibility that increased Ca^{2+} influx is due to activation of L-type channel via cAMP – PKA phosphorylation by the fact that this process is very rapid, takes place within a few milliseconds.

The other possibility that adrenergic stimulation may result in gene transcription and expression of a calcium-conducting cation channel in the plasmalemma seems more

likely. Microarray studies on skeletal muscle mRNA profile during epinephrine infusion showed that cAMP-dependent transcription of genes responsible for carbohydrate, lipid and protein metabolism were up-regulated by adrenergic stimulation (Arner, 2004; Viguerie et al., 2004). These include the enhanced synthesis of enzymes for glycogen mobilization, glucose metabolism, protein anabolism and inhibitory effects on proteolysis (Viguerie et al., 2004). Examining the time constant of real time gene expression in live Escherichia coli cells, Yu et al. measured a time constant of $\tau = 7.0 \pm 2.5$ minutes (Yu et al., 2006). The similarity of time constants shown by our results and the finding of Yu et al., suggests the possibility that adrenergic stimulation may indeed initiate gene expression.

Another possibility could be that ISO promotes the incorporation of some type of cation channel-containing vesicles into the plasmamembrane. An important biological phenomenon involving vesicle-membrane fusion is the incorporation of glucose transporters into the plasma membrane of muscle and fat cells or the fusion of ACh filled vesicles with the presynaptic membrane. Intracellular GLUT-4 traffics to the plasma membrane with a half-time of ~230 min, and insulin reduces the half-time to ~9 min (Karylowski et al., 2004). This half-time is very close to our time constant of 7.0 min. The fusion of ACh vesicles occurs on submilliseconds timescales (200 μs) after the onset of Ca^{2+} influx (Llinás et al., 1981). SNARE-driven fusion of lipid bilayers that did not require Ca^{2+} was measured from 10 minutes half time (Weber T et al., 1998) down to a time constant of 25 ms (Liu et al., 2005). This wide range of time scale of vesicle incorporation would allow us to fit our delay towards the longer end of the range; however the absence of data would make this assumption highly speculative.

4.6 Sudden transient decrease in *fCa* after removal of ISO suggests change in transport of Ca^{2+} from the SR.

Another main finding of this study was the observation of rapid, transient decrease in SR calcium content while ISO was removed from the external solution. After this transient "dip", SR calcium content began increasing again with the same rate as it did during ISO (Fig. 28). These observations suggest two different effects of ISO on the fiber: one is reversible ("dip") and the other (recovery of the rate in increase) is irreversible at least on the short term. This section considers the transient decrease in *fCa* ("dip") after removing ISO.

The initial rate of decline of *fCa* after ISO removal can be described with a single exponential with a time constant of $\tau = 0.91$min (Table 3.5, column 8). From the known time constant we can easily calculate $d[Ca_T]_{SR}/dt$, the rate of total calcium lost in the first minute. The calculation gives the value of 2.27 mM/min (which converts to a rate of 0.038 µM/ms). This rate closely corresponds to the release rate of calcium from the SR by α-RyR for a depolarization to -70 mV observed previously by Pape et al., 1995 (Pape et al., 1995) in frog cut muscle fibers. Although much less than the maximum rate of Ca^{2+} release (of ~150 µM/ms) under the same conditions, it still corresponds to a significant rate of release. It is very important to note that any explanation for this loss of SR calcium has to involve a net efflux across the SR membrane following the removal of ISO. Because of this, it is possible to rule out a few possible explanations for the rapidly reversed component. We can approach this phenomenon from different aspects:

a.) If the removal of ISO reversed the influx pathway across the surface/T -system membrane, it would tend to stop the accumulation of Ca^{2+} in the SR but it would not cause the loss of Ca^{2+} already accumulated. Also, the observation of continuing rise of SR calcium content after the "dip" argues against the assumption that the removal of ISO closes the previously established Ca^{2+} influx pathways.

b.) Another possible explanation to consider is the hypothesis that ISO enhances Ca^{2+} leak from the SR (Reiken et al., 2003). In this case, any Ca^{2+} leak in ISO would have to be masked by the enhanced SERCA, hence the observed increase of SR calcium content during ISO. In this case, removal of ISO would reverse the leak which would cause a transient increase in SR calcium content not a decrease. The presence of the "dip" argues against the hypothesis that ISO enhances a Ca^{2+} leak from the SR.

c.) On the other hand, if ISO directly enhances SERCA by means of involvement of a stimulatory co-factor and/or phosphorylation of the pump itself, the reversal of this effect by removing ISO would expose the leak. It would do so, since prior to the removal of ISO there is a balance established with any Ca^{2+} leaked from the SR being pumped back into the SR. The reversal of the direct enhancement on SERCA would then reveal the SR Ca^{2+} leak thereby causing the "dip". In order to account for the results, this Ca^{2+} leak would also have to be reversed within several minutes following the removal of ISO. Although this explanation can not be ruled out, it is not very likely, since the "dip" indicates a very fast release, and is well described by a single exponential process.

d.) Another possibility is to evaluate the "dip" from the point of view of SERCA. Normally, the major job of SERCA is to remove Ca^{2+} from the sarcoplasm into the SR lumen. It has been shown however, that SERCA can work in reverse mode (Shannon et

al., 2000). In their study, they showed that SERCA behaves as a reversible thermodynamic enzymatic reaction where the forward rate depends on $[Ca^{2+}]_{myo}$, and the reverse rate on $[Ca^{2+}]_{SR}$. The steady state of this system occurs when the energy required to establish the $[Ca^{2+}]$ gradient is balanced by the free energy available from ATP. With the removal of ISO from the external solution, this balance shifts toward the reversal direction of the pump: $[Ca^{2+}]_{SR}$, and likely $[ADP]_{myo}$ and $[Pi]$ are elevated, meantime the adrenergic enhancement of glycolytic ATP production terminates, and with this $[ATP]_{myo}$ stalls or decreases (Shannon et al. (2000). This process, however by itself would not explain the quick release of Ca^{2+} from the SR. In order for this possibility to explain the rapid reversal following ISO removal, it would also require the reversal of a direct stimulation on the pump by ISO (like the ones pointed out in section c. above). This direct enhancement is necessary because the removal of ISO would not cause an immediate change in the conditions for the reversal of the pump (e.g. $[Ca^{2+}]_{SR}$ and $[ATP]_{myo}$).

Both explanations in section c, and d. above require in fact the hypothesis of the presence of a direct enhancing effect of ISO on the SR Ca^{2+} pump; a signal pathway which is independent from the indirect enhancements due to increased $[ATP]_{myo}$ and $[Ca^{2+}]_{myo}$. The observed phenomenon of "dip" therefore can be considered as evidence in support of the idea that ISO directly enhances the SR Ca^{2+} pump despite of the lack of apparent phosphorylation sites for PKA (Odermatt et al., 1998).

4.7 Ca^{2+} influx doesn't change after the removal of ISO

Fig. 28 shows that after the lowest point of the "dip" fCa values begin to rise, until they reach a steady level. The slope of line fit of the steady level after the removal of ISO is not significantly different from the one established in ISO (Table 3.5, columns 2, 3). This finding indicates that removal of ISO does not change the Ca^{2+} influx present before removing ISO. It seems reasonable to conclude that the similar rate of Ca^{2+} influx is due to expressed Ca^{2+} channels in response to ISO stimulation or some type of very slow up-regulation of Ca^{2+} channels, already present when ISO was added.

4.8 Ca^{2+} leak from the SR in ISO is unlikely

As discussed above, the "dip" argues against the enhancement of a Ca^{2+} leak by ISO. This section gives another reason to question this hypothesis.

When we exposed the fiber containing 20 mM EGTA and 0 Ca^{2+} in the internal solution to ISO there was no significant change in the rate of change of fCa values in ISO (Fig. 22 panel D, and Fig. 26, D). If there was a leak, we would expect to see a transient decrease in fCa. This would be expected, since the 20 mM EGTA would buffer the leaked Ca^{2+}, and would compete with SERCA. This process would delay the pumping back of leaked Ca^{2+} in to the SR. This observation provides direct evidence against any Ca^{2+} leak from the SR occurring during ISO exposure; also it argues against the

104

hypothesis made by Marks and co-workers (Reiken et al., 2003) that adrenergic

stimulation causes the RyR channel to be leaky.

4.9 Enhancement of α-adrenergic pathway can explain myoplasmic pH change in ISO

Fig. 30 illustrates the change of myoplasmic pH during ISO. After an initial transient

increase pH values gradually decreased to a steady value of 0.05 pH unit above the initial

value, and remained at this elevated level until ISO was washed out. After washing out

ISO, myoplasmic pH recovered to the value before adding ISO.

Regulation of myoplasmic pH depends on continuous activity of membrane transport

systems that mediate an outflux of H^+ or influx of bicarbonate, so that proton generation

is counterbalanced by proton efflux (JUEL, 1998). The transporters involved in muscle

pH regulation at rest are the Na^+/H^+ exchange system (Moore, 1981; Owen, 1986), as

well as the Na^+-dependent (NBCe), and Na^+-independent (Cl⁻/HCO3⁻X) Cl⁻ - bicarbonate

transport systems (Wang et al., 2000; J. M. Kristensen, 2004). Proton-linked

monocarboxylate transporters (MCT) are also present in skeletal muscle. These proteins

are responsible for efflux of glycolytically derived lactic acid. In fast twitch skeletal

muscle, MTC3 appears to be the major isoform (Wilson et al., 1998).

Lactate/H^+ transporters (MCT) appear to be the major acid extruding system

associated with intense exercise (JUEL, 1998), while the Na^+/H^+ exchanger and the

$Na^+/HCO3^-$ co-transporter (NBC) seem to be active at resting myoplasmic pH levels in skeletal muscle (JUEL, 1998; J. M. Kristensen, 2004).

Since our experiments revealed a myoplasmic pH rise during adrenergic stimulation, the major question is, whether these proteins responsible for pH_i can be affected by isoproterenol?

Owen (1986) proposed that isoproterenol interacts with α-adrenergic receptor to cause IP_3 to rise, which in turn, activates Na/H exchange. This effect could be blocked by the α-antagonist phentolamine, but not by the β-antagonist propranolol. In her studies, she found that 10 μM ISO increased basal pH_i by 0.06 pH unit (Owen, 1986) which is very close to the pH increase of 0.05 in ISO, revealed in our experiment. Our results are very similar to earlier, unpublished results with 20 mM EGTA in the internal solution with frog cut fibers from our laboratory (Pirouzi, 1999). His results indicated a 0.05 pH_i increase, reached after a 4-minute incubation in 10 μM ISO. After removing ISO from the external solution, myoplasmic pH also recovered completely suggesting that isoproterenol is the most likely cause of pH rise.

There is another protein which is responsible for the acid-base homeostasis of skeletal muscle at rest, the Na^+/HCO_3^- co-transporter (NBCe). Kristensen et al., 2004 (J. M. Kristensen, 2004) revealed, that approximately half of the pH recovery is mediated by bicarbonate-dependent transport, by NBCs. They localized two isoforms of the protein in sarcolemmal membranes and suggested that they are present in some internal membranes, probably the T-tubules. The location and function of NBCs would make them another ideal candidate besides the Na/H exchanger for increasing myoplasmic pH if they could be enhanced by adrenergic stimulation. Indeed, Hayashi, 2001 (Hayashi, 2001) reported

that NBCs, found in kidney β-intercalated cells are controlled by isoproterenol via β_1-receptor-cAMP-PKA pathways, but this function has not been verified in skeletal muscle.

Since bicarbonate is not present in our fibers, our results suggest that the increase in myoplasmic pH caused by isoproterenol is likely due to enhanced Na/H effect stimulated via PLC-IP$_3$ pathway.

5. CONCLUSION & PERSPECTIVES

The data presented in this thesis show new findings on the effects of isoproterenol on [Ca^{2+}]$_{SR}$ and [Ca$_T$]$_{SR}$ at rest using TMX, a membrane permeable low affinity Ca^{2+}-indicator. We monitored the fraction of Ca^{2+}-bound TMX (fCa), a direct indicator of free calcium content in the SR ([Ca^{2+}]$_{SR}$).

1. We established that adrenergic stimulation increases Ca^{2+} influx across the sarcolemma in resting fiber. This increased Ca^{2+} influx is non-reversible within the time period of tens of minutes after removing adrenergic stimulation.

2. The isoproterenol effect occurs with a delay with an exponential time constant of τ = 7.0 min until the rate of Ca^{2+} influx reaches a steady level. On the other hand, Ca^{2+} influx in fibers with ISO in the external solution instantaneously increased upon the addition of external Ca^{2+}. Furthermore, after removing ISO, following a transient "dip" the rate of Ca^{2+} influx recovered, and remained constant at the same rate that was established in ISO. These observations suggest that adrenergic stimulation promotes the expression of some type of channel that conducts Ca^{2+} at rest and these channels remain active after the removal of adrenergic stimulation.

3. We showed that the rate of increase of fCa established in ISO increases after some delay following hyperpolarization. Because of the delay, the increase can not be

explained simply by the increased driving force for Ca^{2+} or by inward rectification of a Ca^{2+} conducting channel or by hyperpolarization activated channels. These data suggest therefore that ISO stimulates some, as yet unknown voltage-insensitive Ca^{2+} channel that significantly increases the SR calcium content. Putative candidate may be related to the TRP super family of canonic channels which would be activated at rest.

4. We demonstrated that Ca^{2+} influx across the sarcolemma hence $[Ca^{2+}]_{SR}$ is not enhanced in fibers with lowered $[Ca^{2+}]_{myo}$ to 30% of its normal level. This finding argues against the participation of store-operated mechanisms at this level of depletion.

5. The steady level of fCa in ISO in fibers containing no Ca^{2+} in the external solution and 20 mM EGTA in the internal solution argues against the hypothesis of Marks and colleagues that adrenergic stimulation causes Ca^{2+} leak from the SR. The phenomenon of the "dip", the transient decrease in $[Ca^{2+}]_{SR}$ after the removal of ISO, also argues against the hypothesis that ISO enhanced a Ca^{2+}-leak from the SR during adrenergic stimulation.

6. The occurrence of the "dip", -which is equivalent with a Ca^{2+} release from the SR for a depolarization to -70 mV- its magnitude of Ca^{2+} release, its single exponential time course, and its transient nature suggest that ISO directly enhances the SR Ca^{2+} pump and the removal of ISO brings this enhancement to an end. This enhancement may occur by a direct enhancement of a co-stimulatory factor and/or phosphorylation of the pump itself if possible. After the removal of ISO, with no further adrenergic stimulation the pump quickly turns into "reverse mode" due to the high $[Ca^{2+}]_{SR}$.

7. Our results show an increase in pH by ISO. This pH increase supports the possibility of the involvement of α-adrenergic pathways and its downstream events. Although isoproterenol is primarily a β-adrenergic agonist, its α-adrenergic influence –though in much less extent than that of β – has been previously shown.

In summary, ISO increases Ca^{2+} influx across the surface/T-system membrane which in turn increases SR calcium content ($[Ca_T]_{SR}$) and with this, $[Ca^{2+}]_{SR}$. Increased $[Ca^{2+}]_{SR}$ leads to a greater Ca^{2+} release from the SR which causes a greater tension during muscle contraction.

Our results may give physiological importance to the fact that athletes, directly before their race, relax in a motionless position. It is possible that this concentration before the race not only prepares them mentally but physically as well through the effects of elevated adrenaline levels on their muscles shown in this study.

On the other hand, bedridden patients might benefit from adrenergic stimulation administered directly before their regular physical therapy exercise. The enhancing effects of adrenaline on following muscle contractions could help better maintain –or slower the rate of atrophy- of muscles.

6. APPENDIX - A

The purpose of this appendix is to describe the approach used to calculate the best fit,

using the least sum of squares differences method for the "dip", the transient decrease of

fCa values after the removal of ISO. This phenomenon is illustrated in Fig 27. After

removing ISO, *fCa* values decreased quickly, reaching their lowest value, then recovered,

reaching a steady, positive slope. The shape of this transient decrease could be best

described by an exponential function with a sloping line (y_{FIT}) described by eqn. 3.14:

$$y_{FIT} = C\left(1 - e^{\frac{-t}{\tau}}\right) + mt \qquad (A\text{-}1)$$

where C is the magnitude of exponential, m is the sloping line, reached at $t = \infty$, and

$$t = t' - t_{REF}, \qquad (A\text{-}2)$$

where t' is time after the addition of DYE, and t_{REF} is the time when *fCa* begun to drop,

so $t = 0$ at the beginning of the fit.

The value of *fCa* at $t = 0$ was set to 0, and denoted as y:

$$y = fCa - fCa(t_{REF}), \qquad (A\text{-}3)$$

The least sum of squares fit between the function in eqn. A-1 and y values:

$$SSQ = \sum_{i=1}^{N}(y_i - y_{FIT})^2 \qquad\qquad (A\text{-}4)$$

where y_i are values of fCa of time (t_i) below, in eqn. A-5, after the removal of ISO.

By substituting the function of y_{FIT} into eqn. A-4:

$$SSQ = \sum_{i=1}^{N}\left[y_i - \left(C\left(1-e^{\frac{-t_i}{\tau}}\right) + mt_i\right)\right]^2 \qquad\qquad (A\text{-}5)$$

We obtain the best fit, if the partial derivative of SSQ in respect to m and C are 0. By solving eqn. A-5, first in respect to m:

$$\frac{\partial SSQ}{\partial m} = -2\sum_{i=1}^{N}\left[y_i - \left(C\left(1-e^{\frac{-t_i}{\tau}}\right) + mt_i\right)\right]*t_i = 0, \qquad\qquad (A\text{-}6)$$

rearranging,

$$\sum y_i t_i - C\sum t_i + C\sum t_i e^{\frac{-t_i}{\tau}} - m\sum t_i^2 = 0, \qquad\qquad (A\text{-}7)$$

and solving for m:

$$m = -\frac{C\sum t_i - C\sum t_i e^{\frac{-t_i}{\tau}} - \sum y_i t_i}{\sum t_i^2}.$$ (A-8)

Solving the partial derivative of SSQ in respect to C:

$$\frac{\partial SSQ}{\partial C} = -2\sum\left[y_i - \left(C\left(1-e^{\frac{-t_i}{\tau}}\right) + mt_i\right)\right]\left(1-e^{\frac{-t_i}{\tau}}\right) = 0$$ (A-9)

rearranging:

$$\sum y_i - CN + C\sum e^{\frac{-t_i}{\tau}} - m\sum t_i - \sum y_i e^{\frac{-t_i}{\tau}} + C\sum e^{\frac{-t_i}{\tau}} - C\sum e^{\frac{-2t_i}{\tau}} + m\sum t_i e^{\frac{-t_i}{\tau}} = 0.$$

(A-10)

Substituting in eqn. A-8, and combining $C\sum e^{\frac{-t_i}{\tau}}$ terms:

$$\sum y_i - \sum y_i e^{\frac{-t_i}{\tau}} + 2C\sum e^{\frac{-t_i}{\tau}} - C\sum e^{\frac{-2t_i}{\tau}} \_CN +$$

$$+\frac{C\left(\sum t_i - \sum t_i e^{\frac{-t_i}{\tau}}\right) - \sum y_i t_i}{\sum t_i^2}\left(\sum t_i e^{\frac{-t_i}{\nu}} - \sum t_i\right) = 0,$$ (A-11)

113

and finally solving for C:

$$C = \frac{\sum t_i^2 \left(\sum y_i e^{\frac{-t_i}{\tau}} - \sum y_i \right) - \sum y_i t_i \left(\sum t_i e^{\frac{-t_i}{\tau}} - \sum t_i \right)}{\sum t_i^2 \left(2\sum e^{\frac{-t_i}{\tau}} - \sum e^{\frac{-2t_i}{\tau}} - N \right) + \left(\sum t_i - \sum t_i e^{\frac{-t_i}{\tau}} \right)^2} \quad . \tag{A-12}$$

The function of the fit, y_{FIT} (A-1) with the solutions for variables m (A-8) and C (A-12) were entered in an excel worksheet. The best fit between values of yi and y_{FITi} were obtained by getting the least sum of squares differences between the two sets of values by changing the user-adjustable parameter, τ:

$$SSQ_{y_i, y_{FIT}} = \sum (y_i - y_{FITi})^2 \tag{A13}$$

114

APPENDIX - B

The aim of this appendix is to describe the approach of calculating $[Ca^{2+}]_{SR}$ from the measured fCa values.

Since calcium bound TMX is found explicitly in the SR, and taking the distribution of TMX forms in the fiber into account, the following formula describes fCa:

$$fCa = \frac{V_{SR}[CaTMX]_{SR}}{V_{SR}([CaTMX]_{SR} + [TMX]_{SR}) + V_{myo}[TMX]_{myo}} \qquad \text{(B1)}$$

where V is volume and the subscripts $_{SR}$ and $_{myo}$ refer to sarcoplasm and myoplasm, respectively. This value, however, underestimates SR free calcium, because it contains the myoplasmic component of TMX ($[TMX]_{myo}$). To calculate the fraction of calcium bound TMX in the SR (fCa_{SR}) we have to omit TMX, present in the myoplasm:

$$fCa_{SR} = \frac{V_{SR}[CaTMX]_{SR}}{V_{SR}([CaTMX]_{SR} + [TMX]_{SR})}. \qquad \text{(B2)}$$

Combining eqns (B1) and (B2) and expressing the reciprocal of fCa yields:

$$\frac{1}{fCa} = \frac{1}{fCa_{SR}} + \frac{V_{myo}[TMX]_{myo}}{V_{SR}[CaTMX]_{SR}}. \qquad \text{(B3)}$$

The second part of the right side of eqn (B3) can be broken down into two parts knowing that

$$[TMX]_{SR} = \rho[TMX]_{myo},\qquad\qquad\qquad (B4)$$

where ρ is a constant that explains the difference in $[TMX]_{myo}$ and $[TMX]_{SR}$ based on the pH gradient across the SR membrane. Substituting the ratios of TMX forms present in the SR in (B3) with their fractional ratios and dividing with ρ yields:

$$\frac{V_{myo}}{V_{SR}} * \frac{[TMX]_{myo}}{[CaTMX]_{SR}} = \frac{V_{myo}}{\rho V_{SR}} * \frac{1 - fCa_{SR}}{fCa_{SR}},\qquad (B5)$$

and substituting eqn (B5) into the second expression of the right side of eqn (B3) gives the final solution:

$$\frac{1}{fCa} = \frac{1}{fCa_{SR}} + \frac{V_{myo}}{\rho V_{SR}} * \frac{1 - fCa_{SR}}{fCa_{SR}}.\qquad (B6)$$

The volume ratio (V_{myo}/V_{SR}) is a constant, as well as ρ, therefore eqn (B6) describes the function of fCa_{SR} vs. fCa. Following these calculations with the monitored fCa values, $[Ca^{2+}]_{SR}$ can be calculated with eqn 2.21:

116

$$[Ca^{2+}]_{SR} = \frac{fCa_{SR} * K_d}{1 - fCa_{SR}}.$$

(B7)

It is important to note, however, that in case the turnover rate of the SERCA changes, it should change the constant ρ (which is obtained from the pH gradient across the SR membrane eqn. 3.5), which in turn will change slightly the relationship between fCa and fCa_{SR} and therefore the value of $[Ca^{2+}]_{SR}$.

APPENDIX – C

This section describes how information about the concentrations of Ca-bound and Ca-free TMX ([CaTMX] and [TMX], respectively) and related information is derived from the measurement-derived A_{TMX} signals. Since there are two dye species, TMX and CaTMX, their concentrations can be determined from the dye-related absorbances at two wavelengths. This section describes how [TMX] and [CaTMX] can be obtained utilizing the information from two or more wavelengths using the least-squares method. The measurement-derived absorbance at wavelength λ_n is denoted $A_{dye}(\lambda_n)$ where n can vary from 1 to the number of wavelengths, N. The least-squares best fit absorbance at wavelength λ_n is given by

$$A_{fit}(\lambda_n) = \varepsilon_D(\lambda_n) \cdot [TMX] \cdot l + \varepsilon_{LD}(\lambda_n) \cdot [CaTMX] \cdot l \tag{C1}$$

where l is the optical path length and $\varepsilon_{TMX}(\lambda_n)$ and $\varepsilon_{CaTMX}(\lambda_n)$ are the extinction coefficients at wavelength λ_n. This is simply the sum of the absorbances from each of the dye species using Beer's Law and the best-fit values of [TMX] and [CaTMX]. The sum of squares ($SSQs$) is given by

$$SSQs = \sum_{n=1}^{N} \left(A_{dye}(\lambda_n) - A_{fit}(\lambda_n) \right)^2 \tag{C2}$$

Substituting equation (C1) into (C2), taking the partial derivatives of $SSQs$ with respect to [TMX] and [CaTMX] and solving for [TMX] and [CaTMX] from the two partial derivatives gives that

$$[TMX] = \frac{1}{l} \frac{\sum \varepsilon_{CaTMX}^2 \cdot \sum A_{dye}\varepsilon_{TMX} - \sum \varepsilon_{TMX}\varepsilon_{CaTMX} \cdot \sum A_{dye}\varepsilon_{CaTMX}}{\sum \varepsilon_{TMX}^2 \sum \varepsilon_{CaTMX}^2 - \left(\sum \varepsilon_{TMX}\varepsilon_{CaTMX}\right)^2} \quad (C3)$$

and

$$[CaTMX] = \frac{1}{l} \frac{\sum \varepsilon_{TMX}^2 \cdot \sum A_{dye}\varepsilon_{CaTMX} - \sum \varepsilon_{TMX}\varepsilon_{CaTMX} \cdot \sum A_{dye}\varepsilon_{CaTMX}}{\sum \varepsilon_{TMX}^2 \sum \varepsilon_{CaTMX}^2 - \left(\sum \varepsilon_{TMX}\varepsilon_{CaTMX}\right)^2} \quad .(C4)$$

(N.B. for brevity, the wavelength index, n, for the summations and the function

dependencies on λ_n are omitted.)

119

APPENDIX - D

This section describes the steps used for calculating the time constant of the delay depicted in Fig. 27 A.

The function that describes the change of fCa in ISO, is based on an exponential function and the rate of changes of fCa before ISO and at infinite time, where the rate of change becomes steady:

$$\frac{dfCa}{dt} = \left(\left.\frac{dfCa}{dt}\right|_\infty - \left.\frac{dfCa}{dt}\right|_0\right)\left(1 - e^{\frac{-t}{\tau}}\right) + \left.\frac{dfCa}{dt}\right|_0 \qquad \text{(D1)}$$

where t is the time of addition of ISO,

and $\left.\dfrac{dfCa}{dt}\right|_0$ is the slope of fCa before ISO, denoted m_0,

and $\left.\dfrac{dfCa}{dt}\right|_\infty$ is the steady slope of fCa, reached where $t \gg \tau$, denoted m_∞.

After substituting m_0 and m_∞ in to eqn E1, it simplifies:

$$\frac{dfCa}{dt} = (m_\infty - m_0)\left(1 - e^{\frac{-t}{\tau}}\right) + m_0. \qquad \text{(D2)}$$

Integration gives:

$$fCa(t) = fCa(0) - (m_\infty - m_0)\tau\left(1 - e^{\frac{-t}{\tau}}\right) + m_\infty t \qquad \text{(D3)}$$

where $fCa(0)$ is the value of fCa at the time of addition of ISO

120

Define the function of fCa_{FIT}, the line fit on fCa values when they reached a steady slope as follows:

$$fCa_{FIT} = m_{\infty}t + fCa_{FIT}(0),$$ (D4)

where "$fCa_{FIT}(0)$" is the value of the fit at the addition of ISO, depicted in Fig. 27 A. In the case, when $t \gg 0$, $fCa_{FIT} = fCa$, so eqn E3 and E4 gives:

$$m_{\infty}t + fCa_{FIT}(0) = fCa(0) + m_{\infty}t - (m_{\infty} - m_0)\tau,$$ (D5)

and finally by rearranging, we can express the time constant:

$$\tau = \frac{fCa(0) - fCa_{FIT}(0)}{m_{\infty} - m_0}.$$ (D6)

7. ACKNOWLEDGEMENT

8. REFERENCES

Adams, B., and K. Beam. 1990. Muscular dysgenesis in mice: a model system for studying excitation- contraction coupling. *FASEB J.* 4:2809-2816.

Adrian, R.H., and A.R. Peres. 1977. A gating signal for the potassium channel? *Nature* 267:800-804.

Ahern, G.P., P.R. Junankar, and A.F. Dulhunty. 1997. Subconductance states in single-channel activity of skeletal muscle ryanodine receptors after removal of FKBP12. *Biophys. J.* 72:146-162.

Andersen JP, and Vilsen B. 1998. Structure-function relationships of the calcium binding sites of the sarcoplasmic reticulum Ca(2+)-ATPase. *Acta Physiol Scand Suppl.* 643:45-54.

Andrew M. Bellinger, M.M., Andrew R. Marks. 2008. Stressed out: the skeletal muscle ryanodine receptor as a target of stress. *J Clin Invest.* 118:445-453.

Armstrong, C.M., F.M. Bezanilla, and P. Horowicz. 1972. Twitches in the presence of ethylene glycol bis([beta]-aminoethyl ether)-N,N′-tetraacetic acid. *Biochimica et Biophysica Acta (BBA) - Bioenergetics.* 267:605-608.

Arner, P. 2004. Novel Target Genes for Catecholamines in Skeletal Muscle *J Clin Endocrinol Metab.* 89:1998-1999.

Arredouani, A. 2004. Diversification of Function and Pharmacology in Intracellular Calcium Signalling. *Cellscience Review.* 1:30.

Arredouani, A., Y. Guiot, J.-C. Jonas, L.H. Liu, M. Nenquin, J.A. Pertusa, J. Rahier, J.-F. Rolland, G.E. Shull, M. Stevens, F. Wuytack, J.-C. Henquin, and P. Gilon. 2002. SERCA3 Ablation Does Not Impair Insulin Secretion but Suggests Distinct Roles of Different Sarcoendoplasmic Reticulum Ca2+ Pumps for Ca2+ Homeostasis in Pancreatic {beta}-cells *Diabetes.* 51:3245-3253.

Arreola, J., J. Calvo, M. Garcia, and J. Sanchez. 1987. Modulation of calcium channels of twitch skeletal muscle fibres of the frog by adrenaline and cyclic adenosine monophosphate. *J Physiol (Lond).* 393:307-330.

Balnave, C.D., and D.G. Allen. 1998. Evidence for Na+/Ca2+ exchange in intact single skeletal muscle fibers from the mouse. *Am J Physiol Cell Physiol.* 274:C940-946.

Bates, W.H. 1896. The use of extract of suprarenal capsule in the eye. *New York Medical Journal*:647-650.

Bennett, M. 1999. One hundred years of adrenaline: the discovery of autoreceptors. *Clinical Autonomic Research*. 9:145-159.

Bhat, M.B., J. Zhao, H. Takeshima, and J. Ma. 1997. Functional calcium release channel formed by the carboxyl-terminal portion of ryanodine receptor. *Biophys. J.* 73:1329-1336.

Bianchi, C. P., Bolton, T. C. Effect of thiocyanate on radiocalcium uptake during potassium contracture of frog sartorius muscle. *J. Pharmacol. Exptl. Therap.* 151: 456-463, 1966.

Birks, R.I., and D.F. Davey. 1969. Osmotic responses demonstrating the extracellular character of the sarcoplasmic reticulum. *J Physiol.* 202:171-188.

Birnbaumer, L., K.P. Campbell, W.A. Catterall, M.M. Harpold, F. Hofmann, W.A. Horne, Y. Mori, A. Schwartz, T.P. Snutch, and T. Tanabe. 1994. The naming of voltage-gated calcium channels.[see comment]. *Neuron*. 13:505-506.

Blazev, R., M. Hussain, A.J. Bakker, S.I. Head, and G.D. Lamb. 2001. Effects of the PKA inhibitor H-89 on excitationâ€"contraction coupling in skinned and intact skeletal muscle fibres. *Journal of Muscle Research and Cell Motility*. 22:277-286.

Block, B., T. Imagawa, K. Campbell, and C. Franzini-Armstrong. 1988. Structural evidence for direct interaction between the molecular components of the transverse tubule/sarcoplasmic reticulum junction in skeletal muscle *J. Cell Biol.* 107:2587-2600.

Boron W F, Boulapep E.L. 2003. Medical Physiology, 1st edition. Saunders.

Brandl, C., S. deLeon, D. Martin, and D. MacLennan. 1987. Adult forms of the Ca2+ATPase of sarcoplasmic reticulum. Expression in developing skeletal muscle. *J. Biol. Chem.* 262:3768-3774.

Brillantes, A.B., Ondrias, Scottc, Kobrinsky, E. Ondriaová, M.C. Moschella, T. Jayaraman, M. Landersd, B.E. Ehrlich, and A.R. Marks. 1994. Stabilization of calcium release channel (ryanodine receptor) function by FK506-binding protein. *Cell*. 77:513-523.

Brown, G.L., E. Bulbring, and B.D. Burns. 1948. The action of adrenaline on mammalian skeletal muscle. *J Physiol.* 107:115-128.

Brum, G., R. Fitts, G. Pizarro, and E. Rios. 1988a. Voltage sensors of the frog skeletal muscle membrane require calcium to function in excitation-contraction coupling. *J Physiol (Lond)*. 398:475-505.

Brum, G., E. Rios, and E. Stefani. 1988b. Effects of extracellular calcium on calcium movements of excitation-contraction coupling in frog skeletal muscle fibres. *J Physiol*. 398:441-473.

Cairns SP, D.A. 1993. Beta-adrenergic potentiation of E-C coupling increases force in rat skeletal muscle. *Muscle & Nerve*. 16:1317-1325.

Campbell KP, F.-A.C., Shamoo AE. 1980. Further characterization of light and heavy sarcoplasmic reticulum vesicles. Identification of the 'sarcoplasmic reticulum feet' associated with heavy sarcoplasmic reticulum vesicles. *Biochim Biophys Acta*. 602:97.

Carafoli, E.B., M. 2000. Calcium pumps: structural basis for and mechanism of calcium transmembrane transport. *Curr Opin Chem Biol*. 4:152-161.

Catterall, W.A. 2000. Structure and regulation of voltage-gated Ca2+ channels. *Annual Review of Cell and Developmental Biology*. 16:521-555.

Costantin, L.L., C. Franzini-Armstrong, and R.J. Podolsky. 1965. Localization of Calcium-Accumulating Structures in Striated Muscle Fibers *Science*. 147:158-160.

Curtis, B.A. 1966. Ca Fluxes in Single Twitch Muscle Fibers *J. Gen. Physiol*. 50:255-267.

Curtis, B.M., and W.A. Catterall. 1984. Purification of the calcium antagonist receptor of the voltage-sensitive calcium channel from skeletal muscle transverse tubules. *Biochemistry*. 23:2113-2118.

Curtis, B.M., and W.A. Catterall. 1985. Phosphorylation of the calcium antagonist receptor of the voltage-sensitive calcium channel by cAMP-dependent protein kinase P*NAS*. 82:2528-2532.

Dode, L., F. Wuytack, P.F. Kools, F. Baba-Aissa, L. Raeymaekers, F. BrikÃ©, W.J. van de Ven, R. Casteels, and F. Brik. 1996 cDNA cloning, expression and chromosomal localization of the human sarco/endoplasmic reticulum Ca(2+)-ATPase 3 gene. *Biochem. J.* . 318:689-699.

Endo, M., Tanaka, M., Ebashi, S., Release of calcium from endoplasmic reticulum in skinned fibers of the frog. *Proc. Intern. Congr. Physiol. Sci., 24 th* 1968, vol 7, p. 126.

Ertel, E.A., K.P. Campbell, M.M. Harpold, F. Hofmann, Y. Mori, E. Perez-Reyes, A. Schwartz, T.P. Snutch, T. Tanabe, L. Birnbaumer, R.W. Tsien, and W.A. Catterall. 2000. Nomenclature of voltage-gated calcium channels.[comment]. *Neuron*. 25:533-535.

Fabiato, A. 1983. Calcium-induced release of calcium from the cardiac sarcoplasmic reticulum. *Am J Physiol Cell Physiol*. 245:C1-14.

Fabiato A, F.F. 1978. Cyclic AMP-induced enhancement of calcium accumulation by the sarcoplasmic reticulum with no modification of the sensitivity of the myofilaments to calcium in skinned fibres from a yeast skeletal muscle. *Biochim Biophys Acta*. 539:253-260.

Fatt, P., and B. Katz. 1952. Spontaneous subthreshold activity at motor nerve endings. *J Physiol*. 117:109-128.

Felder, E., and C. Franzini-Armstrong. 2002. Type 3 ryanodine receptors of skeletal muscle are segregated in a parajunctional position *PNAS*. 99:1695-1700.

Fleig, A., and R. Penner. 1996. Silent calcium channels generate excessive tail currents and facilitation of calcium currents in rat skeletal myoballs. *J Physiol*. 494:141-153.

Fleischer, S., E.M. Ogunbunmi, M.C. Dixon, and E.A.M. Fleer. 1985. Localization of Ca2+ Release Channels with Ryanodine in Junctional Terminal Cisternae of Sarcoplasmic Reticulum of Fast Skeletal Muscle *PNAS* 82:7256-7259.

Flockerzi, V., H.-J. Oeken, F. Hofmann, D. Pelzer, A. Cavalie, and W. Trautwein. 1986. Purified dihydropyridine-binding site from skeletal muscle t-tubules is a functional calcium channel. 323:66-68.

Ford, L. E., Podolsky, R. J., Force development and calcium movements in skinned muscle fibers. *Federation Proc*. 27: 375, 1968.

Franzini-Armstrong, C. 1970. STUDIES OF THE TRIAD: I. Structure of the Junction in Frog Twitch Fibers . *J. Cell Biol*. 47:488-499.

Franzini-Armstrong, C., L. Kenney, and E. Varriano-Marston. 1987. The structure of calsequestrin in triads of vertebrate skeletal muscle: a deep-etch study *J. Cell Biol*. 105:49-56.

Gaburjakova, M., J. Gaburjakova, S. Reiken, F. Huang, S.O. Marx, N. Rosemblit, and A.R. Marks. 2001. FKBP12 Binding Modulates Ryanodine Receptor Channel Gating *J. Biol. Chem*. 276:16931-16935.

Garcia, J., T. Tanabe, and K. Beam. 1994. Relationship of calcium transients to calcium currents and charge movements in myotubes expressing skeletal and cardiac dihydropyridine receptors *J. Gen. Physiol.* 103:125-147.

Gonzalez-Serratos, H., L. Hill, and R. Valle-Aguilera. 1981. Effects of catecholamines and cyclic amp on excitation--contraction coupling in isolated skeletal muscle fibres of the frog. *J Physiol (Lond)*. 315:267-282.

Gray, P.C., J.D. Scott, and W.A. Catterall. 1998. Regulation of ion channels by cAMP-dependent protein kinase and A-kinase anchoring proteins. *Current Opinion in Neurobiology*. 8:330-334.

Gray, P.C., V.C. Tibbs, W.A. Catterall, and B.J. Murphy. 1997. Identification of a 15-kDa cAMP-dependent Protein Kinase-anchoring Protein Associated with Skeletal Muscle L-type Calcium Channels *J. Biol. Chem.* 272:6297-6302.

Gruber, C.M. 1914. STUDIES IN FATIGUE: III. The Fatigue Threshold as Affected by Adrenalin and by Increased Arterial Pressure. *Am J Physiol.* 33:335-355.

Hayashi, M. 2001. Phosphorylation of a new member of the bicarbonate cotransporter superfamily. 60:462-465.

Herbette, L., J. Marquardt, A. Scarpa, and J.K. Blasie. 1977. A direct analysis of lamellar x-ray diffraction from hydrated oriented multilayers of fully functional sarcoplasmic reticulum. *Biophys. J.* 20:245-272.

Hille, B., and D. Campbell. 1976. An improved vaseline gap voltage clamp for skeletal muscle fibers *J. Gen. Physiol.* 67:265-293.

Huerta, M., Trujillo, Lomeli. 1991. Adrenergic modulation of the K+ contractures in tonic skeltal muscle fibers of the frog. *Japanese Journal of Physiology*. 41:851 - 860.

Hui, C., and W. Chandler. 1991. Q beta and Q gamma components of intramembranous charge movement in frog cut twitch fibers . *J. Gen. Physiol.* 98:429-464.

Hui, C.S. 1983. Differential properties of two charge components in frog skeletal muscle. *J Physiol.* 337:531-552.

Hutter, O.F., and W.R. Loewenstein. 1955. Nature of neuromuscular facilitation by sympathetic stimulation in the frog. *J Physiol.* 130:559-571.

Huxley, A.F., and R. Niedergerke. 1954. Structural Changes in Muscle During Contraction: Interference Microscopy of Living Muscle Fibres. 173:971-973.

Irving, M., J. Maylie, N. Sizto, and W. Chandler. 1987. Intrinsic optical and passive electrical properties of cut frog twitch fibers *J. Gen. Physiol.* 89:1-40.

Jahn, H., W. Nastainczyk, A. Röhrkasten, T. Schneider, and F. Hoffmann. 1988. Site-specific phosphorylation of the purified receptor for calcium-channel blockers by cAMP- and cGMP-dependent protein kinases, protein kinase C, calmodulin-dependent protein kinase II and casein kinase II. *European Journal of Biochemistry.* 178:535-542.

James, P., T. Vorherr, and E. Carafoli. 1995. Calmodulin-binding domains: just two faced or multi-faceted? *Trends in Biochemical Sciences.* 20:38-42.

Jayaraman, T., A. Brillantes, A. Timerman, S. Fleischer, H. Erdjument-Bromage, P. Tempst, and A. Marks. 1992. FK506 binding protein associated with the calcium release channel (ryanodine receptor). *J. Biol. Chem.* 267:9474-9477.

Johnson, B., T. Scheuer, and W. Catterall. 1994. Voltage-Dependent Potentiation of L-Type Ca2+ Channels in Skeletal Muscle Cells Requires Anchored cAMP-Dependent Protein Kinase PNAS 91:11492-11496.

Jong, D., P. Pape, and W. Chandler. 1995. Effect of sarcoplasmic reticulum calcium depletion on intramembranous charge movement in frog cut muscle fibers *J. Gen. Physiol.* 106:659-704.

Juel, C. 1998. Muscle pH regulation: role of training. *Acta Physiologica Scandinavica.* 162:359-366.

Karylowski, Zeigerer, Cohen, McGraw, 2004. GLUT4 Is Retained by an Intracellular Cycle of Vesicle Formation and Fusion with Endosomes. *Mol. Biol. Cell.* 15(2): 870-882

Keynes, R.D., and D.J. Aidley. 2001. Nerve and Muscle, 3rd edition. Cambridge, University Press, Cambridge.

Kristensen, J. M. M.K., C. Juel,. 2004. Expression of Na+/HCO3 co-transporter proteins (NBCs) in rat and human skeletal muscle. *Acta Physiologica Scandinavica.* 182:69-76.

Lannergren, J. 1987. Contractile properties and myosin isoenzymes of various kinds ofXenopus twitch muscle fibres. *Journal of Muscle Research and Cell Motility.* 8:260-273.

Leeb-Lundberg, L.M.F., S. Cotecchia, J.W. Lomasney, J.F. DeBernardis, R.J. Lefkowitz, and M.G. Caron. 1985. Phorbol Esters Promote alpha 1-adrenergic Receptor Phosphorylation and Receptor Uncoupling from Inositol Phospholipid Metabolism PNAS 82:5651-5655.

Lisman, J., and J. Strong. 1979. The initiation of excitation and light adaptation in Limulus ventral photoreceptors *J. Gen. Physiol.* 73:219-243.

Liu, T., W. Tucker, A. Bhalla, E. ChapmanandJames, and C. Weisshaar. 2005. SNARE-Driven, 25-Millisecond Vesicle Fusion In Vitro. *Biophys J.* 89:2458.

Llinás, R., I.Z. Steinbergand, and K. Walton. 1981. Relationship between presynaptic calcium current and postsynaptic potential in squid giant synapse. *Biophysical Journal.* 33:323-351.

Lutz, G.J., D.B. Cuizon, A.F. Ryan, and R.L. Lieber. 1998. Four novel myosin heavy chain transcripts define a molecular basis for muscle fibre types in Rana pipiens. *J Physiol.* 508:667-680.

Lytton, J., M. Westlin, S. Burk, G. Shull, and D. MacLennan. 1992. Functional comparisons between isoforms of the sarcoplasmic or endoplasmic reticulum family of calcium pumps. *J. Biol. Chem.* 267:14483-14489.

MacLennan, D.H., C.J. Brandl, B. Korczak, and N.M. Green. 1985. Amino-acid sequence of a Ca2+ + Mg2+ -dependent ATPase from rabbit muscle sarcoplasmic reticulum, deduced from its complementary DNA sequence. 316:696-700.

MacLennan, D.H., W.J. Rice, and N.M. Green. 1997. The Mechanism of Ca2+ Transport by Sarco(Endo)plasmic Reticulum Ca2+-ATPases *J. Biol. Chem.* 272:28815-28818.

MacLennan, D.H., and P.T.S. Wong. 1971. Isolation of a Calcium-Sequestering Protein from Sarcoplasmic Reticulum *PNAS.* 68:1231-1235.

Martin, W.H., 3rd, T.K. Tolley, and J.E. Saffitz. 1990. Autoradiographic delineation of skeletal muscle alpha 1-adrenergic receptor distribution. *Am J Physiol Heart Circ Physiol.* 259:H1402-1408.

Marx, S.O., K. Ondrias, and A.R. Marks. 1998. Coupled Gating Between Individual Skeletal Muscle Ca2+ Release Channels (Ryanodine Receptors) .281.5378.818. *Science.* 281:818-821.

Marx, S.O., S. Reiken, Y. Hisamatsu, M. Gaburjakova, J. Gaburjakova, Y.-M. Yang, N. Rosemblit, and A.R. Marks. 2001. Phosphorylation-dependent Regulation of Ryanodine Receptors: A Novel Role for Leucine/Isoleucine Zippers *J. Cell Biol.* 153:699-708.

Maylie, J., M. Irving, N. Sizto, G. Boyarsky, and W. Chandler. 1987a. Calcium signals recorded from cut frog twitch fibers containing tetramethylmurexide *J. Gen. Physiol.* 89:145-176.

Maylie, J., M. Irving, N. Sizto, and W. Chandler. 1987b. Comparison of arsenazo III optical signals in intact and cut frog twitch fibers *J. Gen. Physiol.* 89:41-81.

Meissner, G. 1975. Isolation and characterization of two types of sarcoplasmic reticulum vesicles. *Biochim Biophys Acta.* 389.

Meissner, G., E. Darling, and J. Eveleth. 1986. Kinetics of rapid calcium release by sarcoplasmic reticulum. Effects of calcium, magnesium, and adenine nucleotides *Biochemistry.* 25:236-244.

Meissner G, Gregory E.,C.and.S.Fisher. 1973. Isolation of sarcoplasmic reticulum by zonal centrifugation and purification of Ca2+-pump and Ca2+-binding proteins. *Biochimica et Biophysica Acta (BBA) - Biomembranes.* 298:246.

Michalak, M., K. Famulski, and E. Carafoli. 1984. The Ca2+-pumping ATPase in skeletal muscle sarcolemma. Calmodulin dependence, regulation by cAMP-dependent phosphorylation, and purification. *J. Biol. Chem.* 259:15540-15547.

Moore, R.D. 1981. Stimulation of Na:H exchange by insulin. *Biophysical Journal.* 33:203–210.

Mundina-Weilenmann, C., C. Chang, L. Gutierrez, and M. Hosey. 1991. Demonstration of the phosphorylation of dihydropyridine-sensitive calcium channels in chick skeletal muscle and the resultant activation of the channels after reconstitution. *J. Biol. Chem.* 266:4067-4073.

Nunoki, K., V. Florio, and W.A. Catterall. 1989. Activation of purified calcium channels by stoichiometric protein phosphorylation *PNAS* 86:6816-6820.

Odermatt, A., S. Becker, V.K. Khanna, K. Kurzydlowski, E. Leisner, D. Pette, and D.H. MacLennan. 1998. Sarcolipin Regulates the Activity of SERCA1, the Fast-twitch Skeletal Muscle Sarcoplasmic Reticulum Ca2+-ATPase *J. Biol. Chem.* 273:12360-12369.

Ogawa, Y., and S. Ebashi. 1976. Calcium-releasing action of b,g-methylene adenosine triphosphate on fragmented sarcoplasmic reticulum. *Journal of Biochemistry.* 80:1149-1157.

Oota, I., and T. Nagai. 1977. Effects of Catecholamines on Excitation-Contraction Coupling in Frog Single Twitch Fiber. *Japanese Journal of Physiology:*195-213.

Orbeli, L.A. 1923. Die sympathtitische Innervation der Skelettmuskeln. *Bull. Inst. Soc. Leshaft:*194.

Owen, N. 1986a. Effect of catecholamines on Na/H exchange in vascular smooth muscle cells 10.1083/jcb.103.5.2053. *J. Cell Biol.* 103:2053-2060.

Owen, N. 1986b. Effect of catecholamines on Na/H exchange in vascular smooth muscle cells *J. Cell Biol.* 103:2053-2060.

Pape, P., D. Jong, and W. Chandler. 1995. Calcium release and its voltage dependence in frog cut muscle fibers equilibrated with 20 mM EGTA *J. Gen. Physiol.* 106:259-336.

Pape, P.C., and N. Carrier. 1998. Effect of Sarcoplasmic Reticulum (SR) Calcium Content on SR Calcium Release Elicited by Small Voltage-Clamp Depolarizations in Frog Cut Skeletal Muscle Fibers Equilibrated with 20 mM EGTA *J. Gen. Physiol.* 112:161-179.

Pape, P.C., and K. Fénelon. 2008. The relatively high Ca2+ flux in Ca2+ sparks could be due to the Ca-binding protein calsequestrin in the sarcoplasmic reticulum. *Physiological News.* 71.

Pape, P.C., K. Fenelon, and N. Carrier. 2002. Extra activation component of calcium release in frog muscle fibres *J Physiol.* 542:867-886.

Pape, P.C., K. Fenelon, C.R.H. Lamboley, and D. Stachura. 2007. Role of calsequestrin evaluated from changes in free and total calcium concentrations in the sarcoplasmic reticulum of frog cut skeletal muscle fibres *J Physiol.* 581:319-367.

Patten, G.S., and M.G. Clark. 1983. Ca2+-mediated activation of phosphofructokinase in perfused rat heart. *Biochem. J.* 216:717.

Peachey, L.D. 1965. The sarcoplasmic reticulum and transverse tubules of the frog's sartorius *J. Cell Biol.* 25:209-231.

Peper, K., F. Dreyer, C. Sandri, K. Akert, and H. Moor. 1974. Structure and ultrastructure of the frog motor endplate. *Cell and Tissue Research.* 149:437-455.

Pirouzi, P. 1999. Effet fe la stimulation beta-adrenergique sur le couplage ectitation-contraction dans le muscle squelettique de grenouille. Doctoral dissertation, University of Sherbrooke, Department of Physiology-Biophysics, Sherbrooke.

Reading SA, M.C., Barclay JK. 2003. Increased cAMP as a positive inotropic factor for mammalian skeletal muscle in vitro. *Can J Physiol Pharmacol.* Oct;81(10):986-96.

Reiken, S., A. Lacampagne, H. Zhou, A. Kherani, S.E. Lehnart, C. Ward, F. Huang, M. Gaburjakova, J. Gaburjakova, N. Rosemblit, M.S. Warren, K.-l. He, G.-h. Yi, J. Wang, D. Burkhoff, G. Vassort, and A.R. Marks. 2003. PKA phosphorylation activates the calcium release channel (ryanodine receptor) in skeletal muscle: defective regulation in heart failure *J. Cell Biol.* 160:919-928.

Rios, E., and G. Brum. 1987. Involvement of dihydropyridine receptors in excitation-contraction coupling in skeletal muscle. *Nature*, 325:717-720.

Rios, E., and G. Pizarro. 1988. Voltage Sensors and Calcium Channels of Excitation-Contraction Coupling. *News Physiol Sci*. 3:223-227.

Rios, E., and G. Pizarro. 1991. Voltage sensor of excitation-contraction coupling in skeletal muscle. *Physiological Reviews*. 71:849-908.

Roos, J., P.J. DiGregorio, A.V. Yeromin, K. Ohlsen, M. Lioudyno, S. Zhang, O. Safrina, J.A. Kozak, S.L. Wagner, M.D. Cahalan, G. Velicelebi, and K.A. Stauderman. 2005. STIM1, an essential and conserved component of store-operated Ca2+ channel function *J. Cell Biol*. 169:435-445.

Rubin CS. 1994. A kinase anchor proteins and the intracellular targeting of signals carried by cyclic AMP. *Biochim Biophys Acta*. 1224:467.

Rubio, R., C. Bailey, and C. Villar-Pilasi. 1975. Effects of Cyclic AMP dependent protein kinase on cardiac actomyosin: increase on Ca2+ sensitivity and possible phosphorylation of tropin I. *J. cyclic Nucleotide Res*. 1:143-150.

Rudolf, R., P.J. Magalhaes, and T. Pozzan. 2006. Direct in vivo monitoring of sarcoplasmic reticulum Ca2+ and cytosolic cAMP dynamics in mouse skeletal muscle *J. Cell Biol*. 173:187-193.

Ruehr, M.L., M.A. Russell, D.G. Ferguson, M. Bhat, J. Ma, D.S. Damron, J.D. Scott, and M. Bond. 2003a. Targeting of Protein Kinase A by Muscle A Kinase-anchoring Protein (mAKAP) Regulates Phosphorylation and Function of the Skeletal Muscle Ryanodine Receptor 10.1074/jbc.M213279200. *J. Biol. Chem*. 278:24831-24836.

Ruehr, M.L., M.A. Russell, D.G. Ferguson, M. Bhat, J. Ma, D.S. Damron, J.D. Scott, and M. Bond. 2003b. Targeting of Protein Kinase A by Muscle A Kinase-anchoring Protein (mAKAP) Regulates Phosphorylation and Function of the Skeletal Muscle Ryanodine Receptor *J. Biol. Chem*. 278:24831-24836.

Schmid, A., J. Renaud, and M. Lazdunski. 1985. Short term and long term effects of beta-adrenergic effectors and cyclic AMP on nitrendipine-sensitive voltage-dependent Ca2+ channels of skeletal muscle. *J. Biol. Chem*. 260:13041-13046.

Schneider, M.F., and W.K. Chandler. 1973. Voltage Dependent Charge Movement in Skeletal Muscle: a Possible Step in Excitation-Contraction Coupling. 242:244-246.

Sculptoreanu, A., T. Scheuer, and W.A. Catterall. 1993. Voltage-dependent potentiation of L-type Ca2+ channels due to phosphorylation by cAMP-dependent protein kinase. 364:240-243.

Seeley, R.R., T.D. Stephens, and P. Tate. 2003. Anatomy & Physiology, 7th edition. McGraw-Hill, New York.

Shannon, T.R., K.S. Ginsburg, and D.M. Bers. 2000. Reverse Mode of the Sarcoplasmic Reticulum Calcium Pump and Load-Dependent Cytosolic Calcium Decline in Voltage-Clamped Cardiac Ventricular Myocytes. *Biophys. J.* 78:322-333.

Shen, X., C. Franzini-Armstrong, J.R. Lopez, L.R. Jones, Y.M. Kobayashi, Y. Wang, W.G.L. Kerrick, A.H. Caswell, J.D. Potter, T. Miller, P.D. Allen, and C.F. Perez. 2007. Triadins Modulate Intracellular Ca2+ Homeostasis but Are Not Essential for Excitation-Contraction Coupling in Skeletal Muscle *J. Biol. Chem.* 282:37864-37874.

Shin, D.M., and S. Muallem. 2008. Skeletal muscle dressed in SOCs. 10:639-641.

Slack, J.P., I.L. Grupp, D.G. Ferguson, N. Rosenthal, and E.G. Kranias. 1997. Ectopic Expression of Phospholamban in Fast-Twitch Skeletal Muscle Alters Sarcoplasmic Reticulum Ca2+ Transport and Muscle Relaxation *J. Biol. Chem.* 272:18862-18868.

Smith, J., E. Rousseau, and G. Meissner. 1989. Calmodulin modulation of single sarcoplasmic reticulum Ca2+-release channels from cardiac and skeletal muscle. *Circ Res.* 64:352-359.

Smith, J.S., R. Coronado, and G. Meissner. 1985. Sarcoplasmic reticulum contains adenine nucleotide-activated calcium channels. 316:446-449.

Snutch, T.P., J.P. Leonard, M.M. Gilbert, H.A. Lester, and N. Davidson. 1990. Rat brain expresses a heterogeneous family of calcium channels. *PNAS.* 87:3391-3395.

Stiber, J., A. Hawkins, Z.-S. Zhang, S. Wang, J. Burch, V. Graham, C.C. Ward, M. Seth, E. Finch, N. Malouf, R.S. Williams, J.P. Eu, and P. Rosenberg. 2008. STIM1 signalling controls store-operated calcium entry required for development and contractile function in skeletal muscle. 10:688-697.

Suko, J., I. Maurer-Fogy, B. Plank, O. Bertel, W. Wysowsky, M. Hohenegger, and G. Hellmann. 1993. Phosphorylation of serine 2843 in ryanodyne receptor-calcium release channel of skeletal muscle by cAMP-,CGMP, -and CAM-dependent protein kinase. *Biochem . Biophys. Acta.* 1175:193-206.

Takahashi, M., M.J. Seagar, J.F. Jones, B.F. Reber, and W.A. Catterall. 1987. Subunit structure of dihydropyridine-sensitive calcium channels from skeletal muscle. *PNAS*. 84:5478-5482.

Tasken, K., and E.M. Aandahl. 2004. Localized Effects of cAMP Mediated by Distinct Routes of Protein Kinase A *Physiol. Rev*. 84:137-167.

Toyofuku, T., K. Curotto Kurzydlowski, N. Narayanan, and D. MacLennan. 1994. Identification of Ser38 as the site in cardiac sarcoplasmic reticulum Ca(2+)-ATPase that is phosphorylated by Ca2+/calmodulin-dependent protein kinase. *J. Biol. Chem*. 269:26492-26496.

Tsien, R.W., D. Lipscombe, D.V. Madison, K.R. Bley, and A.P. Fox. 1988. Multiple types of neuronal calcium channels and their selective modulation. *Trends in Neurosciences*. 11:431.

Vergara, J., and C. Caputo. 1983. Effects of tetracaine on charge movements and calcium signals in frog skeletal muscle fibers *PNAS*. 80:1477-1481.

Viguerie, N., K. Clement, P. Barbe, M. Courtine, A. Benis, D. Larrouy, B. Hanczar, V. Pelloux, C. Poitou, Y. Khalfallah, G.S. Barsh, C. Thalamas, J.-D. Zucker, and D. Langin. 2004. In Vivo Epinephrine-Mediated Regulation of Gene Expression in Human Skeletal Muscle *J Clin Endocrinol Metab*. 89:2000-2014.

Wang, C.-Z., H. Yano, K. Nagashima, and S. Seino. 2000. The Na+-driven Cl-/HCO3- Exchanger. Cloning, tissue distribution, and functional characterization *J. Biol. Chem*. 275:35486-35490.

Weber T, Zemelman BV, McNew JA, Westermann B, Gmachl M, Parlati F, Söllner TH, and J. Rothman. 1998. SNAREpins: minimal machinery for membrane fusion. *Cell*. 92:759-772.

Wehrens, X.H.T., S.E. Lehnart, S. Reiken, R. van der Nagel, R. Morales, J. Sun, Z. Cheng, S.-X. Deng, L.J. de Windt, D.W. Landry, and A.R. Marks. 2005. Enhancing calstabin binding to ryanodine receptors improves cardiac and skeletal muscle function in heart failure PNAS 102:9607-9612.

Wilson, M.C., V.N. Jackson, C. Heddle, N.T. Price, H. Pilegaard, C. Juel, A. Bonen, I. Montgomery, O.F. Hutter, and A.P. Halestrap. 1998. Lactic Acid Efflux from White Skeletal Muscle Is Catalyzed by the Monocarboxylate Transporter Isoform MCT3 *J. Biol. Chem*. 273:15920-15926.

Yu, J., J. Xiao, X. Ren, K. Lao, and X.S. Xie. 2006. Probing Gene Expression in Live Cells, One Protein Molecule at a Time *Science*. 311:1600-1603.

Yuan, J.P., W. Zeng, G.N. Huang, P.F. Worley, and S. Muallem. 2007. STIM1 heteromultimerizes TRPC channels to determine their function as store-operated channels. 9:636-645.

Zhang, L., J. Kelley, G. Schmeisser, Y.M. Kobayashi, and L.R. Jones. 1997. Complex Formation between Junctin, Triadin, Calsequestrin, and the Ryanodine Receptor. Proteins of the cardiac junctional sarcoplasmic reticulum membrane *J. Biol. Chem.* 272:23389-23397.

Zurini, M., J. Krebs, J. Penniston, and E. Carafoli. 1984. Controlled proteolysis of the purified Ca2+-ATPase of the erythrocyte membrane. A correlation between the structure and the function of the enzyme. *J. Biol. Chem.* 259:618-627.